Adsorption et stabilité thermique de 2-mercaptobenzothiazole et 2-mercaptobenzimidazole déposés sur la surface du Cu(111) et effet sur les mécanismes d'inhibition de la corrosion

Xiaocui Wu

HAL Id: tel-03551413
https://pastel.hal.science/tel-03551413

Submitted on 1 Feb 2022

PSL★
UNIVERSITÉ PARIS

THÈSE DE DOCTORAT
DE L'UNIVERSITÉ PSL

Préparée à Chimie ParisTech

Adsorption and thermal stability of 2-mercaptobenzothiazole and 2-mercaptobenzimidazole deposited on Cu(111) surfaces and effects on corrosion inhibition mechanisms

Soutenue par
Xiaocui WU
Le 30 septembre 2020

École doctorale nº388
Chimie physique et chimie analytique de Paris centre

Spécialité
Physico-chimie

Composition du jury :

Claire-Marie PRADIER
Directrice de Recherche, CNRS   *Présidente*

Bruno DOMENICHINI
Professeur, Université de Bourgogne   *Rapporteur*

Rob LINDSAY
Senior Lecturer, Université de Manchester   *Rapporteur*

Ingrid MILOSEV
Professeur, Institut Jožef Stefan   *Examinatrice*

Frédéric WIAME
Maître de conférences, Chimie ParisTech   *Examinateur*

Philippe MARCUS
Directeur de Recherche, Chimie ParisTech   *Directeur de thèse*

Chimie Paris | PSL★
ParisTech

Acknowledgments

This thesis work was performed in the Physical Chemistry of Surfaces (PCS) Group, at Institut de Recherche de ChimieParis (IRCP).

CONTENTS

General introduction

Corrosion is an important technical, economic, environmental and safety issue, with an annual global cost estimated to be about 3% of the global GDP (2013) [1]. It is one of the main causes of degradation and destruction of most facilities and equipments.

Copper is widely used in industry for its excellent corrosion resistance property. It does not react with high purity water, but it reacts slowly with humid air to form a dull blue-green patina which protects the metal underneath. However, this metal is not totally immune to corrosion. Under acidic conditions, or in the presence of chloride ions, it may be subjected to corrosion. For metallic materials in environmental conditions in which effective self-protection by passivation does not function, the use of corrosion inhibitors is one of the major means of corrosion protection.

The corrosion inhibitors most commonly used in oil and gas production are imidazolines, amides, amines, phosphate esters, carboxylic acids and their derivatives, and sulfur-containing organic molecules [2]. It is commonly believed that, for inhibition to function, adsorption of the inhibitor molecules on the substrate surface must take place, the interaction must be strong and a protective film must be formed. However, even for the most studied benzotriazole/Cu system [3–14], the chemical details of the inhibiting interaction and the resulting structures of the protective layer formed on metal surfaces are still debated. Most notably, the exact role of the surface oxide in the inhibiting function remains to be studied.

2-mercaptobenzothiazole (2-MBT, $C_7H_5NS_2$) and 2-mercaptobenzimidazole (2-MBI, $C_7H_6N_2S$) are also known as effective corrosion inhibitors used in industry for copper [3], and are selected in this work for their dual functional group. This work aims at bringing new insight into the relationship between local structure and chemical composition of surface interaction and corrosion inhibition efficiency in the presence of oxygen. The objective is to provide the necessary detailed information to understand the corrosion inhibition mechanisms on surfaces, and to offer a rational basis for the design of new inhibitors. The outcome of this research is useful in various industrial areas in which copper and its alloys are used (e.g. drinking water supply system, heat exchangers, microelectronics, materials for nuclear waste storage, etc.).

To this end, a surface science approach on well-defined model surfaces is applied with deposition of the molecules at ultra low pressure from the gas phase. The inhibitor adsorption kinetics and coverage on metallic and pre-oxidized Cu(111) single-crystal surfaces are monitored by Auger Electron Spectroscopy (AES), the chemical composition during growth of the molecular layers is characterized by *in situ* X-ray Photoelectron Spectroscopy (XPS). Scanning Tunneling Microscopy (STM) allows analysing the preferential interaction of the adsorbed molecules with the metallic and pre-oxidized copper surfaces, and characterizing the structure and topography of the molecular layers at different steps of exposure.

This manuscript consists of five chapters. Chapter one presents a state of the art introduction of the different forms of corrosion and various methods for copper protection. An emphasis is given to the use of corrosion inhibitors, where a detailed study is conducted. Finally, a specific investigation on copper corrosion inhibitors is performed. In particular, the interaction of 2-MBT and 2-MBI with copper is studied.

Chapter two describes the experimental techniques used in this work for the characterization of sample surfaces before and after molecule deposition. Detailed informations of three UHV systems where the experiments were carried out are provided, with the characteristic of different surface techniques. Moreover, the experimental conditions used for the preparation of sample surface as well as the protocol applied for the deposition of corrosion inhibitors are specified.

Chapter three and four are dedicated to the study of 2-MBT adsorption on metallic and pre-oxidized Cu(111) surfaces at room temperature. Chapter three consist of a quantitative analysis by *in situ* XPS of the chemical composition and thickness of the adsorbed molecular layers. Their thermal stability and corrosion inhibition efficiency are also investigated. Chapter four gives a topographic characterization by STM of the sample surface at different steps of exposure. The structure of the molecular layers formed on metallic Cu(111) surface after annealing at different temperatures is also determined.

Chapter five reports the study of 2-MBI adsorption on Cu(111) surfaces under similar conditions as for 2-MBT. The growth kinetics of 2-MBI is followed by AES, and the topography of molecular layer is characterized by STM at different steps of exposure. The thermal stability and the corrosion inhibition efficiency of the adsorbed molecular layer are also investigated. Due to technical issues, *in situ* XPS was not performed. Quantitative analysis by XPS is carried out by transferring the sample to XPS system. Finally, a comparative discussion is addressed for a better understanding of the corrosion inhibition mechanisms.

Chapter six focuses on the effect of temperature on the adsorption of 2-MBT. To this end, the molecular deposition is performed by heating the sample to higher temperature. The structure of the molecular layer is followed *in situ* by STM, and the chemical composition is studied by XPS.

The last four chapters presenting the results obtained during this work are in form of articles published or submitted in scientific journals. The main conclusions are given in the final section together with the perspectives. A summary of this work in French is provided in Annex.

CHAPTER 1

STATE OF THE ART

1.1   Copper and its alloys

Copper is a transition metal of atomic number 29, of ground state electronic configuration [Ar]$3d^{10}4s^1$ and of molar mass 63.546 g.mol^{-1}. It is soft and ductile with very high thermal and electrical conductivity [15]. It is widely used in many domains such as electronics, for the conduction of heat and electricity, and on material for the constitution of metal alloys. Copper is present in earth's crust in low concentration, and it is one of the few metals which exists naturally in metallic form, with a red-brown colour. It is also for this reason that it is used in jewellery and for decoration. Copper is one of the first metal used by human, and its first use dates back to around 7000 years BC.

Copper has once been considered as a dangerous poison, especially in the form of verdigris. It is now known that copper is vital for life as a micronutrient. Man and animals need to absorb a few milligrams of copper every day to ensure the proper functioning of organs and metabolic processes, such as the formation of blood hemoglobin [16].

In 2018, the total global copper production from mines amounted to an estimated 21 million tons, and the leading countries in world copper production were Chile, Peru and China. Chile, the world's leading copper producer by far, produced an estimated 5.8 million metric tons of copper. In second place is Peru, with an estimated copper mine production of 2.4 million tons. The world's third-largest copper producer from mines is China, with an estimated 1.6 million tons. Over half of the copper consumption is related to the electrical and electronic applications.

Copper alloys are metal alloys that have copper as their principal component, where other elements are added in order to improve their properties. Due to the variety and combination of the additions employed and their proportions, about 400 different types of copper alloys can be found. The best known traditional types are brass, which is an alloy of copper and zinc, bronze, which generally refers to copper and tin alloys, and cupronickel, a copper-nickel alloy.

Brasses are usually yellow. The zinc content can vary between few % to about 40%. As long as it is kept under 15%, it does not markedly decrease corrosion resistance of copper. Brass has excellent thermal conductivity, making it a first choice for heat exchangers (radiators). Bronzes were the first metallic alloys to be developed by mankind, about four thousand years ago, and were used for coins, weapons, tools, jewellery and ornaments. Copper-nickel alloys are silver in colour, and are used as silver-coloured coins. Cupronickel is also widely used for marine applications for being highly resistant to corrosion by salt water. The addition of nickel to copper improves strength and corrosion resistance without reducing the good ductility.

1.2   Introduction to corrosion

1.2.1   General introduction

Corrosion is the degradation and eventually destruction of materials (mostly metals and alloys) by chemical and/or electrochemical reaction with their environment. The best-known examples are the chemical alterations of metals in air or in water, such as iron and steel rust or the formation of verdigris on copper and its alloys (bronze, brass). Other materials such as plastic, concrete, wood, ceramics and composite materials all suffer deterioration when placed in a chemically aggressive environment. Here are some other examples of corrosion phenomena:

- cracking of brass in the presence of ammonia,

- hot corrosion of a superalloy in a gas turbine,

- degradation of polyvinyl chloride (PVC) by ultraviolet radiation,

- attacks of refractory bricks by slags,

- attack of a mineral glass by an alkaline solution.

Few metals are found in their native form. Some, such as gold or platinum, are thermodynamically stable and are in metallic form, but most of the metals are generally found in the form of oxides, sulphates, sulphides, carbonates or chlorides which constitute the main types of minerals. When reduced to the metallic state, they tend, in the presence of certain environments, to return to the oxidized form which is their thermodynamically stable form. Most metals undergo oxidation phenomena in contact with the ambient atmosphere, liquids or other metals. The kinetics of corrosion can be important and endanger the metal.

There are four main reasons for studying corrosion. Three of those are based on societal issues concerning (i) human life and safety, (ii) the cost of corrosion, and (iii)
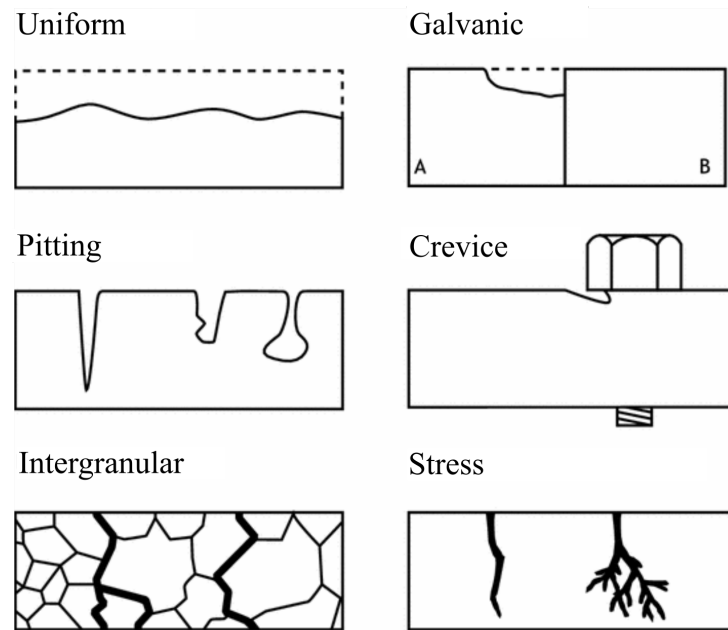
Figure 1.1: Different types of corrosion.

the conservation of materials. The fourth reason is that corrosion itself is a dedicated phenomenon to understand, and its study is a very interesting exercise which will contribute to the development of science.

Corrosion comes in many different forms, as shown in Fig. 1.1. Generalized corrosion accounts for the greatest amount of metal destruction by corrosion and corresponds to a uniform decrease in thickness. The corrosion rate makes it possible to know if the alloy can be used or not. The corrosion rate of an alloy is [17]:

- excellent up to 0.05 mm/year

- good up to 0.5 mm/year

- satisfactory up to 1.25 mm/year

- bad beyond 1.25 mm/year

General attack corrosion is considered as a safe form of corrosion, due to the fact that it is predictable, manageable and often preventable.

In corrosive environments, metals may be exposed to not only uniform corrosion, but also to various types of local corrosion including galvanic, pitting, crevice, intergranular and stress corrosion.

Galvanic corrosion, or dissimilar metal corrosion, occurs when two different metals are located together in a corrosive electrolyte. A galvanic couple forms between the two metals, where one metal becomes the anode and the other the cathode. The anode, or sacrificial metal, corrodes and deteriorates faster than it would alone, while the cathode deteriorates more slowly than it would otherwise.

Three conditions must exist for galvanic corrosion to occur:

- electrochemically dissimilar metals must be present;

- the metals must be in electrical contact;

- the metals must be exposed to an electrolyte.

In the presence of a small hole, or cavity on the metal surface, usually resulting in the de-passivation of a small area, pitting corrosion develops. This area becomes anodic, while part of the remaining metal becomes cathodic, producing a localized galvanic reaction. The deterioration of this small area penetrates the metal and can lead to failure. This form of corrosion is often difficult to detect due to the fact that it is usually relatively small and may be covered and hidden by corrosion products.

Crevice corrosion refers to corrosion occurring in confined spaces to which the access of the working fluid from the environment is limited. These spaces are generally called crevices. Unlike pitting corrosion, the crevice corrosion is a delayed phenomenon that requires a relatively long incubation time. Its propagation is of the same nature as that of pitting corrosion, but its initiation depends on totally different mechanisms. In practice, the condition for crevice corrosion to occur is more difficult to satisfy than that for pitting corrosion.

Intergranular corrosion is a chemical or electrochemical attack on the grain boundaries of a metal. It often occurs due to impurities in the metal, which tend to be present in higher contents near grain boundaries. These boundaries can be more vulnerable to corrosion than the bulk of the metal.

Stress corrosion refers to the degradation of a given metal surface in an electrochemical fluid environment in which the metal is subjected to tensile forces in residual or direct form. Stress corrosion erodes the microscopic granular composition of a metal surface, often causing the surface to crack and disintegrate due to significant tensile stresses. Another comparable phenomenon is the corrosion fatigue, which refers to the mechanical degradation of a material under the simultaneous actions of corrosive environment and cyclic loading, leading to a significant decrease in fatigue strength.

1.2.2   Corrosion of copper

Copper may oxidise when in contact with a specific environment. By forming a thin passivation film on the surface, copper can protect itself from corrosion under appropriate conditions [18], hence its wide usage for roofing and for tubes carrying domestic and industrial water. This native oxide can limit the atomic transport of oxygen and copper. However, it is susceptible to more rapid attack in oxidizing acids, oxidizing heavy-metal salts, sulphur, ammonia, and some sulphur and ammonia compounds. For example, pitting

corrosion can occur in the presence of oxygen and some aggressive anions such as chloride and sulphate ions [19].
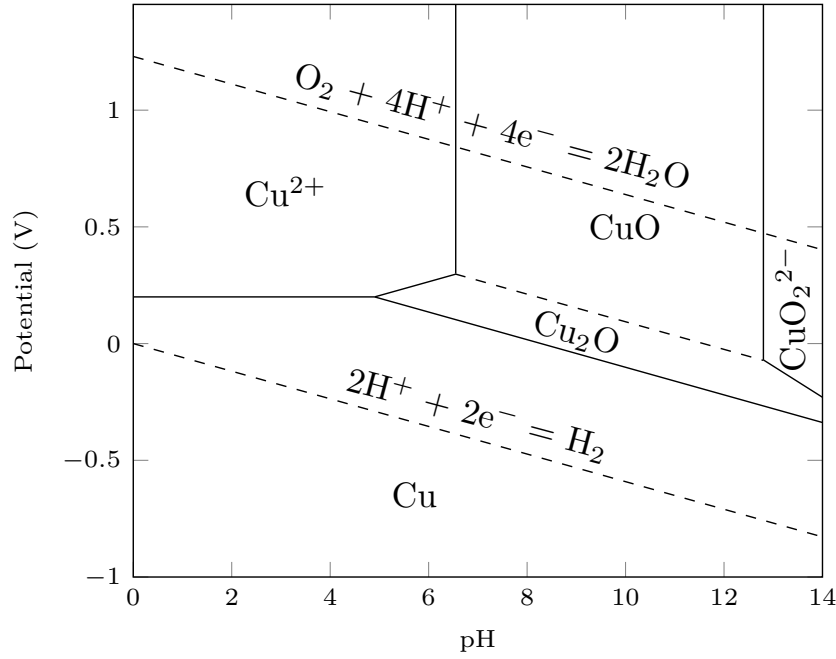
Figure 1.2: Eh-pH diagram of copper [20].

The potential-pH diagram presented in Fig. 1.2 shows the immunity and passivation domains in the water stability domain. Copper can oxidise when interacting with water:

$$2\,Cu + H_2O \longrightarrow Cu_2O + 2\,H^+ + 2\,e^- \tag{1.2.1}$$
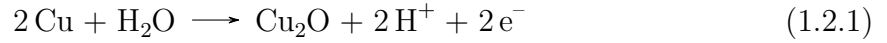
The protective passivating layers formed in neutral and alkaline media consist of either a single layer of Cu_2O oxide or a duplex layer of cuprous oxide Cu_2O and cupric oxide CuO. The formation of CuO oxide takes place only on a sufficiently thick Cu_2O layer. The potential-pH diagram shows that the passive film is stable and protective in neutral and alkaline environments when pH is between 6 and 14.

In acidic conditions, when pH is inferior to 5, copper oxide may dissolve by the following equations:

$$CuO + 2\,H^+ \longrightarrow Cu^{2+} + H_2O \tag{1.2.2}$$

$$CuO + H_2O \longrightarrow CuO_2{}^{2-} + 2\,H^+ \tag{1.2.3}$$
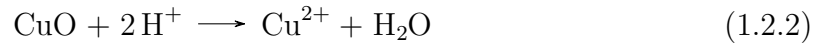
The presence of certain species and in particular chloride ions modifies the resistance of copper to corrosion by promoting the destruction of the passive film.

1.3 Corrosion protection

Different strategies can be employed in order to protect the material from corrosion, acting on the material itself and on the chemical environment, including:

- judicious choice of materials;

- use of coatings;

- adapted form of parts;

- electrochemical protection;

- addition of inhibitors to the corrosive environment.

These methods can be used individually or in combination.

Every metal or alloy has different composition, and thus is used in different environment. For example, the corrosion resistance of stainless steels is mainly due to the surface formation of a passive layer which appears naturally in air and which consists of a resistant chromium-rich oxide, of small thickness (about 2 nm at room temperature). These materials must therefore be used under conditions where they retain this passivity. Provided they have a homogeneous structure, stainless steels are widely used in aerated media or under oxidizing conditions such as nitric acid, organic acids (except formic and oxalic), and various aqueous solutions. On the other hand, their use should be avoided in the presence of hydracids (HCl, HBr, HF), even diluted, oxidizing chlorides (FeCl$_3$, CuCl$_2$), sea water (except cold sea water), and thiosulfates or chlorides plus oxygen in the presence of a stress.

Copper is resistant to corrosion in cold or hot freshwater, deaerated and diluted non-oxidizing acids. Its use should be avoided in the presence of oxidizing acids, ammonia and amines, high-speed circulation water (erosion-corrosion), hydrogen sulphide, sulphur and sulphides. Brasses are used for condenser tubes and cupronickels are sometimes used in pumping systems because they are less susceptible to erosion-corrosion.

The application of a paint coating is a cost-effective way to prevent corrosion. It is a method of corrosion mitigation by applying a thin protective layer on the surface of the materials, which allows for added protection of metal surfaces and acts as a barrier to prevent the contact with chemical compounds or corrosive materials and the transfer of electrochemical charge from the corrosive solution to the metal underneath, making the surface of the material inert in the medium. It is also possible to reduce the risk of corrosion by adapting the form of the objects to their working conditions, and thus significantly increase their lifetime.

Electrochemical protection is also an important way to protect copper. It acts in a controlled manner on the oxidation and reduction reactions that occur during the corrosion

phenomenon. This method consists in imposing on the metal to be protected a potential for which the attack speed becomes very low or even zero. There are two types of protection methods. The cathodic protection consists of lowering the electrode potential of the metal. Its principle has been known for a long time, since the first observations of this phenomenon by Sir H. Davy in 1824 [21]. It was found that when two different metals (Cu and Zn) immersed in a corrosive medium are electrically connected, the corrosion rate of one increases while that of the other decreases. Anodic protection, of more recent origin, is based on the passivation ability of the material in the medium considered. The corrosion of a metal surface is controlled by making it the anode of an electrochemical cell and controlling the electrode potential in a zone where the metal is passive. Anodic protection is used for example for carbon steel storage tanks.

Finally, it is possible to act on the environment with which the material is in contact, i.e. by the use of corrosion inhibitors. The major industries using corrosion inhibitors are oil and gas exploration and production, petroleum refining, chemical manufacturing, heavy manufacturing, water treatment, and product additive industries.

1.4 Corrosion inhibitors

1.4.1 Definition and properties

A corrosion inhibitor [22] is a chemical compound that is added in small quantities in the corrosive environment (liquid or gas) to slow down or even stop the corrosion process of a metal. Inhibitors are often easy to apply and offer the advantage of *in situ* application without causing any significant disruption to the system. Industrial applications have led to the treatments based on the use of corrosion inhibitors in various fields such as aeronautics, boilers, oil and refineries, and cooling systems.

There are several factors to be considered when choosing an inhibitor:

- cost of the inhibitor;

- toxicity of the inhibitor, ill effects should be avoided on human beings and other living species;

- availability of the inhibitor;

- environmental protection, inhibitor should be environment friendly.

A corrosion inhibitor must decrease the rate of corrosion of the metal without changing the physico-chemical characteristics of the latter. It must not only be stable in the presence of other constituents in the medium, but also not affect the stability of the species contained in this environment. An inhibitor is definitely stable at the temperature of usage and effective at low concentration. The inhibitor or reaction products of the inhibitor should

not form any dysfunctional deposits on the metal surface particularly at locations where heat transfer takes place. It can be used for permanent protection (primordial monitoring of the device) or more commonly for temporary protection: during a period when the part is particularly sensitive to corrosion (storage, stripping, cleaning, . . .) or when the part is subjected to very severe machining such as drilling, tapping, threading, etc.

Corrosion inhibitors may perform by:

- adsorbing themselves on the metallic surface by forming a film;

- reducing the anodic or cathodic current densities;

- reducing the movement or diffusion of ions to the metallic surface;

- increasing the electrical resistance of the metallic surface;

- interacting with the metallic surface or the environment near it.

A common mechanism for inhibiting corrosion involves formation of a coating, often a passivation layer, which prevents access of the corrosive substance to the metal.

The nature of the corrosive inhibitor depends on (i) the material being protected, which are most commonly metal objects, and (ii) on the corrosive agent(s) to be neutralized. The corrosive agents are generally oxygen, hydrogen sulphide, and carbon dioxide. Some corrosion inhibitors form a passivating coating on the surface by chemisorption. Benzotriazole is one such species used to protect copper. Volatile amines are used in boilers to minimize the effects of acid. Antiseptics are used to counter microbial corrosion. Orthophosphates may be added in water treatment systems to prevent leaching of lead and copper from pipes.

1.4.2   Types of inhibitors

Corrosion inhibitors can be classified according to several criteria:

- chemical nature: organic or inorganic (mineral) inhibitors;

- effect on electrochemical reactions: anodic, cathodic or mixed inhibitors. The corrosion inhibitor forms a barrier layer on the metal surface, which modifies the electrochemical reactions by blocking either the anodic sites or the cathodic sites;

- principle of protection on the surface. The following protection modes can be distinguished: adsorption, passivation, and precipitation.

Chemical nature

Organic inhibitors generally consist of by-products of the petroleum industry [23], which offer a broad field of application and are nowadays preferentially used because of their effectiveness in wide range of temperatures, compatibility with protected materials, good solubility in water, low costs and relatively low toxicity. Their effectiveness is directly related to their structure. Effective organic corrosion inhibitors have at least one active centre capable of exchanging electrons with the metal or interacting with the metal surface to form π or σ bonds, such as nitrogen, oxygen, phosphorus and sulphur [24]. The usual functional groups, allowing their fixation on the metal, are: the amino radical (–NH$_2$), the mercapto radical (–SH), the hydroxyl radical (–OH) and the carboxyl radical (–COOH).

Organic inhibitors can protect the metallic surface by forming insoluble complex salts at anodic defect sites by adsorption, thus forming a protective film. This process is not either purely physical or purely chemical adsorption. Concentration of corrosion inhibitors has a significant influence on the inhibitor efficiency. The corrosion rate decreases with increasing concentration. Organic inhibitors include azoles, amines, amino acids, calcium alkyl-aryl sulphonates, diamines, metal salts of dinonylnapathalene sulphonates, etc. They can be divided for some clusters with specific elements [25]:

- compounds containing nitrogen: amines, pyridine derivatives, quaternary ammonium salts, triazole derivatives, Schiff base, amino acids and indazole,

- compounds containing nitrogen and sulphur: imidazole derivatives, thiadiazole derivatives and thiazole derivatives,

- compounds containing sulphur: thiourea derivatives and sulphonates,

- compounds containing nitrogen and oxygen: oxazol derivatives, phtalimides and plant extracts/natural.

Certain halogen ions present in the organic inhibitors are known to inhibit corrosion to some extent in acid solutions. The efficiency of the corrosion inhibition is in the following order: $I^- > Br^- > Cl^-$. Fluoride does not show any inhibition characteristics. Synergism of halogen ions can be attributed to the fact that the metal adsorbs halogen ions whose charge shifts the surface in a negative direction, thereby increasing adsorption of the cationic organic inhibitor.

Besides the wide application of organic inhibitors, inorganic inhibitors are used based on the possibility of degradation of organic compounds with time and temperature. The mineral molecules are usually used in neutral to alkaline environment, but rarely in acidic media. The products dissociate in solution and it is their dissociation products (anions or cations) which ensure the inhibition [26]. Inorganic corrosion inhibitors, besides the oldest one, that is, molybdate anion, belong to calcium nitrite, rare earth metals salts,

zinc phosphate, chromates and lanthanide compounds. The main inhibiting anions are $XO_4{}^{n-}$ type oxo-anions such as chromates, molybdates, phosphates, silicates, etc. The cations are essentially Ca^{2+} and Zn^{2+} and those which form insoluble salts with certain anions such as hydroxyl OH^-. The number of molecules used now is going down because most of the effective products have a negative impact on the environment, for example, the toxicity of chromium (VI) oxidation state.

Electrochemical reactions

Anodic inhibitors, also called passivating inhibitors, generally in anionic form, slow down the rate of the anodic oxidation reaction by forming a protective oxide film on the surface of the metal, block the active sites on the metal surface and move the corrosion potential to positive values. Anode inhibitors should be used with caution. Indeed, if the protective film is damaged by scratching or dissolution, and if the amount of inhibitor is insufficient to restore the film, the exposed portion can corrode and form a deep sting. Some examples of such anodic inhibitors are chromates, nitrates, molybdates, and tungstate. The two former are oxidizing anions that can passivate steel in the absence of oxygen, and the two later are non-oxidizing ions that require the presence of oxygen to passivate steel.

Cathodic inhibitors either slow down the rate of the cathodic reaction of the oxidant (oxygen, or H^+ of water) or selectively precipitate on cathodic sites to limit the diffusion of reducing species to the metal surface and increase the surface impedance. The inhibiting action of cathodic inhibitors takes place by three mechanisms:

- cathodic poisoning: The cathodic reduction process is suppressed by impeding the recombination and discharge of hydrogen. Examples of cathodic poisons are compounds of arsenic and antimony. However, they can also increase the tendency of the metal to be susceptible to hydrogen induced cracking,

- cathodic precipitation: Compounds such as calcium, magnesium will precipitate as oxides to form a protective layer which acts as a barrier on the metal surface,

- oxygen scavenging: These compounds react with oxygen present in the system to form a product and reduce corrosion. For example, As^{3+} and Sb^{3+} on the dissolution of Fe in acids.

Mixed inhibitors act on both anodic and cathodic reactions. They are typically film forming compounds that cause the formation of precipitates on the surface blocking both anodic and cathodic sites indirectly. Mixed inhibitors are less dangerous than pure anodic inhibitors. The most commonly used mixed inhibitors are silicates and phosphates used in domestic water softeners to prevent the formation of rust water.

Protection principles

Inhibitors can slow down the corrosion precess by the formation of adsorbed molecular layers. These inhibitors are mainly organic molecules, whether natural or synthetic. They have at least one atom capable of exchanging electrons with the metal atom. These represent the most widely used class of inhibitors.

Two types of adsorption can be distinguished: physisorption and chemisorption. The first, also called physical adsorption, consists of three types of forces:

- the dispersion forces (Van der Waals, London) always present,

- the polar forces, resulting from the presence of an electric field,

- the hydrogen bonds due to hydroxyl or amine groups.

Naturally, the inhibitor must carry a global charge: positive ion, negative ion or dipolar molecule. The force of the electrostatic adsorption will be a function of the difference between the charges carried by the inhibitor on the one hand and by the metal surface on the other hand. The latter is itself a function of the difference between the corrosion potential of the metal and its zero charge potential in the considered corrosive medium.

Chemisorption, on the other hand, consists in the sharing of electrons between the polar part of the molecule and the metal surface, which gives rise to the formation of much more stable chemical bonds since they are based on higher binding energies. The electrons come for the most part from lone pairs of inhibitory molecules such as O, N, S, P, etc. (all these atoms being distinguished from others by their high electronegativity). Chemical adsorption has a significant influence on the distribution of the electronic charges of the adsorbed molecules, and is often thought as an irreversible mechanism.

Besides the corrosion inhibition via adsorption, some inhibitors cause passivation of the metal thus decreasing the rate of corrosion. These inhibitors are also considered as anode inhibitors. A passivating-type inhibitor produce local-action current which anodically polarizes a metal into the passive potential region and thereby provides the means for obtaining a noble mixed potential [27]. Other inhibitors cause the formation of superficial films by precipitation of poorly soluble complexes. Precipitation inducing inhibitors are film forming compounds that have a general action over the metal surface, blocking both anodic and cathodic sites indirectly. Hard water with high calcium and magnesium content is less corrosive than soft water because the salts in the hard water tend to precipitate on the surface of the metal and form a protective film. The most common inhibitors of this category are the silicates and the phosphates, very useful as non-toxic additives [28].

1.4.3 Corrosion inhibitors for copper

Copper corrosion can cause huge economic losses due to the wide applications of copper and copper alloys in the industrial, military and civilian fields, and thus it is particularly

important to find a way to limit that phenomenon. The use of corrosion inhibitor has been proven to be an effective approach to control the corrosion of metals and alloys which are in contact with aggressive environment [29–33].

It is commonly accepted that the corrosion inhibitors take effect through their interaction with the metal surface. The inhibition effect mainly depends on some physicochemical and electronic properties of the organic inhibitor, such as its functional groups, steric effects, the eigenvalues of the highest-occupied (HOMO) and lowest-unoccupied (LUMO) molecular orbitals, the HOMO–LUMO gap, chemical hardness, global softness, electronegativity, dipole moments, electronic density of donor atoms, and orbital character of donating electrons, etc. [34–38].

For each material it exists a family of inhibitors which are effective to limit the corrosion phenomena. Azole derivatives are very often used as corrosion inhibitors of copper and have a remarkable efficiency under certain conditions [3, 39, 40]. The azoles are a class of five-membered heterocyclic compounds containing a nitrogen atom and at least one other atom except the carbon as part of the ring. The presence of a pyridinic nitrogen atom in the azole compounds gives them the possibility to coordinate with other substances and in particular with the metal ions. This ability to complexation leads to interesting applications in corrosion inhibition of metals and alloys.

Benzotriazole (BTA) and its derivatives are the most widely used and effective corrosion inhibitors for copper. A great number of researches have been devoted to the understanding of the inhibition mechanisms of BTA on copper [4–14, 41, 42]. BTA is a heterocyclic compound containing three nitrogen atoms, with the chemical formula $C_6H_5N_3$ (Fig. 1.3). BTA has a remarkable efficiency for the protection against corrosion of copper and its alloys (bronze, brass, cupronickel ...). The use of BTA as a corrosion inhibitor for copper has
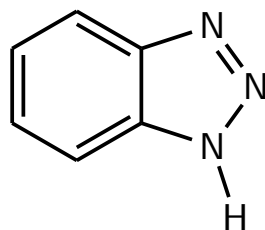
Figure 1.3: Chemical structure of benzotriazole.

been investigated since 1947 [29]. It has been found that in solution, BTA is chemisorbed on copper, with the formation of strong N–Cu chemical bonds and a polymeric Cu(I)-BTA complex that totally covers the copper surface, exhibiting strong corrosion inhibition [4–14, 38, 42].

The adsorption of BTA in vapour phase was also studied under UHV [9, 43], and a chemisorbed monolayer was formed firstly, with N bonded to copper, followed by physisorbed multilayers which were less stable and desorb at around 100°C. Data have
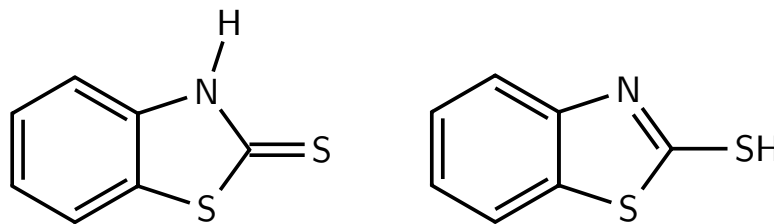
Figure 1.4: Thione (left) and thiol forms (right) of 2-MBT.

also been reported for vacuum evaporation [44, 45] of 1,4-benzenedimethanethiol (BDMT, $C_6H_4(CH_2SH)_2$) on Au(111), Au(110), Cu(100) and Cu(111) single crystal surfaces. The authors found that on Cu(100) and Cu(111) surfaces, which are more reactive than Au, BDMT dissociates in the initial stage of adsorption, resulting in atomic S adsorbed on the Cu surface. This phenomenon was not observed for the adsorption of benzotriazole on Cu(100) [46].

2-mercaptobenzothiazole

2-mercaptobenzothiazole (2-MBT) is also an effective copper corrosion inhibitor widely used in industry besides the well-studied BTA molecule [3, 19, 39, 40, 47–54]. Some works show that it is more effective than BTA [55–57]. 2-MBT is an organosulphur compound with chemical formula $C_7H_5NS_2$, and exists in two forms: the thione (NH) and the thiol (SH) forms, as shown in Fig. 1.4. The former has C double bonded to S, and the latter C double bonded to endocyclic N with hydrogen bonded to S. It is a yellow powder at normal pressure and room temperature.

It has been shown that 2-MBT is only in the thione form in gas phase [58]. The bond lengths and bond angles in the 2-MBT molecule have been determined [59], and by taking into consideration the van der Waals radii of different atoms, we can deduce its molecular dimensions, which gives 7.2 Å × 10.2 Å, as shown in Fig. 1.5.

The presence of nitrogen and sulphur in the organic molecule could improve its capacity as corrosion inhibitor by forming coordinative bonds with copper [3]. The mechanism of inhibition is influenced by the corrosion medium. With few exceptions [44, 45], experimental research concerning corrosion inhibitors have been done by immersion into solutions containing the organic compounds. In aqueous medium, 2-MBT dissolved in solution can react with copper to form a water-insoluble thin polymeric film of Cu(I)MBT which acts as a protective layer at the copper surface [51, 55, 60]. Woods et al. [53] claimed that 2-MBT is attached to the metal surface through interaction with the exocyclic sulphur, as well as the N atom [54, 61], but not by the endocyclic S atom. It was also suggested that 2-MBT adsorbs flat on Ag in the thiol form, while it adsorbs with molecular plane perpendicular on Au in thione form [62].
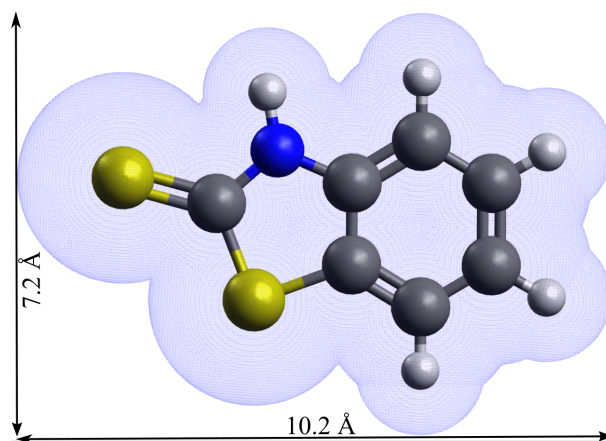
Figure 1.5: Molecular dimensions of the thione form of 2-MBT (the van der Waals surface is presented).
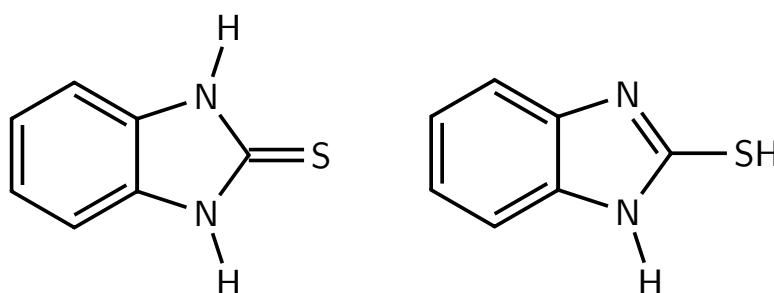
Figure 1.6: Thione (left) and thiol forms (right) of 2-MBI.

However, controversy exists on the chemical nature of the complex formed, as well as on the fundamental mechanisms of the inhibiting interaction. The resulting structures of the protective layer formed on copper are also still not clear. Most notably, the exact role of the surface oxide in the inhibiting function remains to be studied. In order to elucidate the interaction mechanisms, deposition of the molecule evaporated in vacuum could be more insightful, since it allows controlling each step of the deposition process in a well-defined environment and on a well-defined surface.

2-Mercaptobenzimidazole

Another widely used inhibitory molecule which is structurally related to 2-MBT is the 2-Mercaptobenzimidazole (2-MBI). It is an organic compound of the benzimidazole family of formula $C_7H_6N_2S$. 2-MBI is a white to beige powder at normal pressure and room temperature, and exists also in two forms: the thione and the thiol forms, as shown in Fig. 1.6. The former has C double bonded to S, and the latter C double bonded to endocyclic N with hydrogen bonded to S. The thione form is also the preferred form of 2-MBI in solid and gaseous phase [63, 64]. The bond lengths and angles in the 2-MBI molecule have been determined [64], and by taking into consideration the van der Waals radii of

different atoms, we can deduce its molecular dimensions, which gives 7.9 Å × 9.7 Å in the molecular plan, as shown in Fig. 1.7.
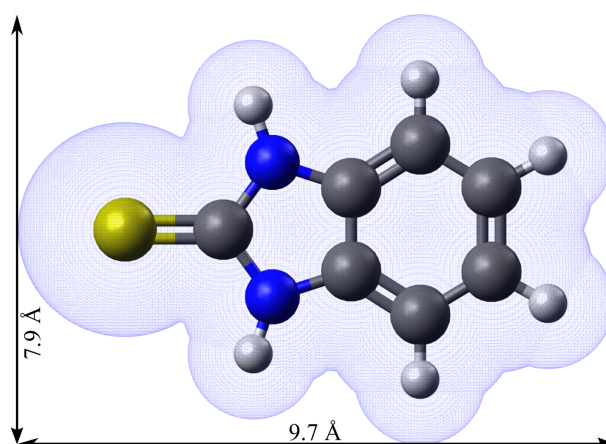
Figure 1.7: Molecular dimensions of the thione form of 2-MBI (the van der Waals surface is presented).

Research has been carried out mostly on the metal/solution interface [52, 65–71], indicating the chemisorption of 2-MBI on copper surface to form a polymeric film which can protect copper from further corrosion. There are two nitrogen atoms and one sulphur atom in the 2-MBI molecule, which can concurrently or individually bond to the metal surface [65, 72]. Finšgar et al. [69, 70] confirmed that 2-MBI molecules are bonded to Cu through their N and S atoms on the oxidized copper surface, forming a tilted position compared to the sample surface, as observed previously by Tooru [73]. Xue et al. [65, 67] reported that 2-MBI is bonded to metallic copper through sulphur atom and the chemisorption is accompanied by a cleavage of the C=S bond, not observed on oxidized copper surface. Hosseini et al. [74] investigated the adsorption of 2-MBI on a less reactive metal surface Au(111), and showed the formation of flat-lying molecules in the monolayer.

However, the molecular deposition by gaseous evaporation under UHV can still be used as an approach to understand the chemistry and strength of the molecule–surface interaction [37, 38]. Density functional theory studies suggest that 2-MBI neutral molecules in gaseous phase can chemisorb perpendicularly on the surface through N–Cu or S–Cu bond and physisorb almost parallel to the surface [37, 75]. Despite the numerous experimental and theoretical studies on copper corrosion inhibitors, the actual mechanism is not yet fully ascertained, neither the chemical nature of the resulting inhibitor films is completely established. The knowledge of the surface chemistry of organic corrosion inhibitors, as well as the mechanism of film formation, would help to elucidate the corrosion inhibition mechanisms.

In this study, the adsorption of the two structurally related corrosion inhibitors, 2-MBT and 2-MBI, on clean and pre-oxidized Cu(111) surfaces for which they are effective inhibitors, by gas evaporation under ultra-low pressure (ULP) in UHV systems was

investigated in order to better understand their interfacial corrosion inhibiting properties and the influence of the substitution of N–H by S in the same position in the heterocyclic compounds. The thermal stability of the adsorbed molecular layers was examined, and the corrosion inhibition efficiency of the adsorbed molecular layer on copper corrosion was studied.

CHAPTER 2

MATERIALS AND METHODS

2.1 Materials

Monocrystalline copper has a face-centred cubic (fcc) crystal structure with lattice parameter a of 0.3615 nm. Copper atoms are found at each corner and in the centre of each face of a cube as described in Fig. 2.1a. In this study, a high purity (99.999%) Cu(111) single crystal sample was used, i.e. the (111) surface of the copper crystal structure, with hexagonal arrangement, as indicated in yellow in Fig. 2.1b. The (111) surface of Cu is considered to be the most stable in terms of surface coordination. Based on the geometry of fcc structure, the lattice parameter of Cu(111) surface is $\frac{\sqrt{2}}{2}a$, which gives 2.556 Å.

(a)

(b)
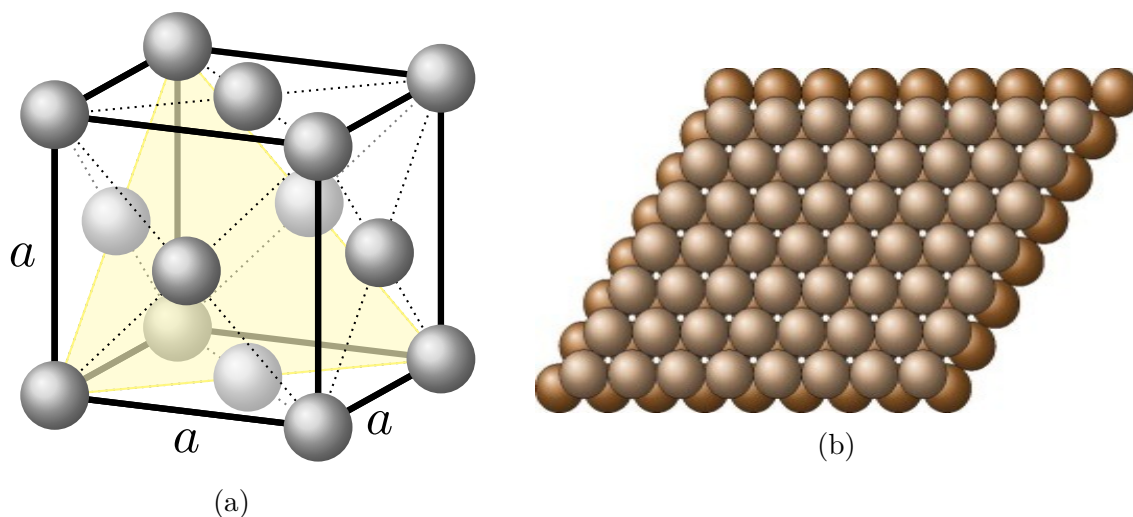
Figure 2.1: (a) fcc configuration of Cu; (b) crystallographic structure of Cu(111).

Two organic molecules with a similar molecular structure were investigated as corrosion inhibitors for copper: 2-MBT and 2-MBI. Both molecules were purchased from Sigma-Aldrich. As shown in Fig. 2.2, 2-MBT is a yellow crystalline powder at normal pressure and room temperature, with a purity higher than 99%, and 2-MBI is a white to beige powder with a purity higher than 98%. The solubility of these two molecules at room temperature

<center>(a)   (b)</center>
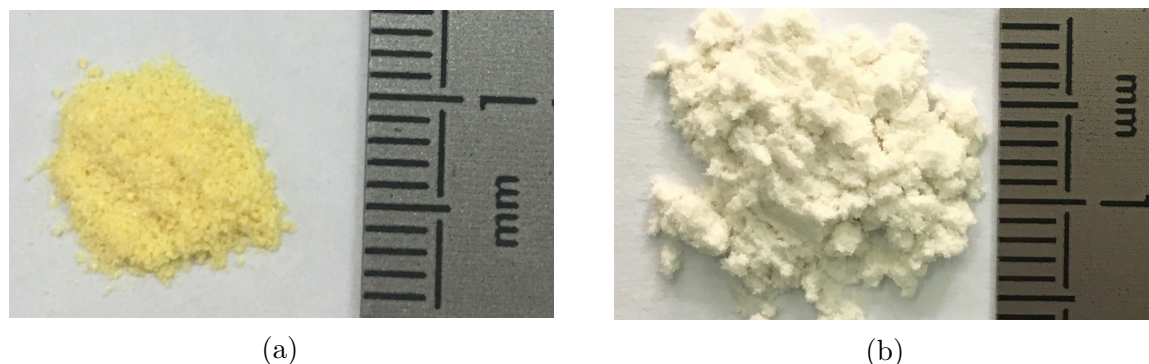
Figure 2.2: Powders at normal pressure and room temperature of (a) 2-MBT; (b) 2-MBI.

is relatively low, i.e. 118 mg/L and 450mg/L for 2-MBT and 2-MBI, respectively. These two compounds should be manipulated with caution. Skin contact may lead to sensitization. Eye contact can cause irritation. When heated to decomposition they emit very toxic fumes of sulphur oxides and nitrogen oxides [76].

2.2   Surface characterization techniques

In this work, experiments were carried out on three different UHV systems. One is equipped with a reactor for molecular deposition and Scanning Tunneling Microscopy (STM), Auger Electron Spectroscopy (AES) as well as Low Energy Electron Diffraction (LEED) for *in situ* characterization of sample surface, and is called STM system in the following text. Another is equipped with the same deposition reactor and X-ray photoelectron spectroscopy (XPS) as well as LEED for *in situ* analysis of the growth of inhibitors, and is called XPS system hereafter. Finally, a UHV platform equipped with STM, XPS and LEED was used to study the properties of the inhibitory layers after exposure to air, and is called plate-forme d'analyse et d'imagerie des surfaces (PAIS).

2.2.1   Scanning tunneling microscopy

Scanning Tunneling Microscopy (STM) is based on the concept of quantum tunneling, and is used to determine the morphology and density of states of conductive or semiconductive surfaces, with a spatial resolution that may be equal to or less than the size of an atom. With this resolution, the atoms on the sample surface can be imaged and manipulated individually.

   The STM was developed in 1981 by Gerd Binning and Heinrich Rohrer [77] who worked at I.B.M. research in Zurich, and this earned them the Nobel Prize in Physics in 1986. Although STM was developed in a 'post academic' context, it remains primarily of academic interest, especially in the domain of surface science. In less than five years, STM
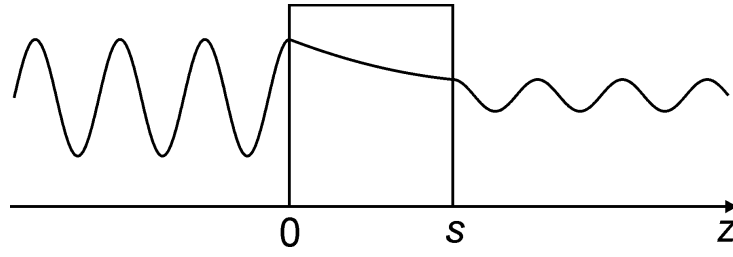
Figure 2.3: Quantum tunneling effect through a one-dimensional barrier.

developed from a difficult measurement performed in a handful of laboratories around the world into a widely accepted and used method of surface characterization.

Principle

Tunneling is often explained in terms of the wave–particle duality that a quantum object can be known as a particle with wave property. In the point of view of classical mechanics, surmounting a potential barrier requires enough potential energy. However, it is possible for a quantum object to cross a potential barrier even if its energy is lower than the classical minimum energy required to cross this barrier, as shown in Fig. 2.3. The probability depends on the accessible states on both sides of the barrier as well as on the spatial extension of the barrier.

In the one-dimensional case and for a barrier of rectangular potential, the probability of tunnel transmission T of a particle of mass m and of energy E through a barrier of height V_0 and of thickness s is given by:

$$T \approx \left(1 + \frac{(k^2 + \kappa^2)^2}{4k^2\kappa^2} \sinh^2(\kappa s)\right)^{-1} \tag{2.2.1}$$

with

$$\kappa = \sqrt{2m(V_0 - E)}/\hbar \tag{2.2.2}$$

where $\hbar$ is the reduced Planck's constant. If we consider a highly attenuating potential barrier ($\kappa s \gg 1$), then:

$$T \approx \frac{16k^2\kappa^2}{(k^2 + \kappa^2)^2} \, \mathrm{e}^{-2\kappa s} \tag{2.2.3}$$

The principle of STM is relatively simple: a conducting tip scans a sample surface, as shown in Fig. 2.4. The tip, consisting for example of W, Au, Rh/Ir or Pt/Ir, is very sharp and its end is terminated ideally by a single atom. A bias is applied to the tip. The distance between the tip and the sample surface is adjusted until a tunneling current is measured. The tip scans the surface to be characterized and a computer adjusts (via a feedback loop) in real time the height of the tip to maintain a constant current (in constant current mode) and records this height which allows to reconstruct the surface topography. It is also possible to keep a constant height and records the variation of tunnel current.
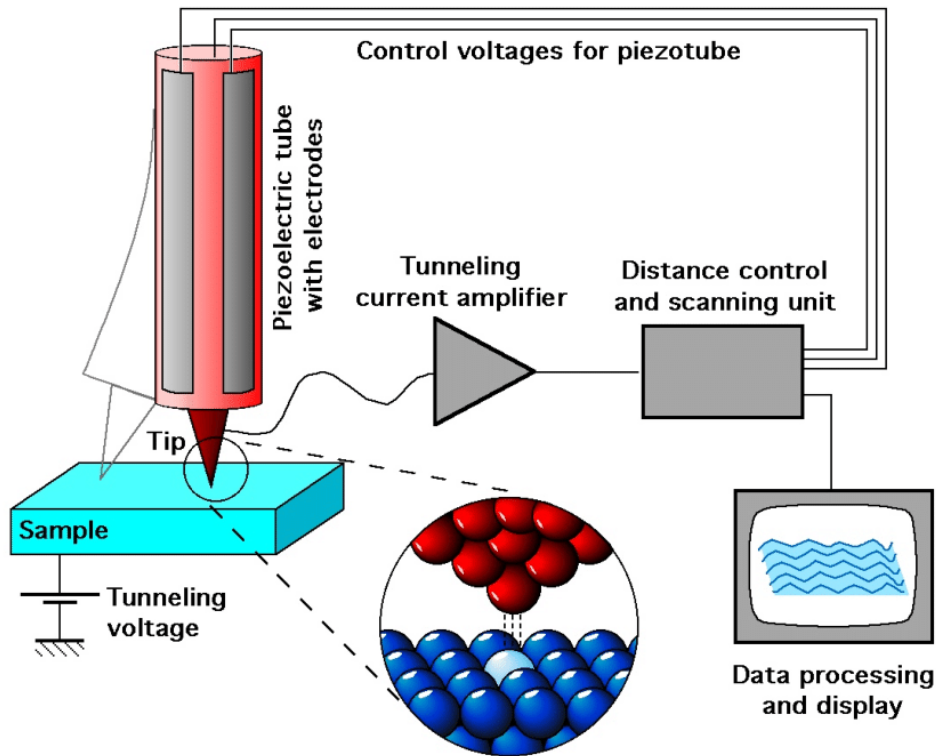
Figure 2.4: Schematic representation of the working principle of STM [78].

This equipment is extremely sensitive because of the exponential variation of the tunneling current with the tip-sample distance (equ. 2.2.3).

Instrumentation

Although simple in conception, several problems had to be solved before invention of STM. Firstly, we need to control precisely the tip's location and movement. Secondly we have to control the vibration. Finally, we need to make a tip with the necessary atomic sharpness.

Piezoelectric ceramics were proven to be the answer for the first problem. It allows control of the tip position thanks to the sensitivity of the piezoelectric elements, more precisely, it allows us to scan the tip with picometre-level control.

The piezoelectric effect was discovered by brothers Pierre and Jacques Curie in 1880. It refers to the generation of an electric charge when applying mechanical stress to certain materials. Reversibly, a piezoelectric material changes its length when an electric field is applied. Both natural and artificial materials exhibit piezoelectric effects, including cane sugar, quartz, Rochelle salt, topaz, tourmaline, and bone (dry bone exhibits some piezoelectric properties due to the apatite crystals, and the piezoelectric effect is generally thought to act as a biological force sensor). An example of man-made piezoelectric materials includes barium titanate and lead zirconate titanate.

Since STM is a sensitive technique with a resolution at atomic scale, it can be disturbed by internal and external vibrations. Early STMs were operated at night in order to reduce

the influence of environmental vibration. Vibration also can be reduced by making the instrument with sufficient mechanical rigidity and through an appropriate configuration of the piezoelectric transducers. STMs operating in air or in solution are often hung on a double bungee cord sling to damp vibration. Further vibration isolation systems have also been made with springs and frames for UHV measurements [79].

Finally, it is very important to make a tip with sufficient sharpness. We explained previously that in the ideal case, a tip only has one atom at its end. However, it is composed of a cluster of atoms in the reality. What is crucial is that one edge of this cluster be sufficiently higher than all the others and itself is atomically sharp, then it can serve as the apex through which the tunneling current passes.

STM can be a complicated and challenging technique. Firstly, the experimental conditions needed to obtain an image of high resolution are difficult to reach, and they are not necessarily reproducible. The STM measurement depends on numerous factors, such as the temperature, non linear piezoelectric effects, drift, depolarization, the electronic state of the tip and sample surface, etc. Secondly, the images that we obtain do not represent the real topography of the sample surfaces and some interpretations are needed. The information obtained depends on many parameters, such as the bias voltage of the sample, the electronic structure of the sample, the state of the tip, etc. It should thus be analysed with a lot of precautions. Especially, STM image calibration is needed.
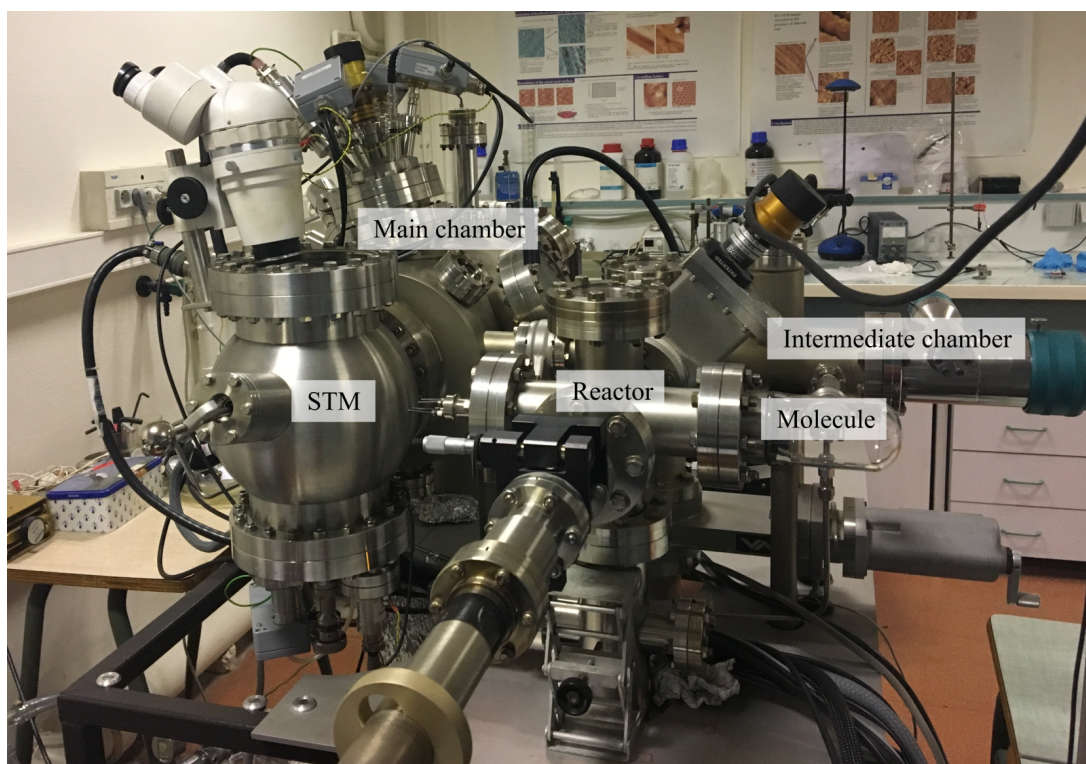
Figure 2.5: Photo of the STM system.

Our STM system for *in situ* characterization is mainly composed of three chambers: a main chamber, an intermediate chamber and a reactor, as shown in Fig. 2.5. Each chamber is separated by a valve.

The main chamber is used for the preparation and characterization of the sample surface. It is equipped with an Ar^+ sputtering gun. Annealing is carried out by filament resistive heating. It is also equipped with AES, LEED and STM for the characterization of the sample surface. An intermediate chamber is used for sample introduction from atmospheric conditions and transfer to the two other chambers. A reactor is designed for molecular deposition. The main chamber is connected to an ionic pump and a Ti sublimator, and the base pressure is 10^{-10} mbar. The intermediate chamber and the reactor are connected each to a pumping system, composed of a turbo pump and a primary pump. The pumping system works continuously to keep the low pressure in these chambers.

(a)   (b)
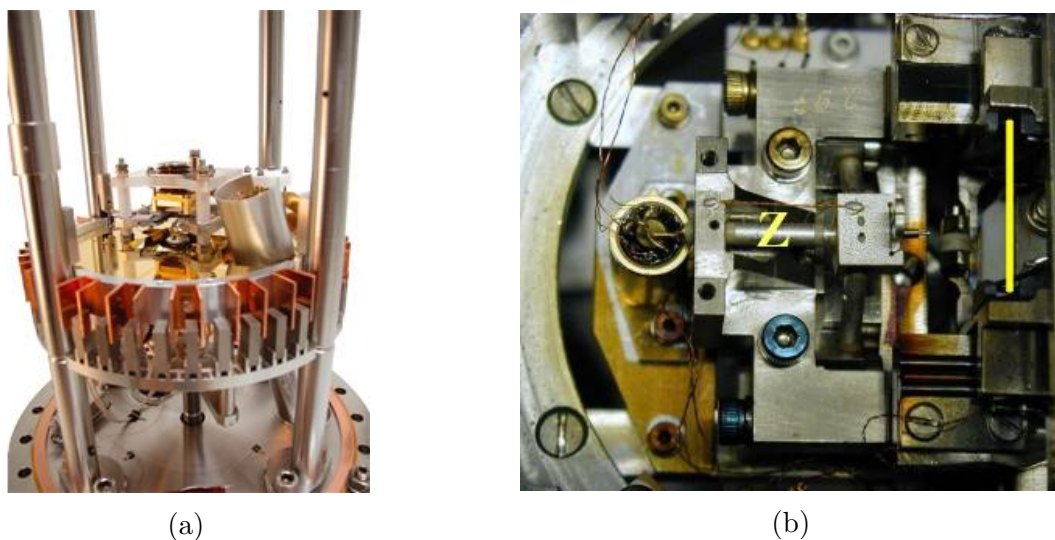
Figure 2.6: Photo of STM unit configuration (a) side view; (b) top view.

The STM used is STM1 with SCALA system from Scienta Omicron, as shown in Fig. 2.6. It is connected to an isolation system in order to avoid the influence of vibration. The STM is suspended in the main chamber using four springs with eddy current dampers. The probe tip is placed in front of the sample, and it is attached to a piezodrive, which consists of three mutually perpendicular piezoelectric transducers for displacement in three directions with very high precision. The STM unit is installed in the main chamber of the UHV system in order to avoid the contamination on the sample surface.

Another STM used is in the PAIS system (Fig. 2.7). PAIS is a UHV system composed of four chambers: an introduction chamber, a preparation chamber and two analysis chambers for STM and XPS analysis, respectively. The system is pumped continuously to keep a UHV environment, with a base pressure of $\sim 10^{-11}$ mbar. The preparation chamber is equipped with an Ar^+ gun and an annealing system with a thermocouple for control of the temperature. The STM used is VT STM XA from Scienta Omicron.
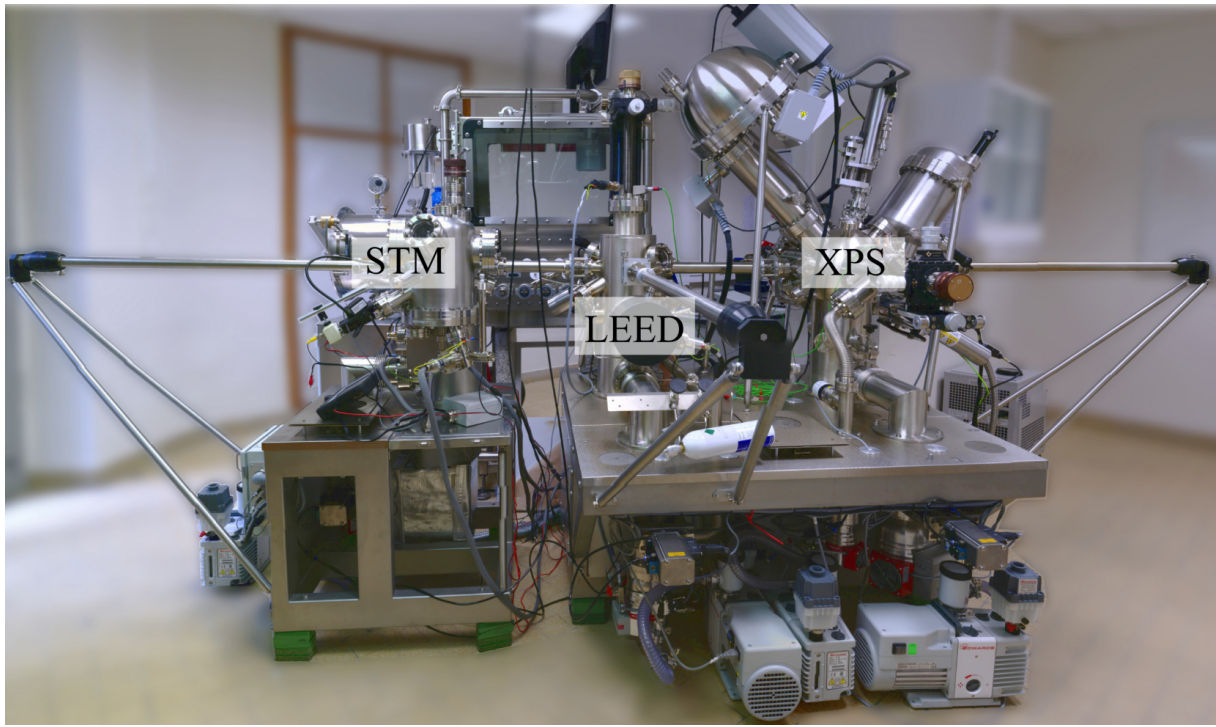
Figure 2.7: Photo of the PAIS system.

STM characterization

Before starting STM measurement, the first step is to prepare a tip. The size, shape and cleanliness of a tip is very important for STM resolution. W tips are frequently used for UHV experiments. The tip is cut from a piece of tungsten wire, and prepared by electrochemical attack in NaOH solution. Then the tip is introduced in UHV where it can be sputtered and annealed for tip cleaning if necessary. Further preparation of the tip is possible in UHV system by voltage pulses. Rapid sweeps on the edges of the steps and voltage scans of a few volts can also improve the quality of the tip.

For STM measurement, we move firstly the sample to approach the tip with a manual controlled stepper motor until a tip-sample distance of the order of 0.1 mm. Then automatic approach is applied by imposing a setpoint of voltage and tunnel current, the position of the tip is controlled by the piezodrive until the setpoint is reached. During STM measurement, we can increase the distance between the tip and sample by increasing the voltage and/or decreasing the tunnel current and vice versa.

The STM characterization was carried out at room temperature and in constant current mode. Image processing was performed using WSxM software (5.0 Develop 9.1) [80]. No filtering was applied except when mentioned and all images were corrected by plane subtraction.
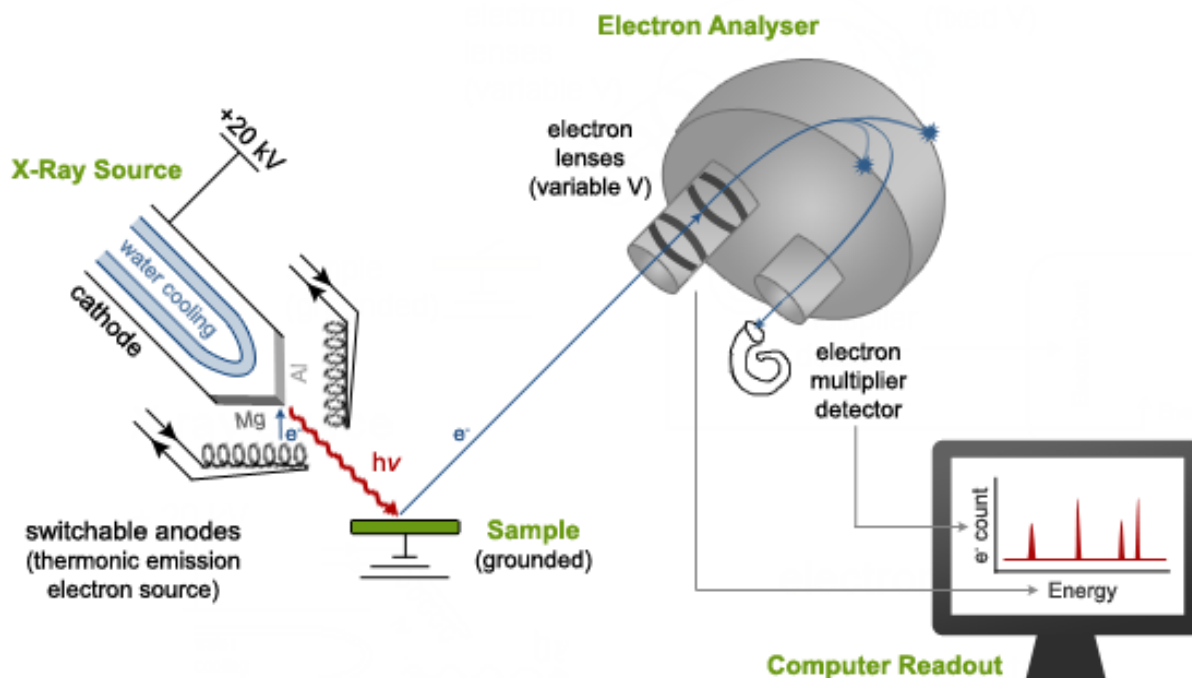
Figure 2.8: Schema of the working principle of XPS [81].

2.2.2 X-ray photoelectron spectroscopy

X-ray photoelectron spectroscopy (XPS) is a quantitative spectroscopic technique that measures the elemental composition and chemical state of the elements present on the surface of a material.

Principle

An X-ray source is used which can produce photons of a certain energy depending on the type of source used. The photons are then directed to the sample surface to be characterized, photoelectrons are thus produced by photoelectric effect and detected. The kinetic energy and the number of electrons that escape from the sample surface are analysed. Since the kinetic energy is characteristic of each element and the number of electrons detected is directly related to the concentration of element within the XPS sampling volume, this technique is proven to be qualitative and quantitative. The schema of the XPS measurement is shown in Fig. 2.8

In order to avoid surface contaminations and ensure free flight of the photoelectrons, UHV conditions are needed and the pressure in the chamber is kept at 10^{-10} mbar in normal operating conditions. Also, the electrons have to escape into the vacuum, meaning that they originate from a limited depth of the sample (0–10 nm). All the photoelectrons emitted from deeper regions of the sample cannot escape from the material without losing some energy. The intensity of the signals depends also on the collection angle of photoelectrons. For normal emission, electrons emitted from sub-surface can be more easily
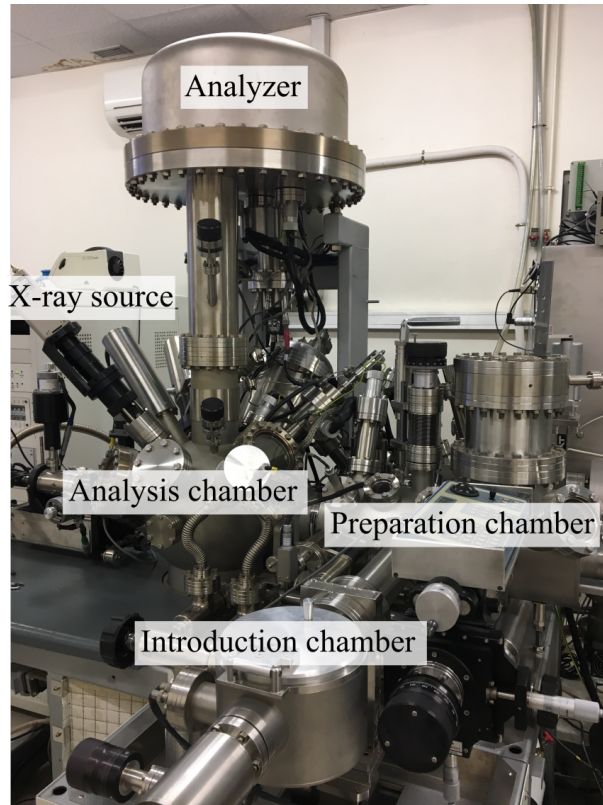
Figure 2.9: Photo of the XPS system.

detected, while for a grazing emission angle, the XPS measurements are more sensitive to surface. Angle-resolved measurements can be performed to obtain information about the chemical composition and the thickness of thin surface films. For thick films, the use of ion sputtering allows to determine in-depth composition profiles as well as film thickness.

Knowing the energy of the incident photons $h\nu$ (h is the Planck constant and ν the radiation frequency), the binding energy of emitted electrons can be determined from their measured kinetic energy, and the relation is given by the following equation:

$$E_b = h\nu - E_k - \phi \qquad (2.2.4)$$

where E_b is the binding energy of the electron, E_k is the kinetic energy of the photoelectrons as measured by XPS, and ϕ the work function dependent on the spectrometer. The work function term ϕ is an adjustable instrumental correction factor.

Instrumentation

In this work, the equipments used are ESCALAB 250 from Thermo Electron Coporation in the XPS system (Fig. 2.9) and ARGUS from Scienta Omicron (Fig. 2.7). The XPS system is mainly composed of an introduction chamber, a preparation chamber and an analysis chamber. The introduction chamber allows the sample transfer from ambient pressure. The preparation chamber is equipped with an Ar^+ gun to clean the sample surface by

ion sputtering. Annealing is performed by heating the filament in the sample holder, and the temperature is measured by a thermocouple connected to sample. Once the sample prepared, it was transferred to the analysis chamber for XPS characterization. The XPS equipment is connected to pumping systems allowing to keep a UHV environment. The base pressure of the UHV system is 10^{-10} mbar. Moreover, a vacuum sealed glass tube for molecular deposition is connected to the preparation chamber of the UHV platform.

XPS analysis

For the analysis of XPS, the sample was placed in front of the photon source and the electron analyser. Two geometries were employed. In order to investigate the elements presented deeper in the surface, the angle between the sample surface and the analyser was fixed to 90° to have a normal emission angle. In order to characterize the first few layers of the sample surface, a take-off angle of 45° was also used in the PAIS system to have a more grazing emission angle.

The photon source used in these two systems was a monochromatic Al K_α X-rays source which can produce monoenergetic photons ($h\nu = 1486.6$ eV). The photoelectrons were filtered through a rectangular slit in the XPS system and a round slit in the PAIS system before entry in the electron analyser. In our experiment, a hemispherical electron energy analyser is used to have a high resolution. It consists of two concentric hemispherical electrodes (inner and outer hemispheres) held at proper voltages, the difference of potential applied to the two electrodes can change the path of electrons, and only electrons with a specific energy can pass through the analyser to arrive at the detector. The transmission of analyser was calibrated by measurement of reference samples. In the XPS system, the survey spectra were recorded with a pass energy of 100 eV corresponding to an overall resolution of 1.8 eV, the high resolution spectra were recorded with a pass energy of 20 eV corresponding to an overall resolution of 360 meV. While in the PAIS system, pass energies of 50 eV and 20 eV was used for survey spectra and high resolution spectra, respectively. The data processing was carried out using the CasaXPS software (version 2.3.19) [82].

Quantitative measurement

The differential intensity $\mathrm{d}I_X^M$ emitted by an element X in a matrix M decreases exponentially with the depth (z) according to the following equation:

$$\mathrm{d}I_X^M = kFSN_X^M \sigma_X T_X \exp\left(-\frac{z}{\lambda_X^M \sin\theta}\right)\mathrm{d}z \qquad (2.2.5)$$

where k is a constant which is characteristic of the equipment used, F the photon flux (constant), S the area of the analysed zone, N_X^M the density of emitting atoms X in the matrix M, σ_X the photoionization cross section of element X, T_X transmission of the
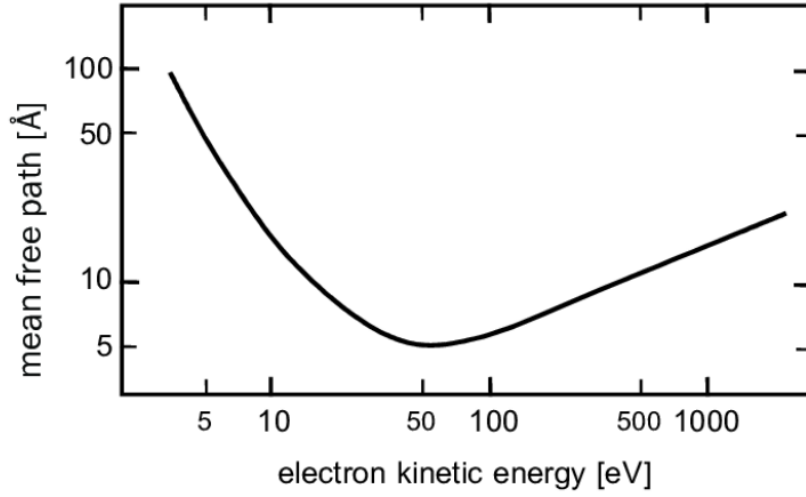
Figure 2.10: Inelastic mean free path of electrons in solids [84].

analyser depending on the kinetic energy of the analysed electron from element X, λ_X^M the inelastic mean free path of emitted electrons from element X in the matrix M, estimated using the Tanuma, Powell and Penn formula (TPP-2M) [83], and θ the take-off angle of photoelectrons. Note that the mean free path corresponds to the average distance travelled by a photoelectron between two inelastic collisions. It depends on the kinetic energy of the electron and the nature of the material, and can roughly be described by a universal curve (Fig. 2.10). The mean free path is very long at low energies, fall to 0.1–0.8 nm for energies in the range 30–100 eV and then rise again as the energy increases further.

The interval of integral depends on the model used. For example, in the case of a metallic surface covered by a homogeneous layer of thickness d, we can consider that the thickness of the metallic substrate is infinite. Then the peak intensities of element X in metallic substrate and upper layer can be given as follows:

$$I_X^d = kFSN_X^d \sigma_X T_X \lambda_X^d \sin\theta \left[1 - \exp\left(-\frac{d}{\lambda_X^d \sin\theta} \right) \right] \tag{2.2.6}$$

$$I_X^{\text{Metal}} = kFSN_X^{\text{Metal}} \sigma_X T_X \lambda_X^{\text{Metal}} \sin\theta \exp\left(-\frac{d}{\lambda_X^d \sin\theta} \right) \tag{2.2.7}$$

From the above equations, we can deduce the thickness of the upper layer, which is given by:

$$d = \lambda_X^d \sin\theta \ln\left(1 + \frac{I_X^d N_X^{\text{Metal}} \lambda_X^{\text{Metal}}}{I_X^{\text{Metal}} N_X^d \lambda_X^d} \right) \tag{2.2.8}$$

In the case of a sample surface covered by two different layers of thickness d_1 and d_2, with d_2 in contact with the metallic surface, integral of eq. (2.2.5) gives:

$$I_X^{d_1} = kFSN_X^{d_1} \sigma_X T_X \lambda_X^{d_1} \sin\theta \left[1 - \exp\left(-\frac{d_1}{\lambda_X^{d_1} \sin\theta} \right) \right] \tag{2.2.9}$$
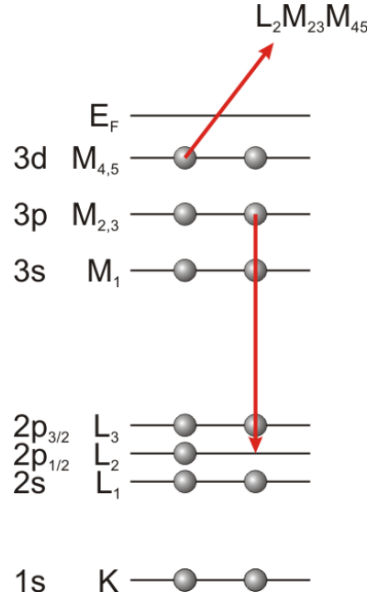
Figure 2.11: Schematic representation of Auger effect.

$$I_X^{d_2} = kFSN_X^{d_2}\sigma_X T_X \lambda_X^{d_2} \sin\theta \left[1 - \exp\left(-\frac{d_2}{\lambda_X^{d_2}\sin\theta}\right)\right]\exp\left(-\frac{d_1}{\lambda_X^{d_1}\sin\theta}\right) \qquad (2.2.10)$$

$$I_X^{\text{Metal}} = kFSN_X^{\text{Metal}}\sigma_X T_X \lambda_X^{\text{Metal}} \sin\theta \exp\left(-\frac{d_1}{\lambda_X^{d_1}\sin\theta}\right)\exp\left(-\frac{d_2}{\lambda_X^{d_2}\sin\theta}\right) \qquad (2.2.11)$$

2.2.3   Auger electron spectroscopy

Auger Electron Spectroscopy (AES) is a widely used analytical technique to investigate the surface composition. It is based on a physical phenomenon called the Auger effect, which is schematically represented in Fig. 2.11.

When an atom is ionized, i.e. an electron is removed from its core level, leaving a vacancy, an electron from a higher energy level may fill the vacancy, resulting in a release of energy (which equals to the difference of energy between these two energy levels). This energy can be released either by emitting a photon by fluorescence, or it can also be transferred to another electron, which can be ejected from the atom. This second ejected electron is called an Auger electron. The Auger effect was first discovered in 1923 by Lise Meitner and later independently discovered once again in 1925 by Pierre Auger [85].

For the AES measurement, the sample surface is bombarded by an electron beam, and the Auger electrons are collected and analysed. The kinetic energy of the Auger electrons is characteristic of the energy of atomic levels of analysed sample surface and is independent of the energy of the incident beam. So by measuring the Auger electron energies, as well as the shape of an Auger peak, we can obtain information on the chemical environment of the sample surface. This technique is routinely used to verify the cleanness of the sample surface. Since the intensity of the Auger spectrum is proportional to the

number of atoms present in the sample, AES can also be used to determine the relative proportion of different elements.

AES is a standard surface analysis technique which is extremely reliable and reproducible. It can provide information on the surface concentration of different elements, and it is only surface sensitive. As for photoelectrons if Auger electrons undergo inelastic scattering, the kinetic energies of the electrons will be less than that of the expected Auger electrons. Therefore, only the Auger electrons originating from the top surface can escape the sample surface without energy loss.

However, in-depth information can be provided using an inert gas ion gun (normally Argon) to sputter off the surface layers. Alternating sputtering and AES spectral acquisition can give chemical depth profiles down to depths of about 1 μm into the bulk. Moreover, by using a field emission gun, information on the chemical imaging can also be obtained, this is called Scanning Auger Microscopy (SAM). Surface chemical maps can be collected with lateral resolutions down to few nanometers.

AES measurement

The AES equipment used in this work is CMA-100 model from Scienta Omicron. It is installed in the main chamber of the STM system. For AES measurement, the sample is moved to be in front of the electron gun. Electron beam is generated by passing a current in a filament, the energy of the electron beam is 3 keV. Auger electrons are emitted from the sample and are detected and analysed. In order to avoid the contamination of the sample surface by the degassing of the filament, the sample is only turned to direction in front of the electron source when the sample current exceeds 2 μA. Reference spectra are often used for identification of the elements present on the surface.

2.2.4   Low-energy electron diffraction

Low-Energy Electron Diffraction (LEED) is a technique for the determination of the surface structure of single-crystalline materials. For the LEED measurement, a collimated low-energy electron beam (typically in the range 20–200 eV) is produced by an electron gun and is directed to the sample surface to be characterized. An electron gun is composed of a cathode filament and a set of electrodes serving as electron lenses. According to the principles of wave-particle duality, the electrons can be considered as electron waves. The energy of the electron beam is adjusted so that its associated wavelength is comparable to atomic spacings, this is the necessary condition for carrying out diffraction experiments on monocrystalline surfaces.

When the electron beam arrives at the sample surface, some of the incident electrons are backscattered elastically, and diffraction can be detected if sufficient order exists on the surface. Only the elastically-scattered electrons contribute to the diffraction pattern;
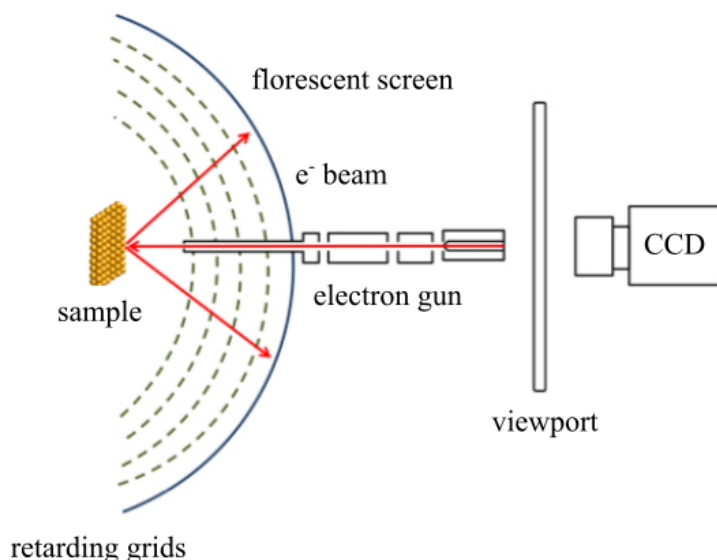
Figure 2.12: Schematic representation of the working principle of LEED [86].

the lower energy (secondary) electrons are removed by energy-filtering grids placed in front of the fluorescent screen that is employed to display the pattern. The experimental setup is shown in Fig. 2.12.

The diffraction pattern is an image of the reciprocal lattice of the surface, it provides information on the periodicity of the surface structure. The existence of symmetrically equivalent domains should also be considered when analysing LEED pattern.

LEED may be used in one of two ways:

- Qualitatively: where the diffraction pattern is recorded and analysis of the spot positions yields information on the size, symmetry and rotational alignment of the superstructure unit cell with respect to the substrate unit cell.

- Quantitatively: where the intensities of the various diffracted beams are recorded as a function of the incident electron beam energy to generate so-called *I-V* curves which, by comparison with theoretical curves, may provide accurate information on atomic positions.

LEED measurement

In this work, three LEED equipments were used. Two are model SpectaLEED from Scienta Omicron, as shown in Fig. 2.13. They are installed in the main chamber of the STM system and in the preparation chamber of the PAIS system. Another is Rear View LEED from Thermo VG Scientific. It is installed in the preparation chamber of the XPS system.

Similarly as for AES, an electron beam is generated by passing a current in a filament. The sample is turned to the direction in front of the LEED screen when the emission current exceeds 0.1 mA.

Figure 2.13: SpectaLEED Scienta Omicron.

2.3 Surface preparation

2.3.1 Cleaning of copper surface

The sample used in this work is a high purity (99.999%) Cu(111) single crystal. In order to prepare a clean and flat copper surface, the sample was firstly mechanically polished from 6 to 1/4 μm by using a diamond paste, and abundantly rinsed with water between each step to eliminate the diamond particles from the previous step. Then it was successively rinsed with acetone, ethanol, and ultra pure (UP) water (resistivity > 18 MΩ·cm). After that the sample was electropolished in 60 wt% H_3PO_4 solution at 1.4 V during 5 min, followed by rinsing with 10 wt% H_3PO_4 solution and UP water to improve the surface finish. Then the sample was annealed under continuous H_2 flow at 725°C during 20 h to reconstruct and recrystallize the surface before introduction in the UHV system.

The sample was further prepared under UHV in the STM system by cycles of ion sputtering and annealing. Ar$^+$ ion sputtering was performed at 600 V and 20 mA of emission current under pressure of 1×10^{-5} mbar during 30 min. Then, in order to eliminate the defect created during the ion sputtering, and to reorganize the sample surface, thermal annealing was performed. The sample was heated progressively until 600°C, and it was kept at 600°C during 30 min. The increase of temperature should be controlled with caution to avoid too important degassing in a short time. Similarly, in XPS system, ion sputtering ($P_{\mathrm{Ar}} = 5 \times 10^{-6}$ mbar, 600 V, 10 mA, 10 min) and annealing (600°C, 10 min) were repeated in order to obtain a clean and well-structured surface.

The surface was systematically checked by AES, XPS, LEED and STM until no contamination was detected in the AES and XPS spectra and a good surface organization

was observed, characterized by a sharp (1×1) LEED pattern and a topography with large and flat terraces as verified by STM. Usually several cycles of sputtering and annealing are needed before getting a clean surface.

2.3.2 Pre-oxidation

In order to study the influence of pre-oxidation on the adsorption of molecules, a pre-oxidized copper surface was prepared under UHV. Oxygen was introduced through a leak valve, and the oxygen partial pressure was kept below 10^{-5} mbar. Before the introduction of oxygen, the ion pump should be shut down at first. In this work, oxidation was carried out at $P_{O_2} = 5 \times 10^{-6}$ mbar and room temperature until saturation. In these conditions, a 2D surface oxide is obtained [87].

2.3.3 Inhibitor deposition

For the deposition of molecules, the inhibitors were placed in a vacuum sealed glass connected directly to the reactor of the UHV systems. The vapor pressure of 2-MBT in the reactor was 2×10^{-9} mbar at room temperature, and that of 2-MBI was 1×10^{-9} mbar at room temperature. The molecular exposure was calculated by multiplying the pressure of 2-MBT by the dosing time (1 L = 10^{-6} torr s). The sample was transferred to the reactor in STM system and to the preparation chamber in XPS system for molecular deposition. A heating system is available in the reactor for high temperature deposition.

CHAPTER 3

2-MBT DEPOSITION ON PRISTINE AND PRE-OXIDIZED Cu(111) SURFACES AT ROOM TEMPERATURE: XPS ANALYSIS

3.1 Abstract

Adsorption of 2-mercaptobenzothiazole (2-MBT) at ultra-low pressure and room temperature on metallic and pre-oxidized Cu(111) surfaces and its thermal stability were investigated using X-ray photoelectron spectroscopy in order to better understand the interfacial corrosion inhibiting properties. 2-MBT is lying flat in the monolayer with two sulphur atoms bonded to Cu and decomposes partially yielding atomic sulphur when interacting with metallic copper prior to forming molecular multilayers. Decomposition is prevented by surface pre-oxidation with 2D oxide dissociation accelerating the 2-MBT initial adsorption kinetics. 2-MBT further decomposes and partially desorbs above 100°C. A pre-adsorbed 2-MBT monolayer on metallic copper inhibits surface corrosion.

3.2 Introduction

Copper is widely used in various applications for its excellent thermal and electrical properties, however it is not immune against corrosion. The use of corrosion inhibitors is considered as an effective way to protect copper [3, 19, 39, 40, 47, 48]. The most studied compound is benzotriazole [4–14, 42], but there are also other nitrogen and/or sulphur

heterocyclic compounds of interest, especially 2-mercaptobenzothiazole (2-MBT) [49–54]. The presence of nitrogen and sulphur in the organic molecule could improve its capacity as corrosion inhibitor by forming coordinative bonds with copper [3]. It has been shown that 2-MBT dissolved in solution can react with copper to form a complex which acts as a protective layer at the copper surface [51]. However, controversy exists on the chemical nature of the complex formed, as well as on the fundamental mechanisms of the inhibiting interaction. The resulting structures of the protective layer formed on copper are also still not clear. Most notably, the exact role of the surface oxide in the inhibiting function remains to be studied.

With few exceptions [9], experimental research concerning corrosion inhibitors have been done by immersion into solutions containing the organic compounds [4–14, 42, 49–54]. However, in order to elucidate the interaction mechanisms, deposition of the molecule evaporated in vacuum could be more insightful, since it allows controlling each step of the deposition process in a well-defined environment and on a well-defined surface. Data have been reported for vacuum evaporation [44, 45] of 1,4-benzenedimethanethiol (BDMT) on Au(111), Au(110), Cu(100) and Cu(111) single crystal surfaces. The authors found that on Cu(100) and Cu(111) surfaces, which are more reactive, BDMT dissociates in the initial stage of adsorption, resulting in atomic S adsorbed on the Cu surface. This phenomenon was not observed for the adsorption of benzotriazole on Cu(100) [46].

In this work, the adsorption of 2-MBT at ultra-low pressure (ULP) and room temperature on clean and pre-oxidized Cu(111) surfaces and its effect on the oxidation of copper were investigated using ultra-high vacuum (UHV) spectroscopic techniques. The results were compared to those obtained for ULP deposition on the oxide-covered Cu(111) surface prepared in air. The thermal stability of the adsorbed molecular layer under UHV was also studied. This work brings new insight into the interaction of 2-MBT with copper, which allow us to better understand its corrosion inhibition mechanisms.

3.3   Material and methods

A high purity (99.999%) Cu(111) single-crystal was used in this work. The surface was mechanically polished to $1/4$ μm (diamond paste), successively rinsed with acetone, ethanol, and ultra pure (UP) water (resistivity > 18 MΩ·cm), and then electropolished in 60 wt% H_3PO_4 solution at 1.4 V during 5 min, followed by rinsing with 10 wt% H_3PO_4 solution and UP water before introduction in UHV.

For ULP exposure on metallic Cu(111), the sample was further prepared in a UHV platform equipped with X-ray photoelectron spectroscopy (XPS, Thermo Electron Corporation, ESCALAB 250) with base pressure of $\sim 10^{-10}$ mbar. UHV sample preparation was performed by Ar$^+$ ion sputtering ($P_{Ar} = 5 \times 10^{-6}$ mbar, 600 V, 10 mA, 10 min) followed by 10 min of annealing at 600°C. Sputtering/annealing cycles were repeated until a clean
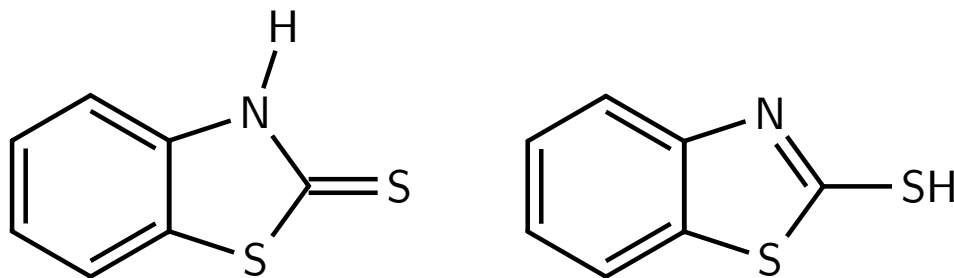
Figure 3.1: Thione form (left) and thiol form (right) of 2-MBT.

surface was obtained with no contamination detected in the XPS survey spectrum and a sharp (1×1) LEED pattern.

2-MBT with chemical formula $C_7H_5NS_2$ exists in two forms as shown in Fig. 4.1, with thione form prevailing in solid and gas phase [88]. A reactor for molecular deposition is connected to the preparation chamber of the UHV platform. 2-MBT yellow powder (Sigma-Aldrich) with purity of 99% was placed in a vacuum sealed glass tube connected directly to the reactor. The tube was kept at room temperature, and the partial pressure of 2-MBT was 2×10^{-9} mbar. The molecular exposure was calculated by multiplying the pressure of 2-MBT by the dosing time (1 L = 10^{-6} torr s). The sample was exposed to 2-MBT vapour at room temperature, and the surface after exposure was analysed by XPS.

A monochromatic Al K_α source (1486.6 eV) was used and the binding energy was referenced by measuring the Fermi level position of the sample. The transmission of analyser was calibrated by measurement of reference samples. The survey spectrum was recorded with a pass energy of 100 eV corresponding to an overall resolution of 1.8 eV, the high resolution spectra were recorded with a pass energy of 20 eV corresponding to an overall resolution of 360 meV. The take-off angle of the analysed photoelectrons was 90° for all analyses except when mentioned. The data processing was carried out using the CasaXPS software (version 2.3.19) [82].

In order to investigate the influence of pre-oxidation on the adsorption of 2-MBT, the ULP dosing experiments were carried out on a pre-oxidized copper surface prepared by introducing oxygen in the main chamber via a leak valve (5×10^{-6} mbar) until saturation at room temperature. In this case, a 2D oxide layer is formed [87]. ULP exposure was also carried out on Cu(111) surface prepared in air as described above without further preparation under UHV in order to study the influence of a native 3D oxide layer on the interaction mechanism of 2-MBT. Finally, the oxidation of a surface covered by a 2-MBT film was investigated by Auger electron spectroscopy (AES, Omicron model CMA-100) in order to determine the inhibition capacity of the 2-MBT films.
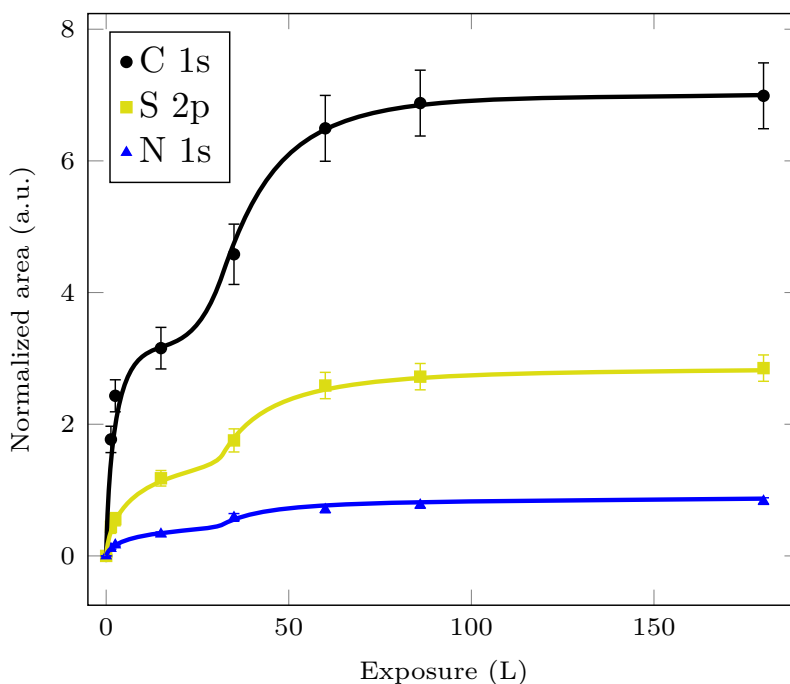
Figure 3.2: Growth kinetics of 2-MBT on clean Cu(111) surface at RT. Change in the XPS normalized area of the S 2p, C 1s and N 1s core level peaks as a function of 2-MBT exposure at 2×10^{-9} mbar. Lines are added to guide reader's eye.

3.4   Results and discussion

3.4.1   Bare Cu(111) exposed to 2-MBT and thermal stability of adsorbed multilayer

The growth kinetics of 2-MBT on clean, metallic Cu(111) at ULP (2×10^{-9} mbar) and room temperature was followed by XPS. The area of the S 2p, C 1s and N 1s core level peaks were normalized by the transmission of analyser, the photoionization cross section and the inelastic mean free path. The normalized peak area is proportional to the density of atoms. Fig. 4.2 shows the change in the XPS normalized area of the S 2p, C 1s and N 1s core level peaks as a function of exposure to 2-MBT. Lines showing the evolution of different signals are added to guide the reader's eye.

Fast increases of the S 2p, C 1s and N 1s signals with exposure are observed, indicating the deposition of 2-MBT on the sample surface, followed by a decrease in the adsorption rate until saturation of the measured signals for an exposure of about 90 L. The atomic ratios of S and N versus C were calculated, and we obtain a N to C atomic ratio of 0.10 $\pm$ 0.01, which is similar to the theoretical value for the stoichiometry of the molecule (1/7). The slight difference could be explained by possible geometric effects. The S to C atomic ratio was calculated to be 0.42 $\pm$ 0.01, which is 1.5 times the theoretical value (2/7).

In order to explain this excess of S, a detailed high resolution XPS analysis of the molecular layers formed after different exposures was performed in order to determine
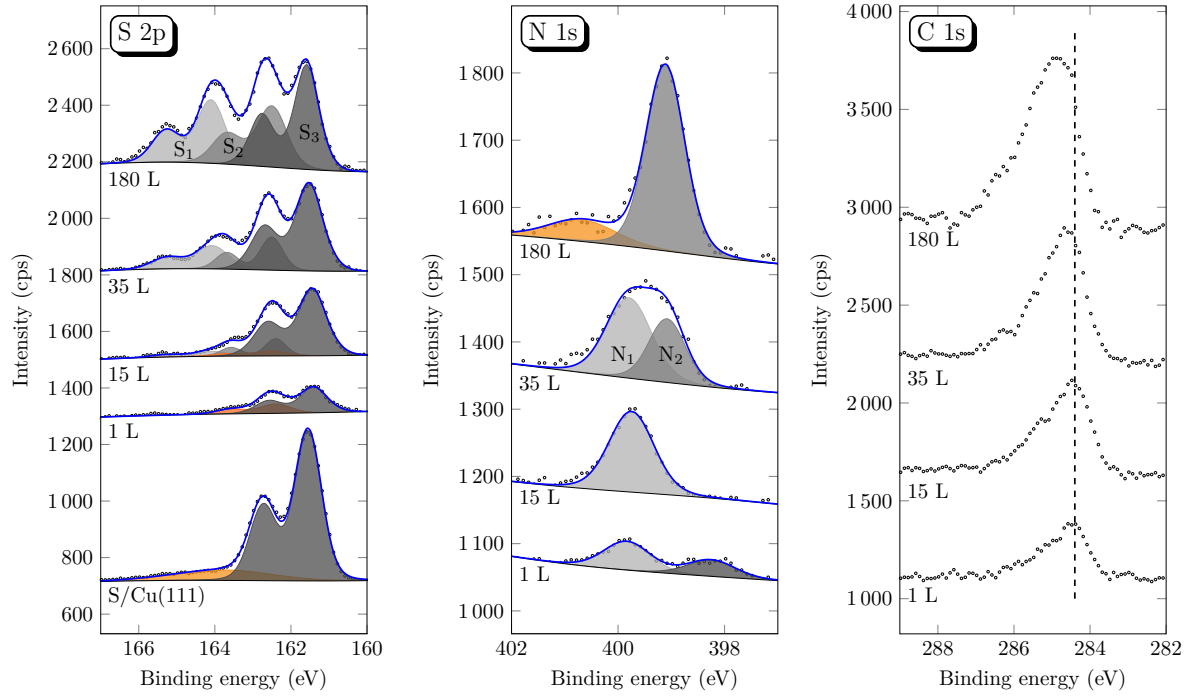
Figure 3.3: XPS spectra of the S 2p, N 1s and C 1s core levels after 2-MBT exposure on metallic Cu(111) surface at 2×10^{-9} mbar and RT. S 2p spectrum for a $(\sqrt{7} \times \sqrt{7})$R19.1° S/Cu(111) surface is shown for comparison.

their chemical composition. The results are shown in Fig. 3.3. The S 2p spectra were decomposed using spin-orbit doublets S $2p_{1/2}$ and S $2p_{3/2}$, with a branching ratio of 0.5 and spin-orbit splitting of 1.18 eV [45, 54]. At low exposure, i.e. 1 L, the S 2p spectrum is mainly composed of one S_3 component, with the $2p_{3/2}$ at 161.4 eV. This peak is at the same position as that of the $(\sqrt{7} \times \sqrt{7})$R19.1° S/Cu(111) surface obtained by exposing clean Cu(111) surface to H_2S, suggesting a partial decomposition of 2-MBT by the cleavage of the C=S and C–S bonds when interacting with metallic copper, and the adsorption of atomic S, as also confirmed by STM [89]. This phenomenon could be explained by the high affinity of sulfur to copper [90–94]. Moreover, angle resolved measurements confirm that S_3 is a component at the interface. The S_3 component is thus attributed to S bonded to metallic copper.

At higher exposure (15 L), besides the increase of S_3 component, two other components S_1 and S_2 appear, with the $2p_{3/2}$ at 164.1 eV and 162.5 eV, corresponding to the endocyclic and exocyclic S atoms in the 2-MBT molecule, respectively [54, 95]. The intensities of S_1 and S_2 components were set to be the same, their full widths at half maximum (FWHM) were limited to 1.0 eV, and the fit is in good agreement with the measured XPS spectra. The appearance of S_1 and S_2 indicates the formation of a molecular layer above the layer directly bonded to metallic copper, which is in agreement with the formation of a full monolayer at 10 L observed by STM [89]. Further exposure to 2-MBT results in an increase of S_1 and S_2, indicating a multilayer growth on Cu(111) surface.
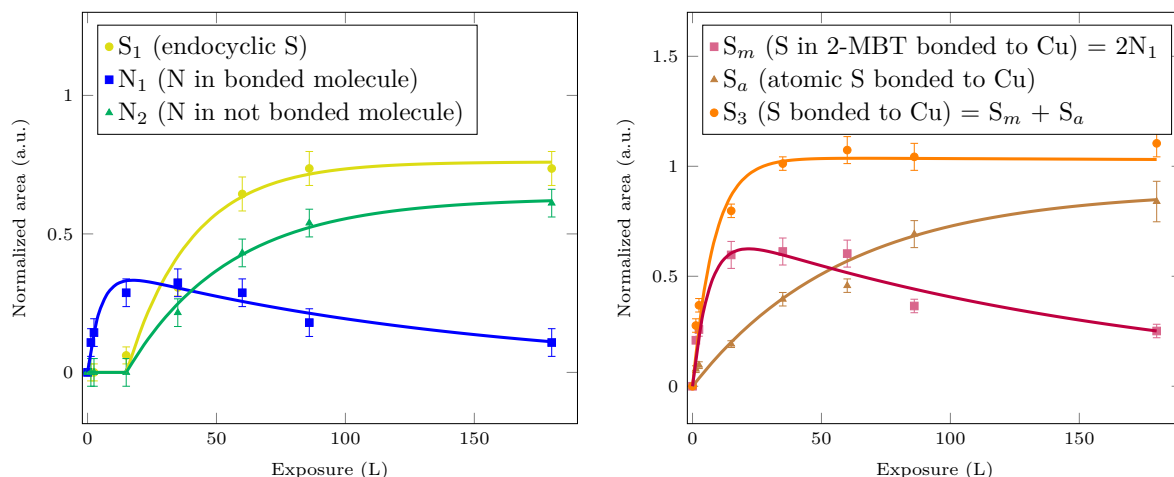
Figure 3.4: Evolution of the different S and N components with exposure to 2-MBT. Lines are added to guide reader's eye.

A transition of N 1s spectra from N_1 (399.8 eV) to N_2 (399.1 eV) was observed, N_2 is assigned to N in non bonded molecule. As for N_1, two possibilities exist to explain the shift of 0.7 eV in binding energy. N may bond directly to copper at the interface, or, since S is bonded to copper, it may change the electronic density of other elements in the molecule. The presence of N_1 component suggests the adsorption of 2-MBT on copper in its molecular form, thus the S_3 component should be considered as the sum of the components corresponding to S bonded to Cu, i.e. atomic S (resulting from the molecule decomposition) and S in the molecule. The binding energies of molecular and atomic S interacting with metallic copper being too close to be distinguished. Moreover, the two S atoms are both bonded to Cu in the molecular form, as indicated by a good fit with one S_3 component and two identical components S_1 and S_2. A shift to higher binding energy until 0.4 eV in C 1s region was observed. Due to low signal-to-noise ratio and non-obvious peak separation, as well as the direct interaction of 2-MBT with copper, the decomposition of C 1s region can not give reliable information and is thus not performed.

We can follow the evolution of different S and N components with exposure, as shown in Fig. 3.4. Smooth lines allowing to better follow the evolution of different components are added. The XPS peak area is normalized as in Fig. 4.2 to be proportional to the density of atoms. The relative components associated to atomic (S_a) and molecular S (S_m) in S_3 can be disentangled by imposing the atomic ratio between S_m and N_1. Firstly, we observe an increase of N_1 and S_m followed by a slow decrease, with maximum value at around 15 L. The absence of S_1 and N_2 during the initial stage indicates the formation of a first monolayer which becomes complete at around 15 L. After 15 L, S_1 and N_2 begin to appear, indicating the formation of 2-MBT multilayer. Finally a stationary regime is reached. S_a is found to increase continuously with increasing exposure, which may be
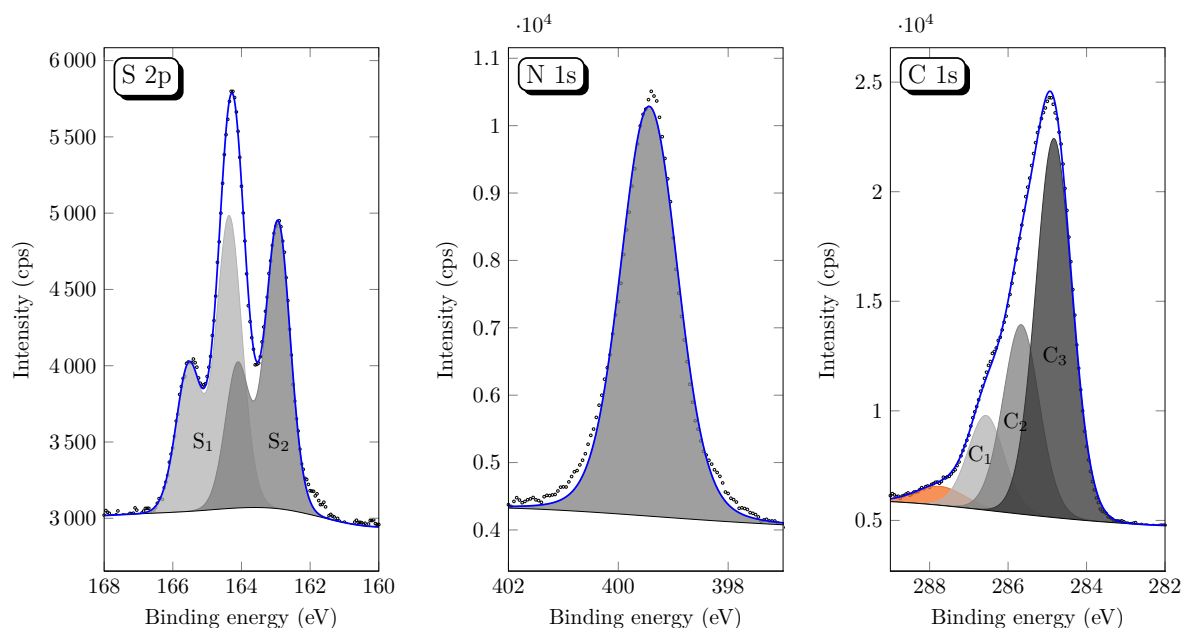
Figure 3.5: XPS spectra of the S 2p, N 1s and C 1s core levels after exposures to 2-MBT at ULP (180 L) and RT on Cu(111) prepared in air.

explained by a further decomposition and a possible densification of the monolayer at higher exposure.

In order to better understand the interaction of 2-MBT with copper, exposure was also carried out in the same conditions on Cu(111) prepared in air, and the results are shown in Fig. 3.5. In this case, a 3D oxide formed in air is covering the Cu(111) surface before 2-MBT deposition, and the presence of S 2p, N 1s and C 1s signals indicates the adsorption of the molecule. However, the S 2p spectrum shows only two components S_1 and S_2 corresponding to S in molecules which are not bonded to copper. This confirms that S_3 component is effectively associated to S bonded to metallic Cu. The pre-adsorbed 3D oxide prevents the direct interaction with metallic Cu and the dissociation of the molecule.

The high signal-to-noise ratio and the absence of direct molecule/copper interaction allow the decomposition of the C 1s region. There are theoretically seven inequivalent carbon environments within the molecule, however, XPS may not distinguish between the four benzene-like carbon atoms not in direct contact with N or S [96, 97]. We assume thus mainly three types of carbon, C_1, C_2 and C_3. The FWHMs (1.0 eV) of these three components were set to be the same, the intensity of C_1 was set to be half of C_2, which itself was half of C_3, and the fit is in agreement with the measured spectrum. We obtain three components at binding energies of 284.8 eV, 285.6 eV and 286.6 eV for C_3, C_2 and C_1, respectively. C_1 is then assigned to C=S, C_2 to C–N and C–S, and C_3 represents the remaining C atoms in the benzene ring. The good fit with the experimental data confirms non-dissociative molecular adsorption on the surface pre-covered by a 3D oxide layer. In the case of exposure on metallic Cu(111) prepared under UHV (Fig. 3.3, 180 L), a slight
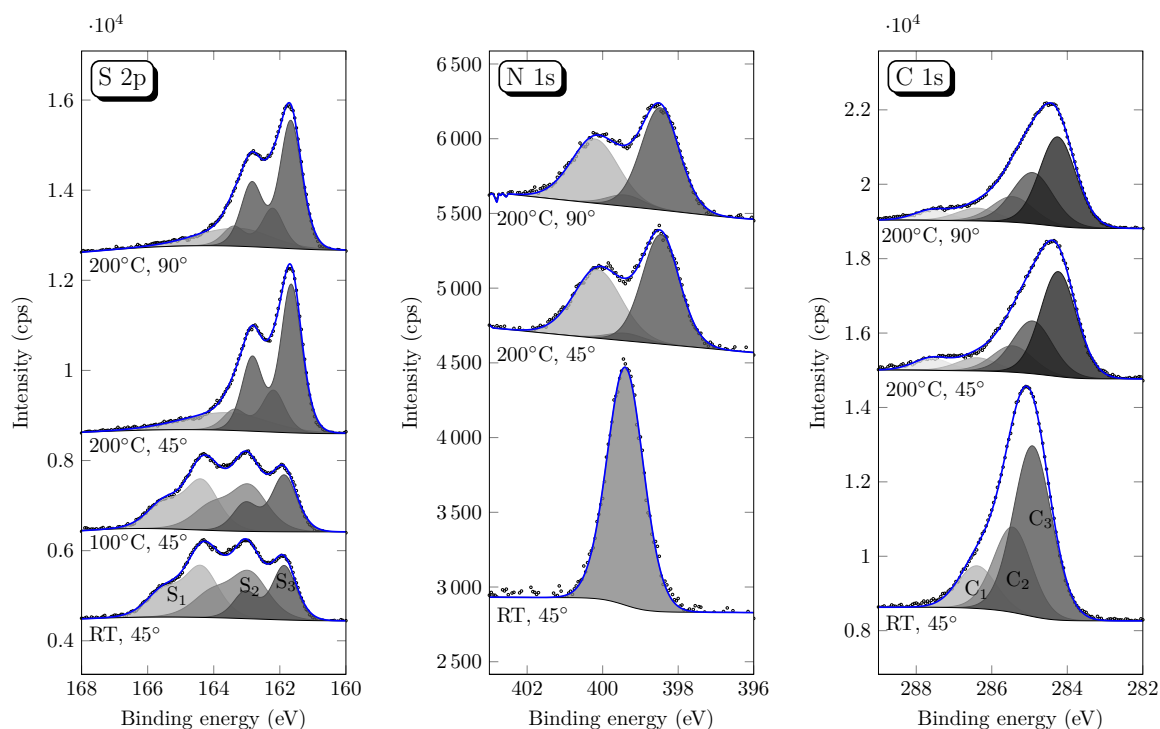
Figure 3.6: XPS spectra of the S 2p, N 1s and C 1s core levels for Cu(111) saturated with 2-MBT (ULP) before and after annealing during 20 min (take-off angle: 45° or 90° as indicated).

shift of 0.1 eV to lower binding energy of C 1s spectrum is observed, indicating a change in the C bonding in the molecule interacting with metallic copper. The same phenomenon is observed for the N 1s region, with a shift of 0.3 eV to lower binding energy and a decrease in FWHM (0.9 eV) of about 25%. The increase in FWHM and the small deviations in the fit of S 2p and N 1s spectra for exposure on Cu(111) prepared in air may be explained by the presence of surface contaminations when exposed to air. The C 1s component at binding energy of 287.7 eV is assigned to carboxylic groups (air contamination) [70].

In order to examine the thermal stability of the 2-MBT layer deposited under ULP conditions on oxide-free Cu(111), annealing at different temperatures during 20 min was carried out on saturated surfaces. XPS analyses performed before and after annealing are shown in Fig. 3.6. Firstly, XPS spectra were recorded at a take-off angle of 45°. After annealing at 100°C, the S 2p spectrum shows almost no change. We find the three S components associated to sulphur in non bonded molecule (S_1 and S_2) and sulphur interacting with metallic copper (S_3), with almost the same intensity and FWHM compared to those obtained before annealing. In contrast, when the sample was heated to 200°C, the total intensity of S increased by 8%, and the fraction of S_3 was twice that before annealing, while that of molecular S (S_1 and S_2) was reduced by half. The relative proportion of molecular C was reduced to half, and that of molecular N strongly decreased, with appearance of other C and N components at lower and higher binding energies, suggesting
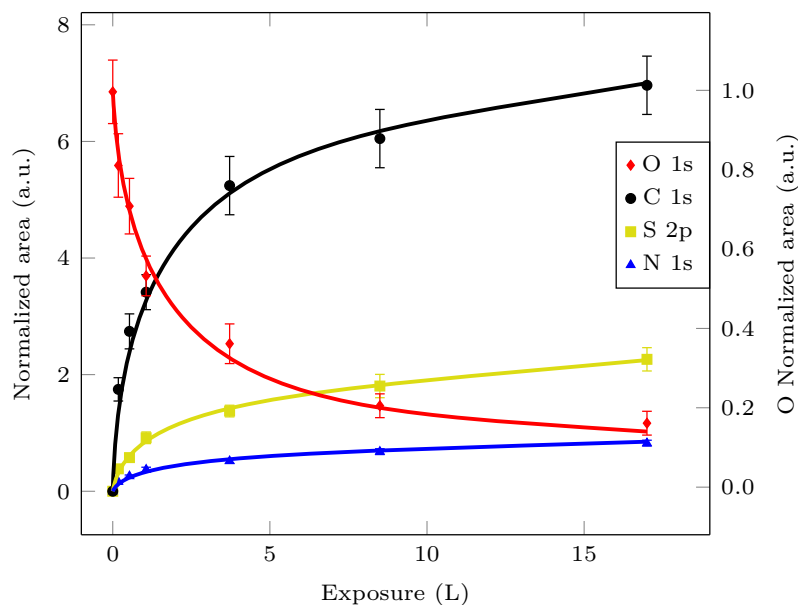
Figure 3.7: Growth kinetics of 2-MBT on pre-oxidized Cu(111) at RT. Changes in XPS normalized area of the S 2p, C 1s, N 1s and O 1s core level peaks as a function of 2-MBT exposure at 2×10^{-9} mbar. Lines are added to guide reader's eye.

decomposition of 2-MBT. At the same time, the total intensity of C decreased by about 30%, and that of N decreased by 17%, indicating the partial desorption of the molecular layer. This dissociative desorption of the molecular layer contributes to the increase of the remaining S component associated to S bonded to Cu(111) through a reduced attenuation of the signal.

In order to determine any stratification of the molecular layer after annealing, XPS measurements were also carried out in more sub-surface-sensitive conditions, at a take-off angle of 90° (Fig. 3.6). Compared to the spectra obtained at 45°, the relative proportion of S_3 versus molecular S (S_1 and S_2) increased slightly, as well as the relative proportion of molecular C and N versus that of C and N after molecule decomposition. This seems to indicate that the surface is firstly covered by sulphur, followed by the 2-MBT molecule, and finally by decomposition products (C and N).

3.4.2 Pre-oxidized Cu(111) exposed to 2-MBT and thermal stability of adsorbed multilayer

In order to study the influence of surface oxidation on the adsorption of 2-MBT, the Cu(111) surface was pre-oxidized ($P_{O_2} = 5 \times 10^{-6}$ mbar, 15 min, RT), and exposure of 2-MBT was then performed at room temperature under ULP at 2×10^{-9} mbar. The conditions of pre-oxidation were selected so as to saturate the surface with a 2D oxide layer [87].
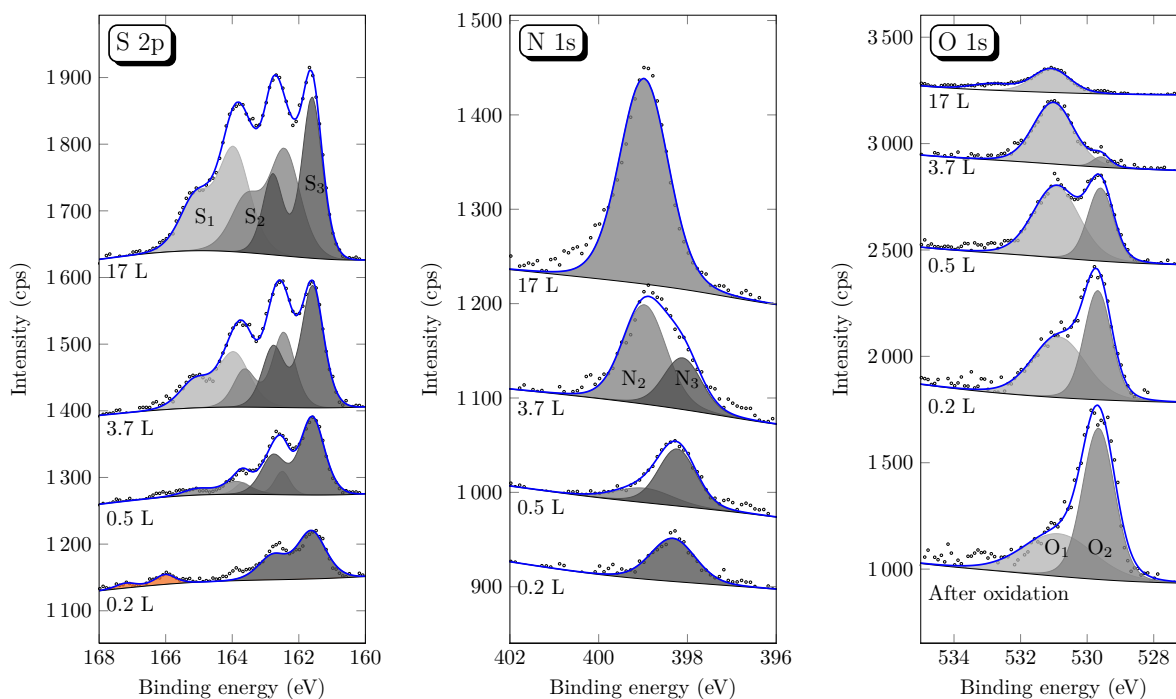
Figure 3.8: XPS spectra of the S 2p, N 1s and O 1s core levels after 2-MBT exposure on pre-oxidized Cu(111) surface at 2×10^{-9} mbar and RT.

Fig. 4.8 shows the variation of the XPS normalized area of the S 2p, C 1s, N 1s and O 1s core level peaks with 2-MBT exposure. The XPS peak area is normalized similarly as above to be proportional to the density of atoms, and lines showing the evolution of different signals are added to guide the reader's eye. A rapid increase of the S 2p, C 1s and N 1s signals is observed, indicating the growth of 2-MBT on the pre-oxidized copper surface. It is important to notice that the growth of 2-MBT layer is accompanied by a continuous decrease of the oxygen signal. Oxygen is substituted by 2-MBT with dissociation of the initial 2D oxide layer, and it may desorb as gaseous O_2 [98, 99]. The results are in agreement with that obtained by AES [89], where a complete disappearance of oxygen was observed after about 25 L. The atomic ratios of S and N versus C were calculated, we obtain values close to the stoichiometry of the molecule, indicating the adsorption of 2-MBT in its molecular form on the pre-oxidized Cu(111) surface.

Similarly, a high resolution XPS analysis of the molecular layer formed on pre-oxidized Cu(111) after different exposures was performed, and the results are shown in Fig. 3.8. At low exposure (0.2 L), the S 2p region is mainly composed of S_3 component at 161.6 eV, and a decrease in the O 1s spectrum of 19% compared to that obtained before exposure is observed, indicating the substitution of oxygen by 2-MBT and direct bonding between S and Cu. The N 1s spectrum gives a component N_3 at 398.3 eV, which is assigned to N in the bonded molecule. At an exposure of 0.5 L, we observe an increase of S_3 component and the appearance of two other components S_1 and S_2 corresponding to S in non bonded 2-MBT. Moreover, the N_2 component at 399.0 eV representing N in non bonded molecule
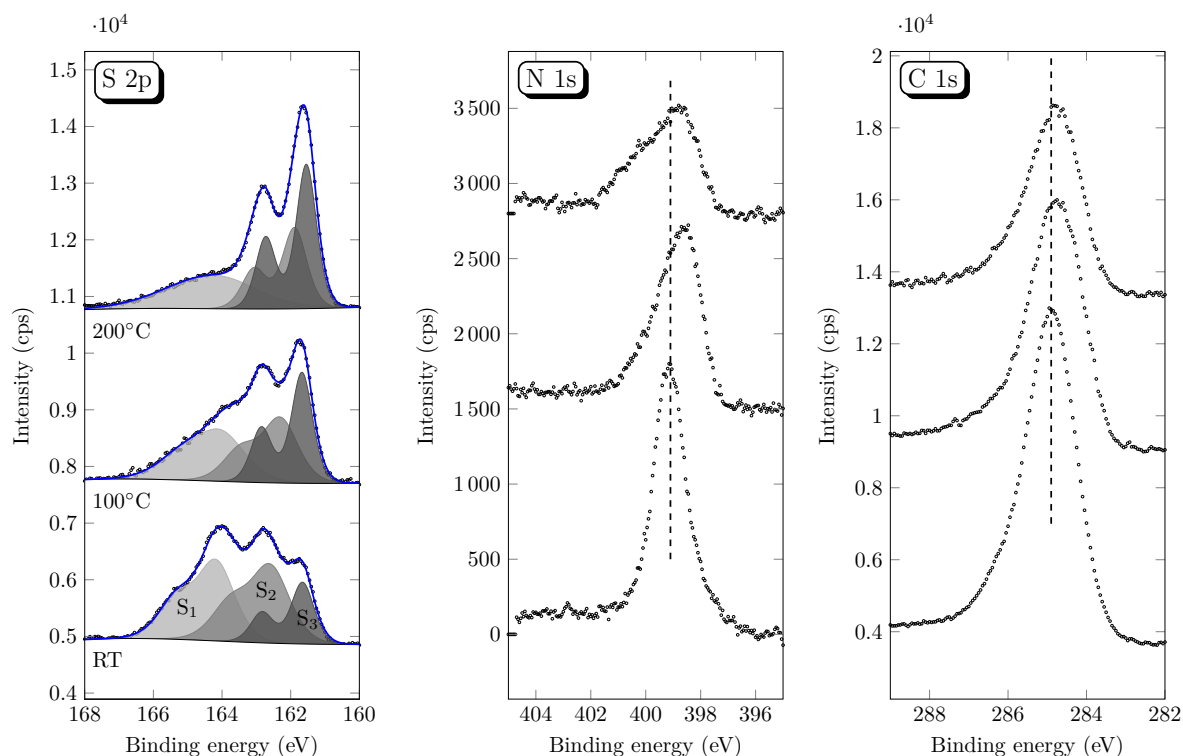
Figure 3.9: XPS spectra of S 2p, C 1s and N 1s core levels for pre-oxidized Cu(111) saturated with 2-MBT (ULP) before and after annealing during 20 min (take-off angle: 45°).

begins to appear. This seems to indicate the formation of a second layer from 0.5 L. The presence of O 1s signal at 0.5 L indicates that the surface is partially covered by 2-MBT molecular layer where oxygen has been substituted. Compared to the spectra obtained for adsorption of 2-MBT on the clean metallic copper surface, a difference of 1.5 eV towards lower binding energy from N_1 to N_3 is observed, indicating a stronger interaction of N with metallic Cu, which may be assigned to direct bonding between N and Cu. This explains the slight shift of the S_3 component. Further exposure to 2-MBT leads to the growth of molecular layer as indicated by the increase of S_1 and S_2 components, and continuous decrease of O 1s spectra.

In order to assess the thermal stability of the 2-MBT layer formed on pre-oxidized surface, annealing at different temperatures was carried out (Fig. 3.9). Decomposition and partial desorption of the molecule were observed when the sample was heated above 100°C, as shown by an increase of the relative proportion of S_3 component and a decrease of intensities of C 1s and N 1s, as well as a shift to lower binding energy of the XPS spectra. However, compared to annealing of adsorbed molecular layer on metallic Cu(111), difference in the N 1s region can be observed, with non-obvious peak separation, which may be explained by the bonding between N and Cu for exposure on metallic Cu(111). A schematic illustration of the adsorption of 2-MBT on clean and pre-oxidized Cu(111)
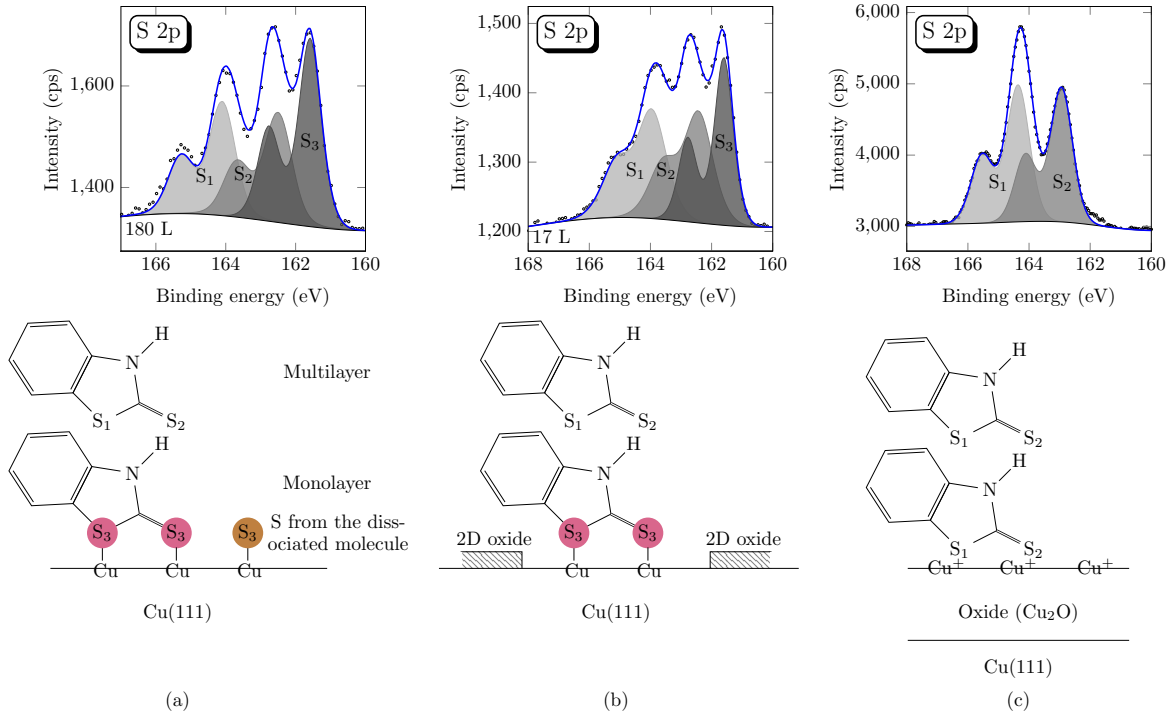
Figure 3.10: Schematic illustration of 2-MBT adsorption on different copper surfaces and the corresponding chemical state of S measured by XPS: (a) metallic; (b) oxidized (2D oxide); (c) oxidized (3D oxide).

surfaces is summarized in Fig.3.10. The inclination angle between the molecule and the sample surface is not considered.

3.4.3   Thickness of the 2-MBT layers

Quantitative analysis of the XPS data was performed in order to determine the thickness of the molecular layers (d_{MBT}) formed at ULP on metallic and pre-oxidized Cu(111) surfaces. We assume that the sample surface was covered by a homogeneous layer of 2-MBT on metallic Cu(111) surface. In the presence of a 2D oxide, we assume a homogeneous molecular layer on Cu(111) surface where oxide has been replaced by 2-MBT.

The thickness of the inhibitor layer was calculated from the intensities of the S 2p, N 1s, O 1s and Cu 2p spectra, using the following set of equations.

$$I_{\text{S 2p}}^{\text{MBT}} = (1-\phi)kFSN_{\text{S}}^{\text{MBT}}\sigma_{\text{S 2p}}T_{\text{S 2p}}\lambda_{\text{S 2p}}^{\text{MBT}}\sin\theta\left[1-\exp\left(-\frac{d_{\text{MBT}}}{\lambda_{\text{S 2p}}^{\text{MBT}}\sin\theta}\right)\right] \qquad (3.4.1)$$

$$I_{\text{N 1s}}^{\text{MBT}} = (1-\phi)kFSN_{\text{N}}^{\text{MBT}}\sigma_{\text{N 1s}}T_{\text{N 1s}}\lambda_{\text{N 1s}}^{\text{MBT}}\sin\theta\left[1-\exp\left(-\frac{d_{\text{MBT}}}{\lambda_{\text{N 1s}}^{\text{MBT}}\sin\theta}\right)\right] \qquad (3.4.2)$$

$$I_{\text{Cu 2p}}^{\text{Cu}} = (1-\phi)kFSN_{\text{Cu}}^{\text{Cu}}\sigma_{\text{Cu 2p}}T_{\text{Cu 2p}}\lambda_{\text{Cu 2p}}^{\text{Cu}}\sin\theta\exp\left(-\frac{d_{\text{MBT}}}{\lambda_{\text{Cu 2p}}^{\text{MBT}}\sin\theta}\right) + \phi I_{\text{Cu 2p}}^{\text{Cu(2D oxide)}}$$

$$(3.4.3)$$
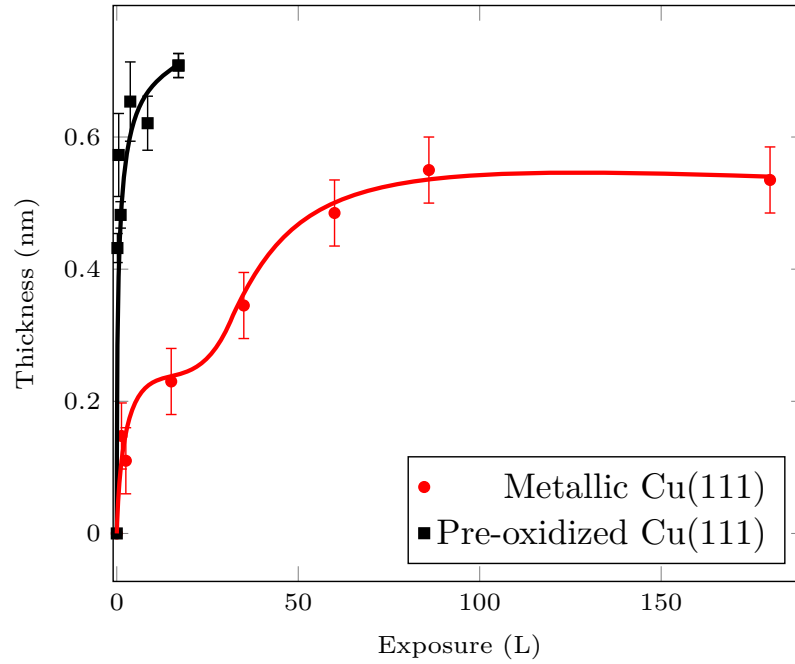
Figure 3.11: Thickness of the molecular layer formed on metallic and pre-oxidized Cu(111) surfaces. Lines are added to guide reader's eye.

where I is the intensity of the photoelectrons, ϕ the surface coverage by the 2D oxide, N the density of emitting atoms, λ the inelastic mean free path, estimated using the Tanuma, Powell and Penn formula (TPP-2M) [83], and θ the take-off angle of photoelectrons. $\phi = 0$ for exposure on the metallic Cu(111) surface, and $\phi = I_{\text{O 1s}}/I_{\text{O 1s}}^{\text{2D oxide}}$ for exposure on the pre-oxidized Cu(111) surface.

The results are shown in Fig. 3.11. Lines are added to show the thickness evolution. Growth of molecular layer is observed with a fast increase of the inhibitor layer thickness at initial stage, followed by a decrease in the growth rate until saturation for exposure on the metallic Cu(111) surface. Moreover, an acceleration of the initial growth kinetics of 2-MBT is observed in the presence of oxygen, which may be explained by the activation of the molecule bonding to copper by the dissociation of the pre-formed surface oxide.

We concluded above on the formation of a complete monolayer at 15 L on the metallic Cu(111) surface, which corresponds to a thickness of about 0.2 nm. Taking into account the dimension of the 2-MBT molecule [59], we can deduce that 2-MBT in the monolayer adsorbs with its plane almost parallel to the sample surface. This is consistent with the fact that S-containing molecules can adsorb on metallic surface with small tilt angle [100, 101]. Multilayers are formed at higher exposure, with a total thickness of 0.6 nm at saturation. On pre-oxidized Cu(111) surface, the monolayer formed is 0.4 nm after an exposure of 0.2 L, which indicates that the molecule adsorbs in a tilted position. Multilayers of thickness of 0.7 nm are formed at 17 L. For 2-MBT exposure at ULP on Cu(111) prepared in air until saturation, by assuming a homogeneous oxide layer covered by a homogeneous layer
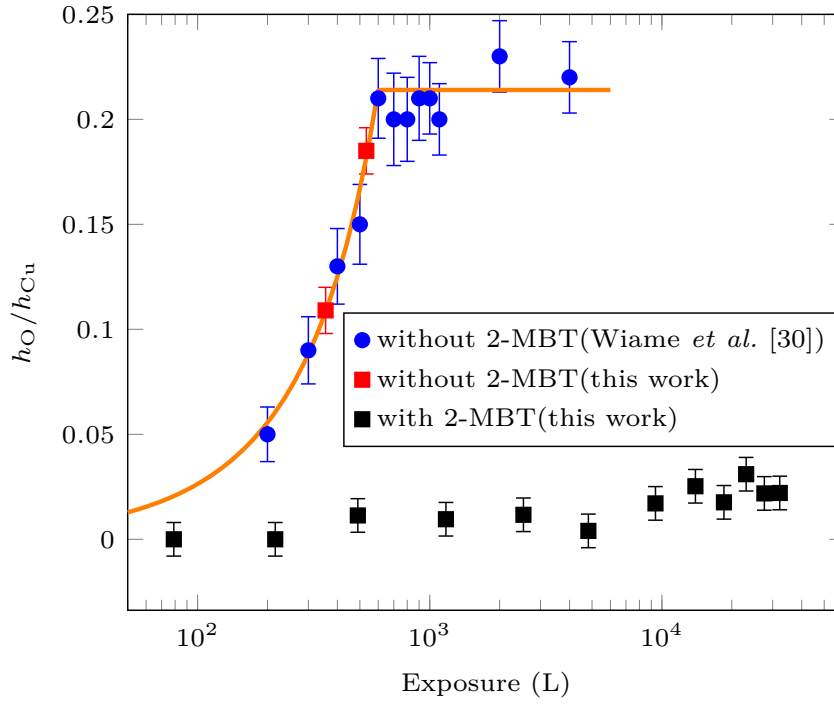
Figure 3.12: Oxidation kinetics of Cu(111): effect of adsorbed 2-MBT (8 L of 2-MBT at RT prior to oxidation).

of 2-MBT, we can calculate the thickness of oxide and molecular layers, which gives 0.6 $\pm$ 0.1 nm and 1.0 $\pm$ 0.1 nm, respectively. The 2-MBT layer formed on Cu in aqueous solution was reported to be 1.5 $\pm$ 0.5 nm [54]. This indicates that the presence of oxygen prior to exposure can promote the growth of 2-MBT.

3.4.4 Inhibition effect of pre-adsorbed 2-MBT on oxidation of Cu(111)

In order to confirm if 2-MBT pre-adsorbed under ULP conditions could inhibit copper corrosion, we recorded the oxidation kinetics on the Cu(111) surface first exposed to 8 L of 2-MBT at room temperature, corresponding to the formation of about one monolayer of 2-MBT. Oxidation of the sample was then performed at $P_{O_2} = 5 \times 10^{-6}$ mbar at RT. Fig. 3.12 shows that in the presence of the pre-adsorbed monolayer of 2-MBT, there is almost no increase in the oxygen intensity, whereas without 2-MBT copper is oxidized and the oxidation kinetics agree with previous reported data [87]: the intensity of oxygen increases with exposure until the formation of a monolayer of oxide, then the surface is saturated with oxygen, with a value of $h_O/h_{Cu} \sim 0.22$ corresponding to the completion of the 2D oxide layer. The comparison between the oxidation kinetics with and without pre-adsorbed 2-MBT indicates that a monolayer of 2-MBT can effectively protect the copper surface from oxidation in these conditions of temperature and pressure, and thus prevent the formation of copper corrosion products. The residual uptake of oxygen is

likely due to the formation of copper oxide at the local sites of the 2-MBT layer where protection is defective. The defective sites cover about 8% of the surface area.

3.5 Conclusions

In this work, the adsorption of 2-MBT deposited from the vapour phase on metallic and pre-oxidized Cu(111) surfaces under ULP conditions was investigated by XPS. When 2-MBT molecules arrive on a clean metallic copper surface (prepared under UHV), the XPS spectra show that the two sulphur atoms are involved simultaneously in the interaction with copper, confirmed by the presence of a S $2p_{3/2}$ peak at 161.5 ± 0.1 eV. The adsorption is accompanied by a partial decomposition of the molecule giving atomic sulphur adsorbed on copper. On the pre-oxidized Cu(111) surface, the 2D oxide initially formed is dissociated and substituted by 2-MBT, without decomposition of the molecule.

A complete monolayer of 2-MBT is formed at an exposures of 15 L on metallic Cu(111) surface, with a thickness of 0.2 nm. This is consistent with the adsorption of flat-lying molecule. Further exposure to 2-MBT leads to the formation of multilayers, with a thickness of 0.6 nm at saturation. On pre-oxidized Cu(111), a monolayer covers partially the surface with a thickness of 0.4 nm, suggesting the adsorption of 2-MBT in a tilted configuration. On the Cu(111) surface covered by a native 3D oxide formed in air, 2-MBT also adsorbs without decomposing and the multilayer is 1.0 nm thick at saturation.

By comparing the growth kinetics of 2-MBT on metallic and pre-oxidized Cu(111) surfaces, we can deduce that the presence of a 2D oxide layer accelerates the initial uptake of 2-MBT on copper (< 20 L), and leads to the formation of a thicker molecular layer. This may be explained by the activation of the molecule bonding to copper by the dissociation of the pre-formed surface oxide and substitution of oxygen by 2-MBT.

After heating metallic and pre-oxidized Cu(111) saturated with 2-MBT to above 100°C, molecules decompose. The C and N resulting from decomposition leave the surface, while the atomic S remains adsorbed on copper.

2-MBT is relatively efficient for corrosion inhibition after adsorption under ULP conditions at room temperature. A monolayer of 2-MBT effectively prevents the oxidation of Cu(111) at low O_2 pressure and room temperature.

CHAPTER 4

2-MBT DEPOSITION ON PRISTINE AND PRE-OXIDIZED Cu(111) SURFACES AT ROOM TEMPERATURE: STM CHARACTERIZATION

4.1   Abstract

2-mercaptobenzothiazole (2-MBT) is used for its corrosion inhibition properties. In this study, the adsorption of 2-MBT on metallic and pre-oxidized Cu(111) surfaces was investigated using Auger Electron Spectroscopy and Scanning Tunneling Microscopy. Growth and structure of molecular films adsorbed at ultra low pressure and room temperature on clean and pre-oxidized Cu(111) surfaces were characterized. On clean metallic Cu(111) surface, local triangular $(\sqrt{7} \times \sqrt{7})$R19.1° structures are formed at low exposures (3–4 L), which are assigned to the adsorption of atomic S resulting from partial decomposition of 2-MBT. At 10 L, a full non-ordered monolayer of 2-MBT is formed, and further exposure leads to the formation of a non-ordered multilayer. The thickness of the outermost 2-MBT layer is 1.3 Å, which suggests that the outermost molecules of the multilayer are lying flat. Oxidation of the copper surface prior to exposure to 2-MBT results in more compact and homogeneous molecular films. The initial 2D oxide is dissociated and replaced by 2-MBT. Thermal stability at different temperatures was studied on clean and pre-oxidized copper surfaces saturated with 2-MBT. A $(\sqrt{7} \times \sqrt{7})$R19.1° structure is observed in both cases for temperatures higher than 100°C, indicating the decomposition of 2-MBT and a copper surface covered with atomic S.
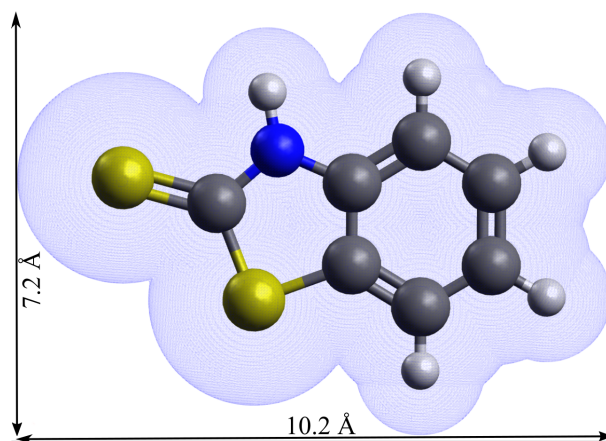
Figure 4.1: 2-MBT chemical structure (thione form) and associated molecular dimensions (the van der Waals surface is presented.)

4.2   Introduction

The corrosion of metals and alloys is an important issue in industrial applications with an annual global cost estimated to be about 3.4% of the global GDP (2013) [1]. In order to mitigate corrosion, inhibitors are widely used and developed. On copper, numerous studies [3, 9, 19, 39, 40, 47, 48, 53–55, 58–62, 102–104] have been carried out for a better understanding of the surface interaction with corrosion inhibitors, as well as the inhibition mechanisms.

2-mercaptobenzothiazole (2-MBT) is one of the corrosion inhibitors used in industry besides benzotriazole (BTAH) [3, 19, 39, 40, 47, 48, 102–104]. Its chemical formula is $C_7H_5NS_2$, and it exists in two forms: the thione (NH) and the thiol (SH) forms. The former has C double bonded to S, and the latter C double bonded to endocyclic N with hydrogen bonded to S. It has been shown that 2-MBT is only in the thione form in gas phase [58]. The bond lengths and bond angles in the 2-MBT molecule have been determined [59], and by taking into consideration the van der Waals radii of different atoms, we can deduce its molecular dimensions, as shown in Fig. 4.1.

It has been shown that Cu reacts with 2-MBT in solution to form a complex which can protect it from corrosion [55, 60]. Woods et al. [53] claimed that 2-MBT is attached to the metal surface through interaction with the exocyclic sulfur, as well as the nitrogen [54, 61, 103], but not by the endocyclic S atom. It was also suggested that 2-MBT adsorbs flat on Ag in the thiol form, while it adsorbs with molecular plane perpendicular on Au in thione form [62]. 2-MBT can also protect aluminium alloy from corrosion by forming a thin organic layer on the substrate surface [105]. Besides the molecular deposition in solution, the adsorption of BTAH on Cu(111) surface has been investigated by gas evaporation under ultra-high vacuum (UHV) and analyzed by scanning tunneling microscopy (STM) [9]. A chemisorbed monolayer was formed firstly, followed by physisorbed multilayer which were less stable and desorb at around 100°C.

In this work, we studied the interaction of 2-MBT with a single crystalline Cu(111) surface using Auger Electron Spectroscopy (AES) and STM. It allows us to determine the adsorption process and address the adsorbed molecular structure at nanometric and atomic scales. The influence of surface pre-oxidation and the effect of temperature were also investigated. This study brings new insight into the inhibition mechanism of 2-MBT on copper, which contributes to the knowledge-based development of more efficient corrosion inhibitors for the corrosion protection of copper and its alloys.

4.3 Experimental

A Cu(111) single crystal of high purity (99.999%) was used. The surface was mechanically polished down to 0.25 μm (diamond paste), and then electro-polished in 60 wt% H_3PO_4 solution at 1.4 V during 5 min before introduction into the UHV system, where it was further prepared by cycles of ion sputtering ($P_{Ar} = 1 \times 10^{-5}$ mbar, 600 V, 20 mA, 30 min) and annealing (600°C, 30 min) in order to obtain a clean and well-structured surface. The base pressure of the UHV system is 10^{-10} mbar, and it is equipped with STM (Omicron, STM1 with SCALA system), AES (Omicron model CMA-100) and Low Energy Electron Diffraction (LEED, Riber, OPD-304). The surface was systematically checked by AES, LEED and STM until no contamination and a good surface organization were observed, characterized by a sharp (1×1) LEED pattern and a topography with large and flat terraces as verified by STM.

The 2-MBT molecule used was 99% pure (Sigma-Aldrich). It is a yellow powder at room temperature. The 2-MBT powder was placed in a vacuum sealed glass connected directly to a reactor attached to the UHV system. The pressure of 2-MBT in the reactor was 2×10^{-9} mbar at room temperature. The sample was kept at room temperature during the deposition process. In order to investigate the influence of pre-oxidation on the adsorption of 2-MBT, oxidation of the copper surface was performed by introducing oxygen gas in the chamber through a leak valve ($P_{O_2} = 5 \times 10^{-6}$ mbar) until saturation. In these conditions, a 2D surface oxide is formed [87, 106, 107]. After 2-MBT depositions on clean and pre-oxidized copper surfaces, the growth kinetics was followed by AES, and the surface structures were characterized by STM.

The STM measurements were performed at room temperature and in constant current mode. Image processing was carried out using WSxM software (5.0 Develop 9.1) [80]. No filtering was applied except when mentioned. All images were corrected by plane subtraction.
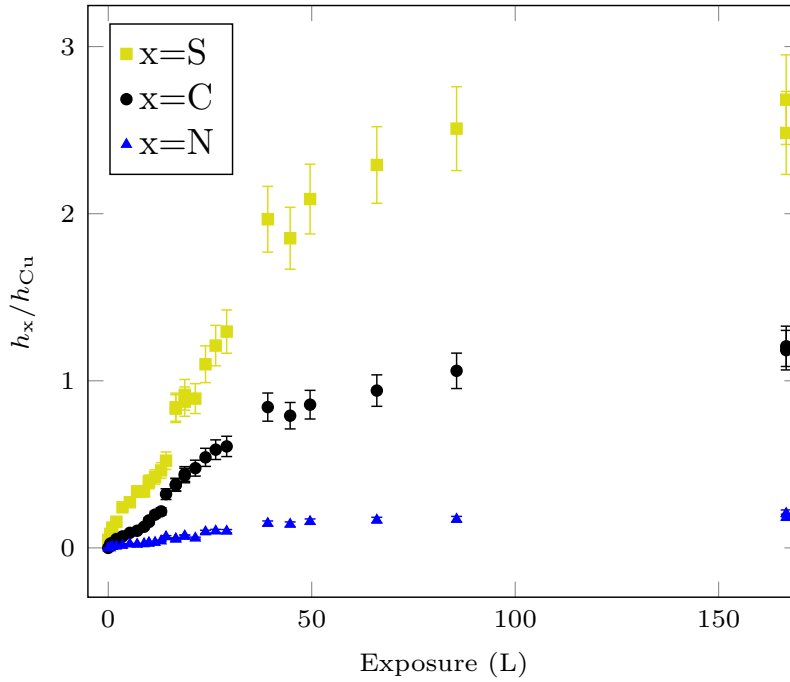
Figure 4.2: Growth kinetics of 2-MBT on Cu(111) at room temperature. Change in the AES peak-to-peak height ratios h_S/h_{Cu}, h_C/h_{Cu} and h_N/h_{Cu} as a function of 2-MBT exposure at 2×10^{-9} mbar.

4.4   Results and discussion

4.4.1   2-MBT adsorption on metallic Cu(111) surface

A clean oxide-free and organized copper surface was prepared under UHV, then the sample was exposed to 2-MBT at ultra low pressure (2×10^{-9} mbar) and room temperature and analyzed by AES. Fig. 4.2 shows the change in the peak-to-peak height ratios of S (151 eV), C (271 eV) and N (380 eV) to Cu (920 eV) signals as a function of exposure to 2-MBT. The adsorption of 2-MBT is initially characterized by fast increase of the S, C and N signals with increasing exposure, indicating the deposition of 2-MBT on the sample surface, and then a decrease in the adsorption rate until saturation of the measured signals after an exposure of about 100 L. The limit values for h_S/h_{Cu}, h_C/h_{Cu} and h_N/h_{Cu} are 2.6 $\pm$ 0.3, 1.2 $\pm$ 0.1 and 0.19 $\pm$ 0.02, respectively.

In order to verify that the increase of the S, C and N signals corresponds to the adsorption of 2-MBT, their relative ratios are corrected using the relative sensitivities S_x of the Auger transitions. The results are shown in Fig. 4.3. The corrected N to C ratio calculated after different exposures is close to the theoretical (molecule stoichiometry) value (1/7), deduced from the number of N and C atoms in the molecule, indicating the adsorption of 2-MBT on Cu(111). However, the S to C ratio first decreases and then increases slightly after about 10 L until reaching its saturation value. This seems to indicate that there is a transition in the growth mode of 2-MBT at about 10 L, also
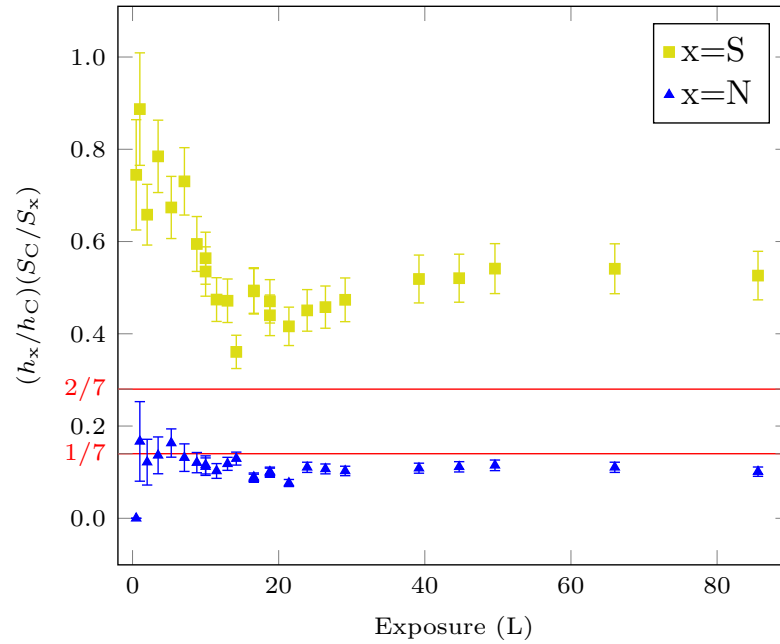
Figure 4.3: Evolution of S and N to C atomic ratios as measured by AES with 2-MBT exposure at ultra low pressure and RT.

suggested in Fig. 4.2 by the change in slope. Another point to notice is that the ratio between S and C at stationary regime is almost 2 times the theoretical value (2/7).

In order to explain this excess of S, STM measurements were carried out at different exposures to characterize the surface structure.

Low exposure, i.e. 4 L, is characterized by the formation of ordered local structures along the step edges and on the terraces, as shown in Fig. 4.4a. These local structures are triangles having variable dimension (side length of 2–3 nm). The triangles are either isolated or aggregated. Similar triangles have been observed for atomic S adsorbed on the Cu(111) surface [108, 109], which seems to indicate the adsorption of S atoms on the copper surface in the present case. However, in the case of S/Cu(111), due to the high mobility of atomic S at low coverage, the triangles were mainly at the step edges. Here, adsorbed molecules on Cu(111) may play the role of a barrier, thus preventing the displacement of S, which could explain the formation of triangles on the terraces and not only at the step edges.

A higher resolution image of these triangles is presented in Fig. 4.4b. Substrate crystallographic directions, derived from atomic resolution STM images and LEED pattern obtained on pristine Cu(111) surface, are shown. An ordered local structure can be observed inside the triangles with the presence of three or six protrusions depending on the size of triangles. The lattice unit cell is shown by the black rhombus. The distance between protrusions in different directions and from different STM images was measured to be 0.67 ± 0.02 nm, thus we identified the lattice as a $(\sqrt{7} \times \sqrt{7})R19.1°$ structure,

(a)   (b)
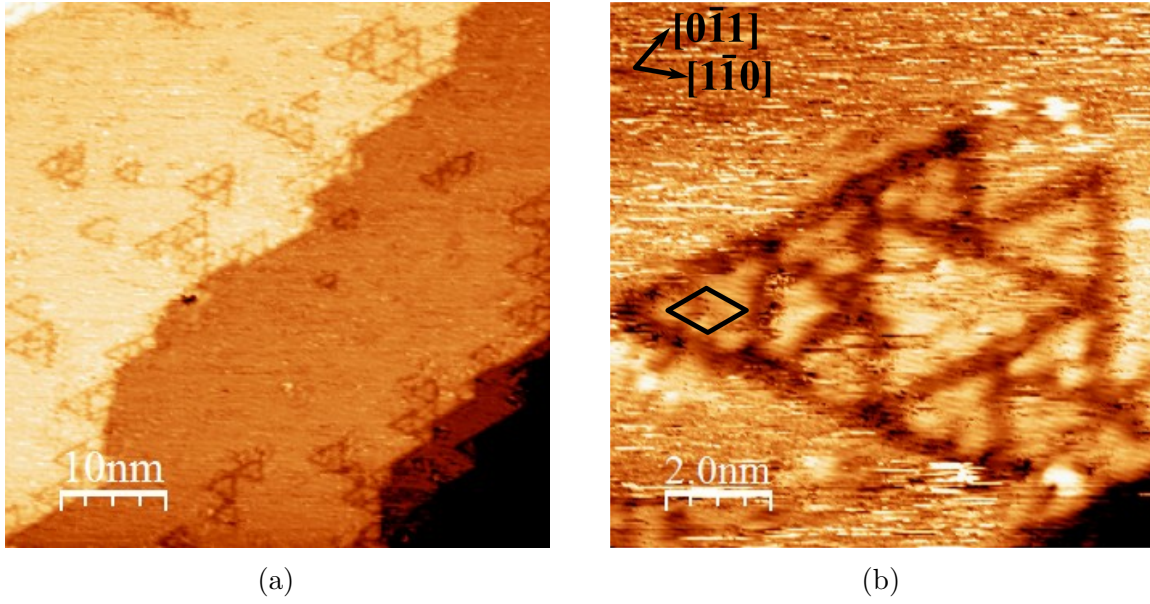
Figure 4.4: STM images for 4 L (exposure) of 2-MBT on Cu(111) (a) 50 nm × 50 nm, $V = -1.0$ V, $I = 1.0$ nA; (b) 10 nm × 10 nm, $V = -1.0$ V, $I = 0.5$ nA.

which is similar to that obtained for the S/Cu(111) system at saturation [110, 111]. This suggests the local adsorption of atomic S on copper, and a partial decomposition of 2-MBT when interacting with the clean, metallic Cu(111) surface, which explains the excess of S observed in Fig. 4.3. By counting the number of protrusions inside the triangles of different sizes in Fig. 4.4a, we estimate their density on the surface to be $\sim 2 \times 10^{13}$ cm^{-2}. Given that the atomic density of copper atoms on Cu(111) surface is 1.78×10^{15} cm^{-2}, we estimate a surface coverage (ratio between the density of protrusion and the atomic density of the substrate) of $\sim 1\%$. A well-organized $(\sqrt{7} \times \sqrt{7})$R19.1° surface gives a coverage of 14%, assuming one adsorbate per unit cell.

   Further exposure of the sample to 2-MBT up to 10 L (Fig. 4.5) preserves the surface topography. Small darker local structures are observed on the terraces, as indicated by the white triangle. These structures are similar in size and orientation to the triangular structures observed on Cu(111) at 4 L, and can be assigned to the adsorption of atomic S. The apparent height difference between these structures and the terraces nearby is about 0.7 Å, which is smaller than that between two successive Cu(111) planes, i.e. 2.0 Å. This seems to indicate the formation of a quasi-complete layer of molecules which lie almost flat on the sample surface by referring to the size of the molecule, with the adsorption of both atomic S resulting from molecular partial decomposition and 2-MBT in its molecular form. The results are in good agreement with AES measurements (Fig. 4.3) showing a change of slope at 10 L and an excess of S. No local ordering was evidenced by Fast Fourier Transform (FFT) of the images.

   At higher exposure, 2-MBT continues to adsorb on Cu, and finally more than one molecular layer is formed. The surface obtained after an exposure of 1300 L (Fig. 4.6a) is
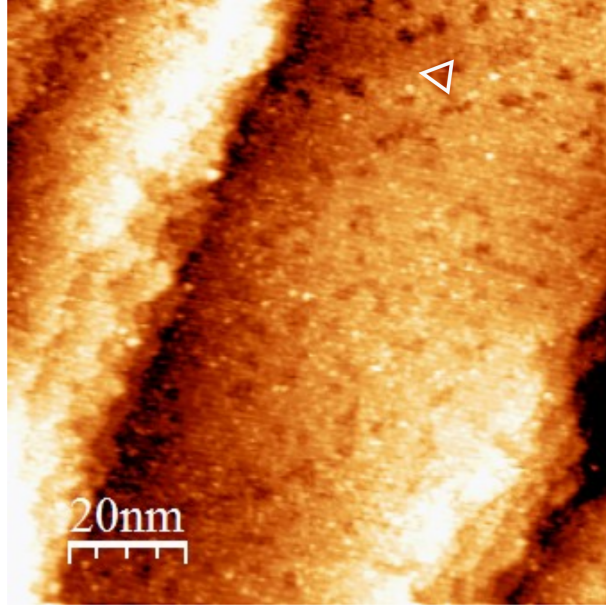
Figure 4.5: STM image for 10 L (exposure) of 2-MBT on Cu(111) (100 nm × 100 nm, $V = -2.0$ V, $I = 0.2$ nA).

rougher than that obtained for 10 L. One can still see different terraces but the contrast between different zones on terraces is increased (Fig. 4.6b). This corresponds to difference in height, i.e. the thickness, due to adsorption of the last molecular layer. This contrast also indicates that the last molecular layer is incomplete. We can plot the height distribution of a terrace, as shown by the height histogram (Fig. 4.6c), obtained from Fig. 4.6b with a bin size of 5 pm. Fitting of the histogram with gaussian distributions gives a layer thickness of 1.3 Å and a surface covered fraction of 55% for the last molecular layer. Taking into account the molecular dimensions of 2-MBT, this indicates that the 2-MBT in the last molecular layer adsorbs with its plane almost parallel to sample surface. FFT did not reveal any ordered local structure.

4.4.2   2-MBT adsorption on pre-oxidized Cu(111) surface

In order to investigate the influence of pre-oxidation on the adsorption of 2-MBT, the Cu(111) surface covered previously with a 2D surface oxide was prepared by exposing the clean surface to gaseous oxygen ($P_{O_2} = 5 \times 10^{-6}$ mbar) during 15 min at room temperature [87].

Fig. 4.7 shows the evolution of the peak-to-peak height ratios of S (151 eV), C (271 eV) and N (380 eV) to Cu (920 eV) Auger signals with 2-MBT exposure at room temperature. Similarly to Fig. 4.2, a first region with rapid increase of the S, C and N signals is observed, indicating the growth of the 2-MBT layer on the pre-oxidized copper surface, followed by a saturation regime, characterized by the plateau in the S, C and N signals. At saturation, the value of h_S/h_{Cu} ($\sim 2.8 \pm 0.3$) is similar to that obtained without pre-oxidation.

(a)   (b)   (c)
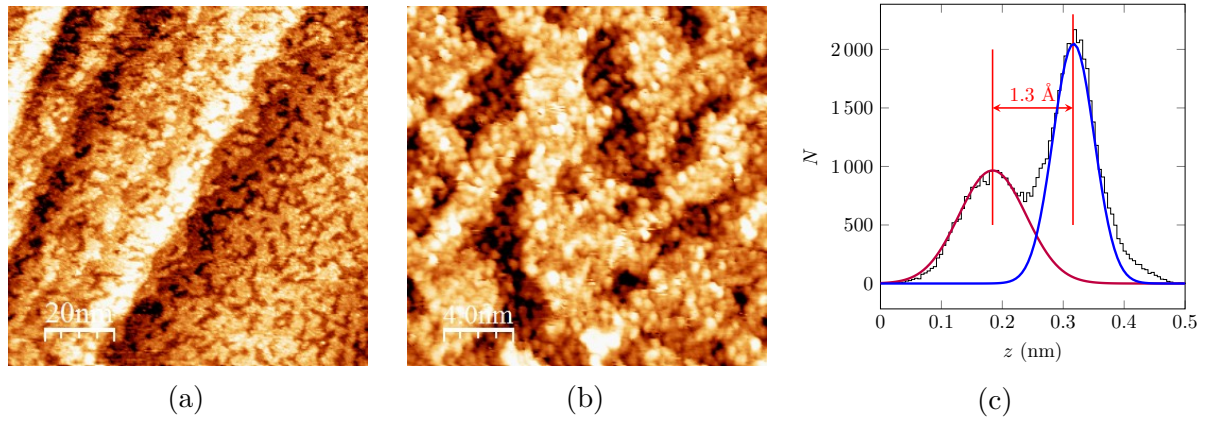
Figure 4.6: STM images for 1300 L (exposure) of 2-MBT on Cu(111) (a) 100 nm × 100 nm, $V = 1.0$ V, $I = 0.2$ nA; (b) 20 nm × 20 nm, $V = 1.0$ V, $I = 0.3$ nA; (c) Height histogram of image (b).
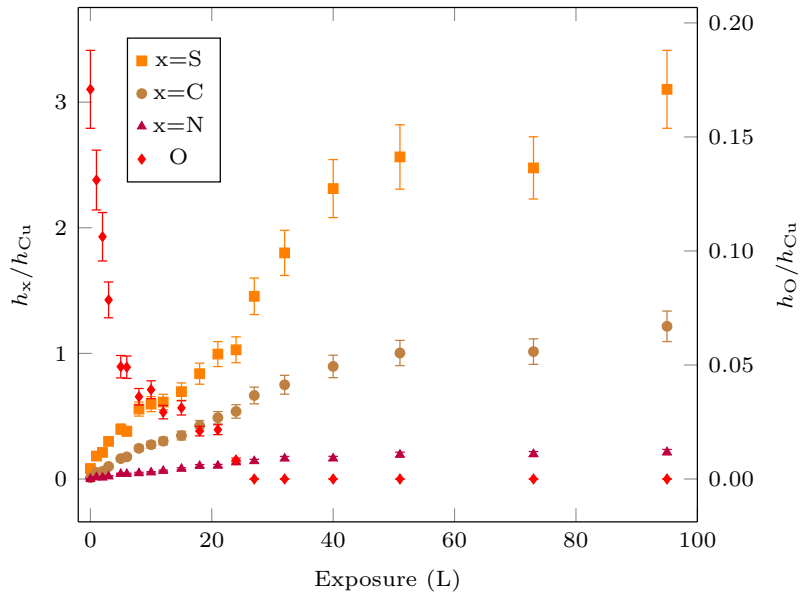
Figure 4.7: Growth kinetics of 2-MBT on pre-oxidized Cu(111) at room temperature. Changes in Auger peak-to-peak height ratios as a function of 2-MBT exposure at 2×10^{-9} mbar.
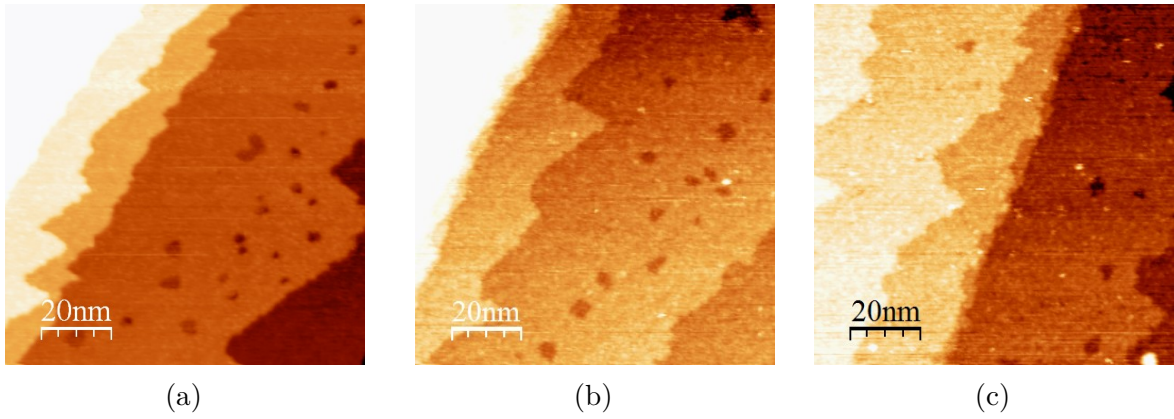
Figure 4.8: STM images of pre-oxidized Cu(111) surface (a) before exposure to 2-MBT (100 nm × 100 nm,
$V = 1.0$ V, $I = 0.2$ nA); (b) after 21 L of 2-MBT (100 nm × 100 nm, $V = 1.0$ V, $I = 0.6$ nA); (c) after 40 L of 2-MBT (100 nm × 100 nm, $V = 0.7$ mV, $I = 0.3$ nA).

It is important to notice that the growth of the 2-MBT layer is accompanied by a continuous decrease of the h_O/h_{Cu} signal from 0.17 ± 0.02 to zero. Oxygen initially present on the sample surface is thus substituted by 2-MBT and completely desorbs at 2-MBT exposure of about 25 L at room temperature. The substitution of oxygen by sulfur has also been observed for H_2S exposure on pre-oxidized Cu(111) surface [92].

The STM image of the pre-oxidized surface (Fig. 5.8a) confirms the formation of a flat bi-dimensional copper oxide covering the atomically flat substrate terraces, with a reconstruction of the step edges. Moreover, local defects exist on the terraces, and they appear darker than the terraces, with a difference in height of about 2 Å, corresponding to the height of one atomic step of Cu(111).

The pre-oxidized surface was then exposed to 2-MBT, and no obvious change of the surface topography is observed, as shown in Fig. 4.8b and Fig. 4.8c (high frequency noise has been filtered in Fig. 4.8c). The terraces remain flat and homogeneous after exposure to 2-MBT, and the step edges keep a similar form as before exposure. Local defects are always present on the terraces with similar height compared to that measured on the pre-oxidized copper surface before exposure. No ordered local structure was observed.

Compared to the multilayer-covered surface obtained by exposing clean, metallic Cu(111) to 2-MBT (Fig. 4.5 and Fig. 4.6), the terrace topography is more compact and uniform on the pre-oxidized surface, indicating that the last molecular layer is almost complete. So we can conclude that pre-oxidation of copper prior to exposure can effectively change the morphology of the adsorbed 2-MBT multilayer. It appears likely that the Cu atoms released by the dissociation of the 2D copper oxide favor the formation of a more homogeneous and compact multilayer of 2-MBT.
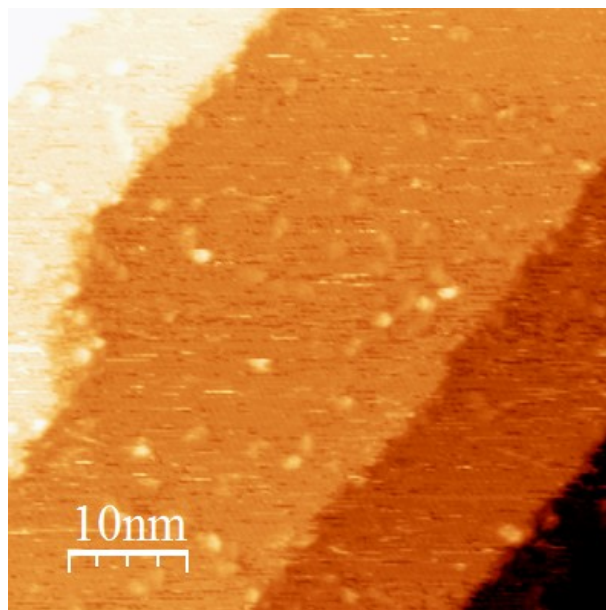
Figure 4.9: STM image of clean Cu(111) surface exposed to MBT (saturation) after annealing at 160°C (50 nm × 50 nm, $V = -1.0$ V, $I = 0.2$ nA).

4.4.3   Thermal stability of 2-MBT layers

In order to test the stability of the adsorbed molecular layer, annealing at different temperatures was carried out for multilayer deposited on metallic and pre-oxidized Cu(111) surfaces, which were then characterized by STM and LEED after annealing.

Fig. 5.10 shows that the topography of clean Cu(111) surface saturated with 2-MBT changes after annealing at 160°C. Reorganization of the steps can be observed, with the formation of straight and parallel step edges. The step edges become aligned along the principal direction of the surface layer, as can be seen from the comparison of Fig. 5.10 and Fig. 4.10a. Moreover, bright spots can be evidenced on the terraces, with size of 1–2 nm, and height of about 1 Å. They may be assigned to the decomposition products after annealing.

If we zoom in on a terrace (Fig. 4.10a), we can see that the $(\sqrt{7} \times \sqrt{7})$R19.1° structure is formed, also confirmed by FFT (Fig. 4.10b). This is the characteristic structure obtained when Cu(111) surface is exposed to atomic S until saturation [110, 111]. The annealing tests were performed at different temperatures, and the $(\sqrt{7} \times \sqrt{7})$R19.1° structure was observed once the sample was heated above 100°C, also confirmed by LEED as shown in Fig. 6.12d. Two overlapped mirror domains are observed by LEED, as indicated in Fig. 4.10d. Mirror domains are also observed in STM images obtained from different area on the surface. Taking into account the possible elements present on the surface (S, C, N, O) measured by AES, we can deduce that 2-MBT dissociates when heated to temperatures above 100°C, and atomic S remains adsorbed on the copper surface. The same phenomenon is observed on pre-oxidized Cu(111) surface saturated with 2-MBT after
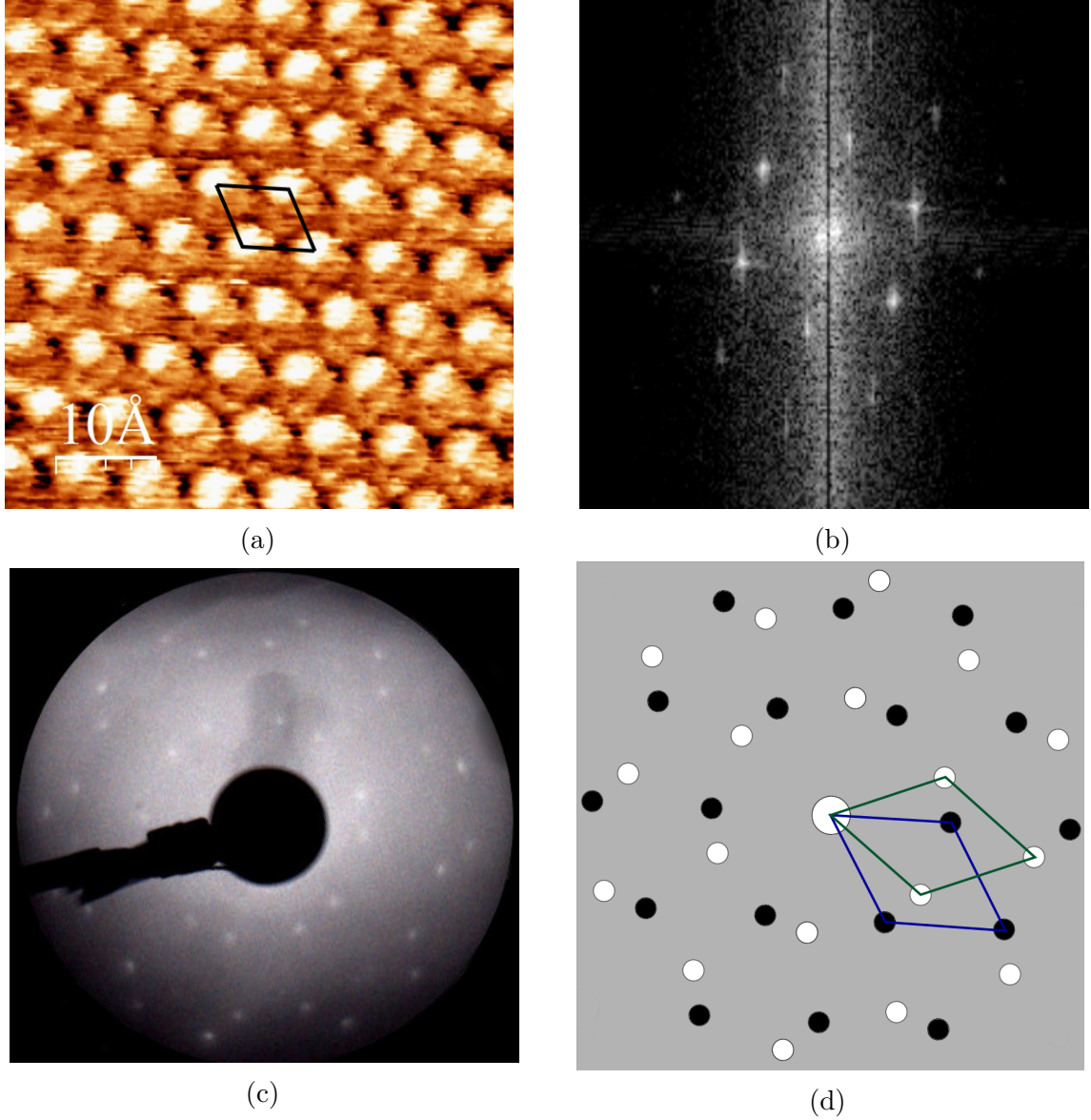
Figure 4.10: Clean Cu(111) surface exposed to MBT (saturation) after annealing (a) at 160°C observed by STM (5 nm × 5 nm, $V = -0.1$ V, $I = 2.5$ nA); (b) FFT of (a); (c) at 200°C observed by LEED (Ep = 50 eV); (d) schematics with the unit cells associated with the two variants of the superstructure.

annealing at temperatures superior to 100°C, indicating the decomposition and partial desorption of molecular layers adsorbed on pre-oxidized Cu(111) surface.

4.5   Conclusions

In this study, the morphology and structure of 2-MBT layers adsorbed on metallic and pre-oxidized Cu(111) surfaces at room temperature and their thermal stability were investigated by AES and STM in order to bring nanometric and atomic scale insight on the interaction of the molecule with copper, which is of paramount importance for its corrosion inhibition properties. On clean, metallic Cu(111) surface, local $(\sqrt{7} \times \sqrt{7})$R19.1° ordered triangular structures, typical of atomic S adsorption on Cu(111), are observed at low exposures, suggesting a partial decomposition of 2-MBT and adsorption of atomic S on Cu(111). 2-MBT forms a monolayer of adsorbed molecules at an exposure of about 10 L which is almost lying flat on copper. A non ordered 2-MBT multilayer is formed at higher exposure, with an incomplete outermost molecular layer of thickness of 1.3 Å and of surface covered fraction of 55%. Taking into account the dimension of 2-MBT, we can conclude that the outermost molecules adsorb flat on the surface.

When Cu(111) is pre-oxidized and covered by a 2D surface oxide layer, the sample surface remains flat and homogeneous after 2-MBT dosing, and the last molecular layer formed is complete. The 2D oxide layer is replaced by 2-MBT and the presence of Cu atoms from the dissociated 2D oxide promotes a homogeneous morphology of the molecular layer with a local structure that remains non ordered.

The stability of the molecular multilayer adsorbed on clean and pre-oxidized Cu(111) surfaces was investigated by annealing. In both cases, when the sample was heated above 100°C, the step edges are reorganized, and the surface is completely covered by a $(\sqrt{7} \times \sqrt{7})$R19.1° structure, typical of S/Cu(111) system at saturation, indicating the decomposition and partial desorption of 2-MBT and the adsorption of S atoms on the sample surface.

CHAPTER 5

2-MBI DEPOSITION ON PRISTINE AND PRE-OXIDIZED Cu(111) SURFACES AT ROOM TEMPERATURE

5.1 Abstract

2-mercaptobenzimidazole (2-MBI) is considered as an effective corrosion inhibitor for copper. In this study, the adsorption of 2-MBI on pristine and pre-oxidized Cu(111) surfaces was investigated by sublimation at ultra low pressure, using Auger Electron Spectroscopy, Scanning Tunneling Microscopy and X-ray Photoelectron Spectroscopy in order to understand its corrosion inhibition properties. 2-MBI adsorbs with S and N atoms bonded to Cu. On pristine Cu(111) surface, a self-assembled monolayer is formed at about 5 L, with the adsorption of atomic S resulting from molecule decomposition to form a $(\sqrt{7} \times \sqrt{7})$R19.1° structure, and that of the molecule forming a (8×8) structure. 2-MBI is lying flat in the adsorbed multilayer. Oxidation of copper prior to exposure results in compact and homogeneous molecular films, with dissociation and substitution of 2D oxide by 2-MBI, but much more slower than that for 2-mercaptobenzothiazole (2-MBT). A multilayer of 2-MBI can block the initial stages of oxidation of copper under low oxygen pressure at room temperature, and the molecular layer is stable until 500°C. The comparison with 2-MBT suggests that the latter is a better corrosion inhibitor for copper at room temperature.
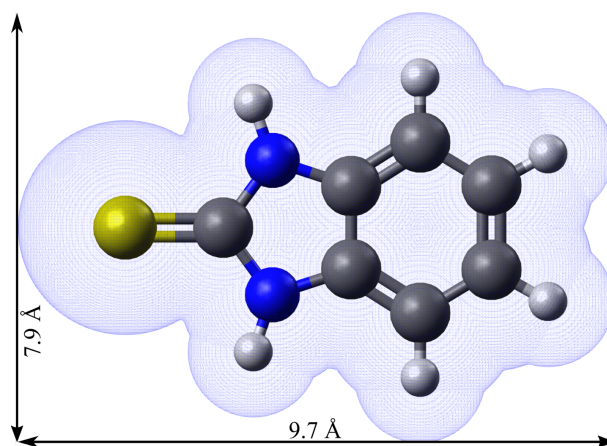
Figure 5.1: 2-MBI chemical structure (thione form) and associated molecular dimensions (the van der Waals surface is presented).

5.2 Introduction

Corrosion is one of the main causes of alteration and destruction of most facilities and equipments. Copper corrosion can cause huge economic losses due to the wide applications of copper and copper alloys in the industrial, military and civilian sectors, and thus it is particularly important to find a way to limit that phenomenon. The use of corrosion inhibitor has been proven to be an effective approach to control the corrosion of metals and alloys which are in contact with aggressive environments [29–33].

It is commonly believed that, for inhibition to function, adsorption of the inhibitory molecules on the substrate surface must take place, that the interaction must be strong and that a protective film must be formed. Azole derivatives such as 2-mercaptobenzimidazole (2-MBI, $C_7H_6N_2S$) are very often used as corrosion inhibitors for copper and have a remarkable efficiency under certain conditions [3, 39, 40].

2-MBI exists in two forms: the thione and the thiol forms. The former has C double bonded to S, and the latter C double bonded to endocyclic N with hydrogen bonded to S. The thione form is the preferred form of 2-MBI in solid and gaseous phase [63, 64]. The bond lengths and angles of 2-MBI have been determined [64], and by considering the van der Waals radii of different atoms, its molecular dimensions can be deduced (see Fig. 5.1).

Research has been carried out mostly on the metal/solution interface [52, 65–71], indicating that the chemisorption of 2-MBI on copper surface forms a polymeric film which can protect it from corrosion. There are two nitrogen atoms and one sulfur atom in the 2-MBI molecule, which can concurrently or individually bond to the metal surface [65, 72]. Finšgar et al. [69, 70] confirmed that 2-MBI molecules are bonded to Cu through their N and S atoms on the oxidized copper surface, tilted relatively to the sample surface, as observed previously by Tooru [73]. Xue et al. [65, 67] reported that 2-MBI is bonded to metallic copper through sulfur atom and the chemisorption is accompanied by a cleavage

of the C=S bond, not observed on oxidized copper surface. Hosseini et al. [74] investigated the adsorption of 2-MBI on a less reactive metal surface, namely Au(111), and showed the formation of flat-lying molecules in the monolayer.

Molecular deposition by evaporation under ultra-high vacuum (UHV) can also be used as an approach to understand the molecule/surface interaction [37, 38]. Density functional theory studies suggest that 2-MBI neutral molecules in gaseous phase can chemisorb perpendicularly on the surface through N–Cu or S–Cu bond and physisorb almost parallel to the surface [37, 75], and that a monolayer of MBI adopting a $(\sqrt{7} \times \sqrt{7})$R19.1° superstructure could form [112]. Despite these experimental and theoretical studies on copper corrosion inhibition by 2-MBI, the inhibition mechanism is not yet fully ascertained, neither the chemical nature of the resulting inhibitor films is completely established.

In this study, the adsorption of 2-MBI under ultra-low pressure (ULP) at room temperature on pristine and pre-oxidized Cu(111) surfaces by sublimation was investigated using Auger Electron Spectroscopy (AES), Scanning Tunneling Microscopy (STM), and X-ray Photoelectron Spectroscopy (XPS). The corrosion inhibition efficiency and thermal stability of the adsorbed molecular layers were examined.

Previously, we have investigated the adsorption of another structurally related inhibitor, 2-mercaptobenzothiazole (2-MBT), on Cu(111) surfaces using a similar approach [89, 113]. The molecule was found to adsorb flat with S bonded to Cu, accompanied by a partial decomposition on metallic Cu(111). In this work, a comparative discussion will be included for better understanding of corrosion inhibition mechanisms, and to provide a rational basis for the design of new inhibitors.

5.3   Experimental

In this study, a high purity (99.999%) Cu(111) single-crystal was used. The surface was mechanically polished down to 0.25 μm (diamond paste), and then electro-polished in 60 wt% H_3PO_4 solution at 1.4 V during 5 min, followed by annealing under H_2 flow at 725 °C during 20 h to reconstruct and recrystallize the surface. It was then introduced into the UHV system for further preparation by cycles of ion sputtering ($P_{Ar} = 1 \times 10^{-5}$ mbar, 600 V, 20 mA, 30 min) and annealing (600°C, 30 min) in order to obtain a clean and well-structured surface. The base pressure of the UHV system is 10^{-10} mbar, and it is equipped with STM (Omicron, STM1 with SCALA system), AES (Omicron, model CMA-100) and Low Energy Electron Diffraction (LEED, Omicron, spectaLEED). The surface was systematically checked by AES, LEED and STM until no contamination and a good surface organization were observed, characterized by a sharp (1×1) LEED pattern and a topography with large and flat terraces as verified by STM.

2-MBI molecule was purchased from Sigma-Aldrich. It is a white to beige powder with a purity higher than 98%. The 2-MBI powder was placed in a vacuum sealed glass

connected directly to a reactor attached to the UHV system. The pressure of 2-MBI in the reactor was 10^{-9} mbar at room temperature. The sample was kept at room temperature during the deposition process. Pre-oxidation of the copper surface was performed by introducing oxygen gas in the main chamber through a leak valve ($P_{O_2} = 5 \times 10^{-6}$ mbar) until saturation. In these conditions, a 2D surface oxide is formed [87, 106, 107]. The growth kinetics of 2-MBI on clean and pre-oxidized copper surfaces was followed by AES, and the surface structure changes were characterized by STM.

The STM measurements were performed at room temperature and in constant current mode. Image processing was carried out using WSxM software (5.0 Develop 9.1) [80]. No filtering was applied. All images were corrected by plane subtraction.

In order to determine the chemical composition of adsorbed molecular layers, the sample after 2-MBI deposition was transferred quickly to another UHV platform, equipped with XPS (Thermo Electron Corporation, ESCALAB 250) of base pressure of 10^{-10} mbar. A monochromatic Al K_α source (1486.6 eV) was used and the binding energy was referenced by measuring the Fermi level position of the sample. The transmission of the analyzer was calibrated by measurement of reference samples. The survey spectra were recorded with a pass energy of 100 eV corresponding to an overall resolution of 1.8 eV, the high resolution spectra were recorded with a pass energy of 20 eV corresponding to an overall resolution of 360 meV. The take-off angle of the analyzed photoelectrons was 90°. The data processing was carried out using the CasaXPS software (version 2.3.19) [82].

5.4   Results and discussion

5.4.1   2-MBI deposition on pristine Cu(111)

A pristine Cu(111) surface was prepared as described previously, 2-MBI exposure was then performed at ULP (1×10^{-9} mbar) at room temperature and the growth kinetics was followed by AES. The peak-to-peak height ratios of S (151 eV), C (271 eV) and N (380 eV) to Cu (920 eV) signals were recorded and corrected by the relative sensitivity S_x of the Auger transitions. The normalized ratios are proportional to the atomic densities of each element, and plotted as a function of exposure to 2-MBI. The results are shown in Fig. 5.2.

We can see from the growth kinetics curves that the C, S and N signals increase firstly with increasing exposure, indicating the adsorption of 2-MBI on copper. A decrease of the adsorption rate is then observed, and finally a stationary regime is reached at an exposure of about 110 L, indicating a copper surface saturated with 2-MBI.

In order to verify the stoichiometry of the molecule in the adsorbed layer, the atomic ratios of S and N to C were calculated, and were compared to the theoretical (molecule stoichiometry) values. At early stage of growth, the N to C atomic ratio increases rapidly
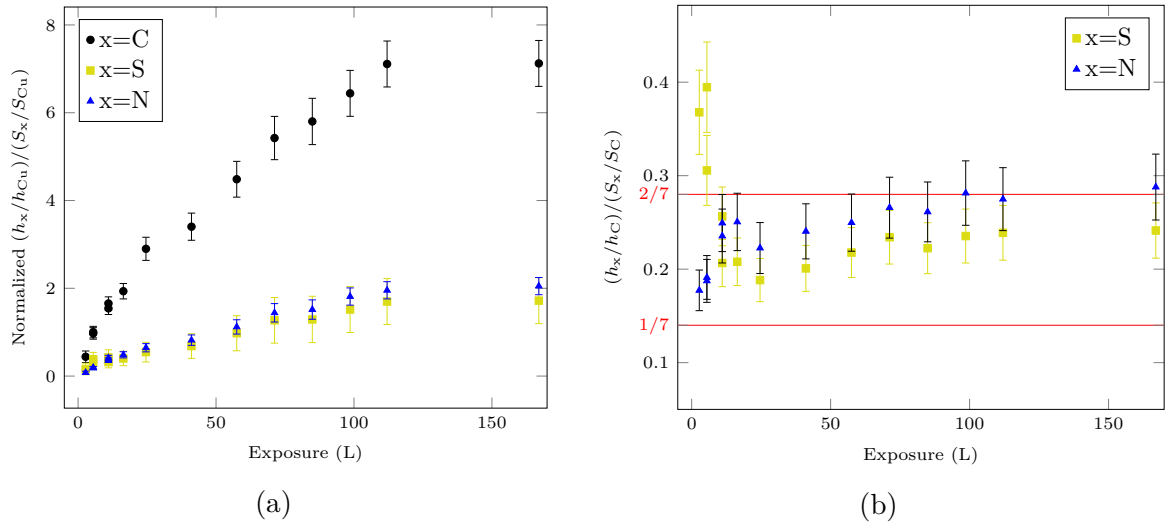
Figure 5.2: Growth kinetics of 2-MBI on pristine Cu(111) at room temperature: (a) change in the normalized AES peak-to-peak height ratios as a function of 2-MBI exposure at 1×10^{-9} mbar and RT; (b) evolution of S and N to C atomic ratios with 2-MBI exposure.

with increasing exposure, and stabilize at the theoretical value (2/7) within the error bars after about 11 L. At the same time, a fast decrease of the S to C atomic ratio was observed, followed by a slight increase to stabilize at about 1.5 times the theoretical value (1/7). This seems to indicate that there is a transition in the growth mode of 2-MBI at about 11 L, and the excess of S suggests that the molecule may partially decompose when adsorbed on metallic Cu(111). Similar results were observed on 2-MBT, with a saturation regime reached at about 100 L and an excess of S attributed to the decomposition of 2-MBT [89].

The surface topography after different exposures was characterized by STM. After an exposure of 5 L, STM images show the formation of self-assembled monolayer on Cu(111), as can be seen in Fig. 5.3. The surface remains flat and homogeneous. Different structures coexist on the sample surface, and the lattice unit cell is marked by the black rhombus. A $(\sqrt{7} \times \sqrt{7})$R19.1° structure is formed as shown in Fig. 5.3a. This is the characteristic structure formed by atomic S on Cu(111) surface at saturation [110, 111], suggesting the adsorption of atomic S resulting from molecular decomposition. This could explain the excess of S observed by AES. A long-range hexagonal structure with lattice parameter of 2.0 ± 0.2 nm is observed, as shown in Fig. 5.3b, and is assigned to a (8×8) structure. Images of different aspects are observed at different applied potentials, and only one is chosen to be presented. The size of one pattern is 1.5 ± 0.3 nm, which is 2–3 times the size of one 2-MBI molecule. Thus the (8×8) structure may correspond to the adsorption of 2-MBI clusters. Moreover, a structure with lattice constant of (8.6 ± 0.2) Å $\times$ (10.7 ± 0.01) Å is also observed (Fig. 5.3c). This structure with intermediate lattice parameter may serve as a transition between the two previous structures.

Further exposure of the sample to 2-MBI up to 11 L leads to the formation of a second molecular layer, as can be seen in Fig. 5.4. This is in good agreement with AES
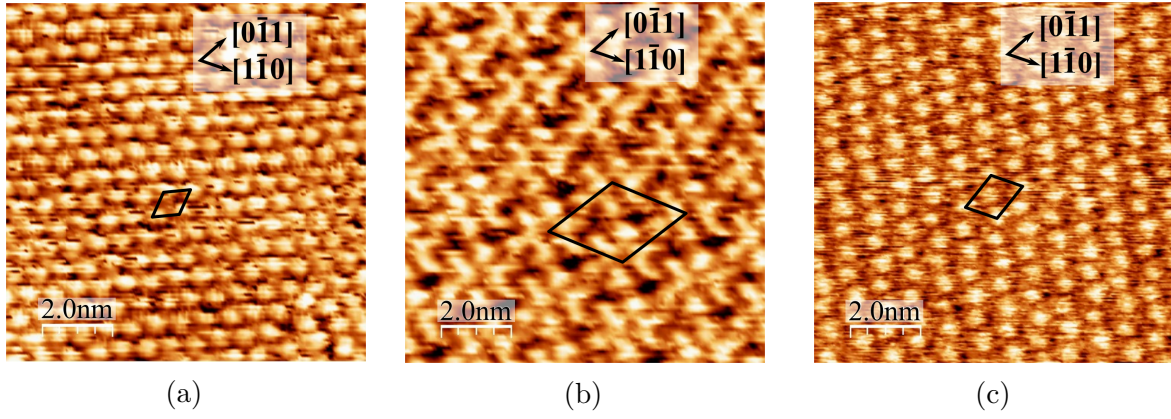
Figure 5.3: Drift-corrected STM images for 5 L of 2-MBI on Cu(111) obtained at different locations on the surface: (a) $(\sqrt{7} \times \sqrt{7})$R19.1° structure (10 nm × 10 nm, $V = -1.5$ V, $I = 2.0$ nA); (b) (8×8) structure (10 nm × 10 nm, $V = -1.5$ V, $I = 2.0$ nA); (c) 10 nm × 10 nm, $V = 2.0$ V, $I = 1.5$ nA. Main directions of the Cu surface are indicated as well as the superstructure unit cell formed by the adsorbate.
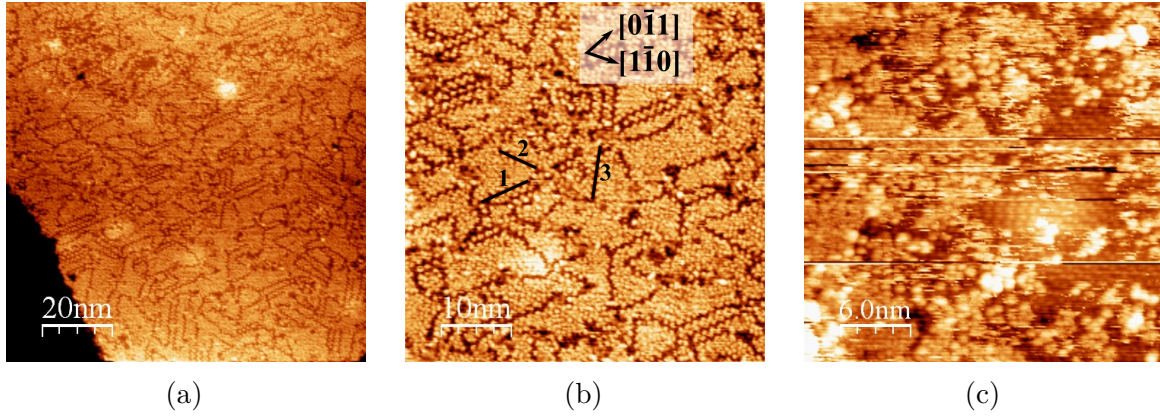
Figure 5.4: STM images for 11 L of 2-MBI on Cu(111): (a) 100 nm × 100 nm, $V = -1.5$ V, $I = 0.5$ nA; (b) 50 nm × 50 nm, $V = -1.5$ V, $I = 0.5$ nA; (c) 30 nm × 30 nm, $V = -1.0$ V, $I = 1.0$ nA.

measurements (Fig. 5.2) showing a change of slope at 11 L. The surface is always flat with large terraces, and the second layer is incomplete, with domains delimited by dark lines following three preferential directions, as indicated in Fig. 5.4b. The two directions marked '1' and '2' are orientated along the principal direction of the (8×8) structure formed on the first monolayer underneath, and the direction '3' is closer to the principal direction of the $(\sqrt{7} \times \sqrt{7})$R19.1° structure. Moreover, local order can be observed but no obvious long range ordering was evidenced by Fast Fourier Transform (FFT) of the second layer.

Fig. 5.4c is a zoom in on a different region in the second layer, and we can see the self-assembled monolayer underneath. No ordered structure is observed by FFT. The apparent height difference between the first and second layer is measured by a profile,
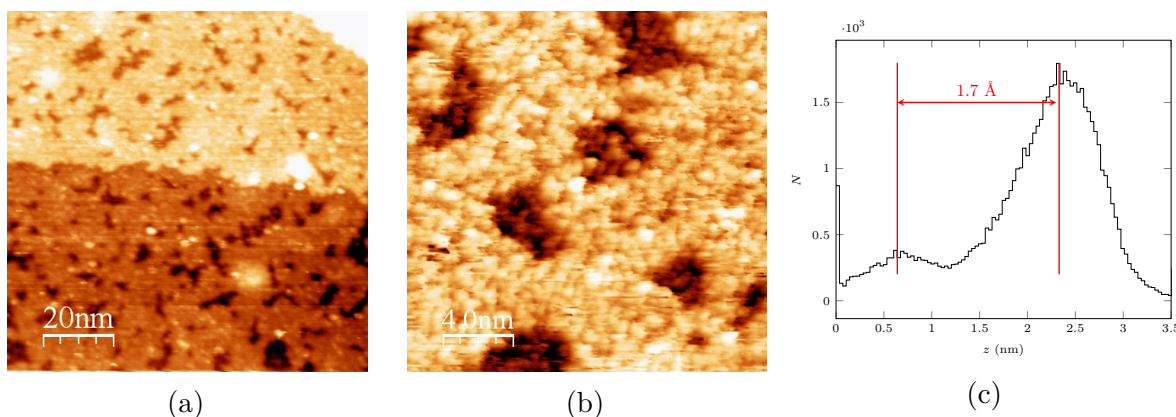
Figure 5.5: STM images for 2-MBI exposure on Cu(111): (a) 41 L (100 nm × 100 nm, $V = 1.5$ V, $I = 0.5$ nA); (b) 57 L (20 nm × 20 nm, $V = -1.8$ V, $I = 0.3$ nA); (c) Height histogram of image (b).

giving a thickness of about 1.2 Å. Taking into account the dimension of the molecule, 2-MBI lies flat in the second layer with its plane almost parallel to the sample surface.

At higher exposure, multilayers of 2-MBI were formed on Cu(111). FFT did not reveal any ordered local structure. The surface becomes rougher but we can still see different terraces. The outermost molecular layer is always incomplete, as shown in Fig. 5.5a and Fig. 5.5b. This contrast corresponds to the difference in height, i.e. the thickness of the outermost molecular layer. The height distribution of Fig. 5.5b was plotted with a bin size of 35 pm, as shown in Fig. 5.5c, and gives a layer thickness of 1.7 Å as well as a surface covered fraction of $86 \pm 1\%$ by the incomplete outermost layer. Taking into account the molecular dimensions of 2-MBI, this indicates that the 2-MBI in the outermost molecular layer adsorbs with its plane almost parallel to the sample surface.

Once the surface topography at different exposures was determined by STM, XPS analyzes were then performed on monolayer (5 L) and multilayer (167 L) of 2-MBI in order to characterize their chemical composition, and the results are shown in Fig. 5.6. The S 2p spectra were decomposed using spin-orbit doublets S $2p_{1/2}$ and S $2p_{3/2}$, with a branching ratio of 0.5 and spin-orbit splitting of 1.18 eV [45, 54]. The S 2p spectrum of the 2-MBI monolayer is composed of a S_2 component, with the $2p_{3/2}$ at 161.8 eV. This component is slightly shifted to higher binding energy (0.4 eV) compared to that observed for a 2-MBT monolayer adsorbed on Cu(111) [113]. This may be explained by the surface oxidation during transfer to XPS which modifies the chemical environment of 2-MBI in the adsorbed monolayer. Taking into account the AES and STM observations, S_2 is assigned to S bonded to metallic Cu, both in the atomic form and in the intact molecule, as also observed for 2-MBT [113]. As for 2-MBI multilayer, the S_2 component at 161.5 eV is also observed, with higher intensity compared to that obtained on Cu(111) with a 2-MBI monolayer, suggesting that the molecules are also bonded to copper in the multilayer, probably due to a reconstruction of the copper substrate. Moreover, another component
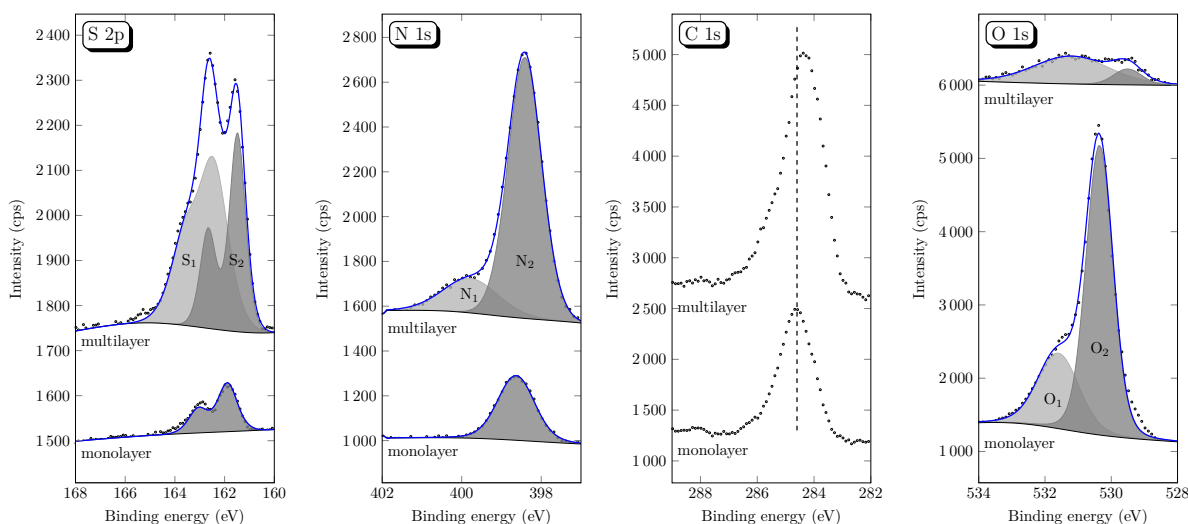
Figure 5.6: XPS spectra of the S 2p, N 1s, C 1s and O 1s core levels after 2-MBI exposure on metallic Cu(111) surface at 1×10^{-9} mbar and RT.

S_1 is observed at binding energy of 162.4 eV for $2p_{3/2}$. This agrees with the position of 2-MBI reported previously [70, 73] and with that of the exocyclic S in 2-MBT [113]. S_1 is thus assigned to S in the 2-MBI molecule non bonded to Cu in the multilayer.

Analysis of the N 1s spectra gives a component N_2 at 398.6 eV in the monolayer of 2-MBI, with full width at half maximum (FWHM) of 1.0 eV. The intensity of this component increases in the multilayer, with appearance of another component N_1 at 399.8 eV with larger FWHM. However, the N 1s peak for the 2-MBI crystalline powder presents only one component at 400.5 eV [70, 73]. It is difficult to determine the nature of N_1 component, but the shift to lower binding energy of N_2 component (1.9 eV) observed in the monolayer and multilayer of 2-MBI suggests that N atoms are involved in the surface interaction with copper, acting as electron acceptor. Similar phenomenon has been observed for 2-MBI interaction with copper in solution [70].

Moreover, because of non-obvious peak separation and the interaction of the molecule with copper leading to a partial decomposition of 2-MBI, as well as the influence of transfer to air, the decomposition of C 1s region does not give reliable information and is thus not performed. The small peak at binding energy of about 288 eV is assigned to carboxylic groups (air contamination). The O 1s spectrum of the 2-MBI monolayer shows two components O_1 and O_2, at binding energies of 531.6 eV and 530.4 eV, respectively. O_2 component is usually attributed to a bulk oxide ligands, and O_1 may be assigned to the OH groups resulting from dissociative adsorption of water and/or oxygenated contaminations [114, 115]. The intensity of the O 1s spectrum decreases to 1/4 with 2-MBI multilayer, indicating a better protection of copper compared to the monolayer. The stronger oxidation of copper with 2-MBI monolayer results in an enhanced attenuation of the molecular layer, thus a decrease in the intensity of the S 2p and N 1s spectra.
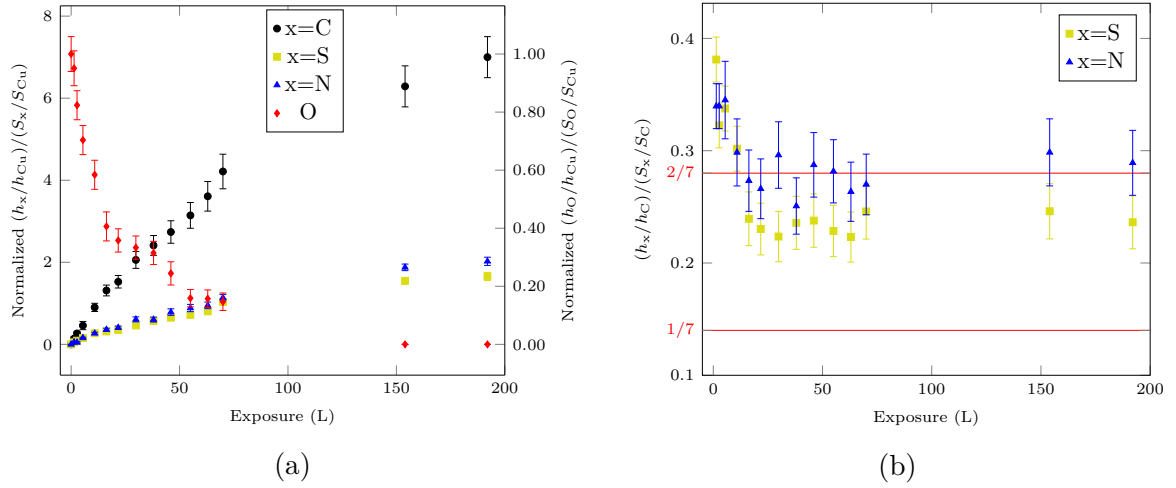
Figure 5.7: Growth kinetics of 2-MBI on pre-oxidized Cu(111) at room temperature: (a) change in the normalized AES peak-to-peak height ratios as a function of 2-MBI exposure at 1×10^{-9} mbar and RT; (b) evolution of S and N to C atomic ratios with 2-MBI exposure.

By assuming a homogeneous and continuous layer of 2-MBI and by applying the same method as in Ref. [113], we estimate an equivalent thickness of the 2-MBI multilayer to be 1.0 ± 0.2 nm, corresponding to 7 ± 2 layers of 2-MBI given the thickness of one layer of 1.5 ± 0.3 Å measured previously by STM. This is almost 2 times that formed by 2-MBT. Note that the presence of oxygen in the 2-MBI multilayer is neglected for the calculation.

5.4.2   2-MBI deposition on pre-oxidized Cu(111)

In order to investigate the influence of oxygen on the adsorption of 2-MBI, a pre-oxidized Cu(111) surface was prepared as described above, then the surface was exposed to 2-MBI at ULP (1×10^{-9} mbar). The growth kinetics of 2-MBI on pre-oxidized Cu(111) surface was followed by AES. Fig. 5.7 shows the change in the peak-to-peak height ratios of S (151 eV), C (271 eV) and N (380 eV) to Cu (920 eV) signals as a function of exposure to 2-MBI.

Firstly, we can see that the S, C and N signals increase with increasing exposure, indicating the growth of 2-MBI layer on the pre-oxidized copper surface. Then a saturation regime is reached, characterized by the plateau in the S, C and N signals. The surface is saturated with 2-MBI after an exposure of about 190 L. No significant change is observed compared to the growth kinetics of 2-MBI on metallic Cu(111). However, compared to the adsorption of 2-MBT which reaches its saturation regime at about 50 L on pre-oxidized Cu(111) [89], a much slower growth kinetics is evidenced for 2-MBI.

Meanwhile, the normalized $(h_O/h_{Cu})/(S_O/S_{Cu})$ signal decreases continuously with increasing exposure until a total disappearance of oxygen at an exposure of about 150 L, indicating the substitution of oxygen by 2-MBI at room temperature taking into account the inelastic mean free path of oxygen and copper Auger electrons. The same phenomenon has been observed for 2-MBT and H$_2$S exposure on pre-oxidized Cu(111) [89, 92]. However,

(a)   (b)
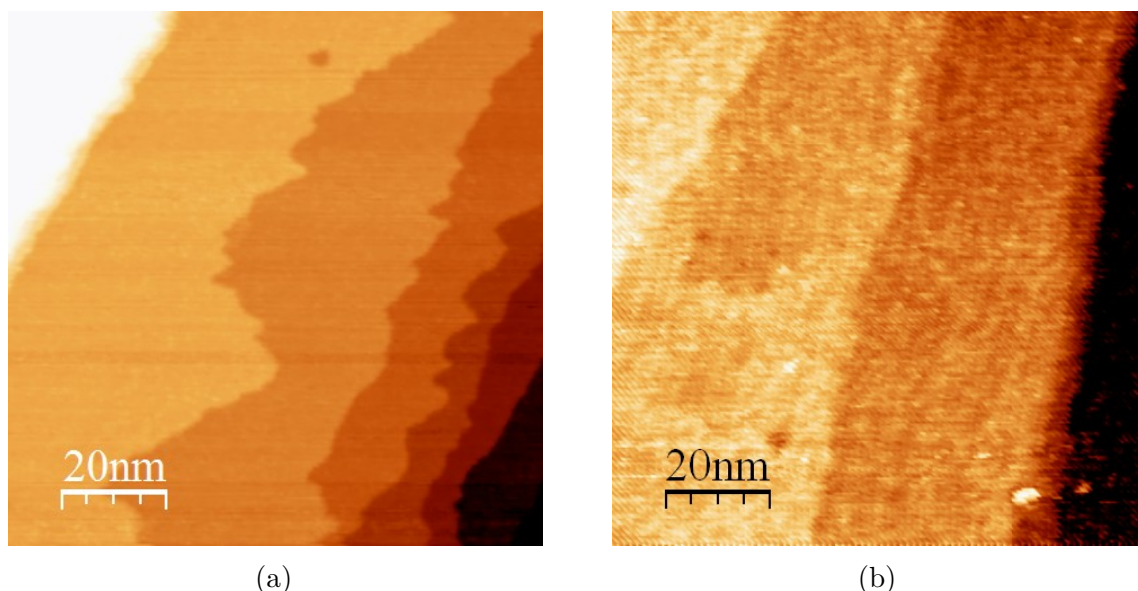
Figure 5.8: STM images of pre-oxidized Cu(111) surface: (a) before exposure to 2-MBI (100 nm × 100 nm, $V = 1.0$ V, $I = 0.2$ nA); (b) after 11 L of 2-MBI (100 nm × 100 nm, $V = 1.0$ V, $I = 0.3$ nA).

in the case of 2-MBT, oxygen desorbs completely at about 25 L. This indicates that 2-MBT is more reactive on pre-oxidized copper surface.

Similarly, the atomic ratios of S and N to C in the adsorbed layer were calculated, and were compared to the theoretical (molecule stoichiometry) values. The S and N to C ratios decrease firstly and reach a stationary regime at about 16 L, with a N to C ratio close to the theoretical value (2/7), confirming the adsorption of 2-MBI, and a S to C ratio about 1.5 times the theoretical value (1/7), suggesting a partial decomposition of 2-MBI. Compared to the deposition on metallic Cu(111), the high values of N to C ratio in the early stage of growth may be assigned to geometric effects due to the difference in the film structure, i.e. the relative orientation of the molecule compared to the sample surface.

The surface topography before and after molecule deposition was characterized by STM, as shown in Fig. 5.8. The STM image of the pre-oxidized surface (Fig. 5.8a) confirms the formation of a flat bi-dimensional copper oxide covering the atomically flat substrate terraces, accompanied by a reconstruction of the step edges. The oxide takes the form of the '29' superstructure. After 2-MBI deposition (Fig. 5.8b), no remarkable change of the surface morphology is observed. The step edges becomes straight, but the terraces remain flat and homogeneous. The influence of noise on the image can be observed but no ordered local structure is evidenced, even when zoom in on one terrace. Moreover, compared to the adsorption of 2-MBI on metallic Cu(111) which leads to the formation of an incomplete outermost molecular film, pre-oxidation of copper prior to exposure effectively change the morphology of the adsorbed 2-MBI layer by forming a complete molecular film.

The chemical composition of multilayer (191 L) of 2-MBI adsorbed on pre-oxidized Cu(111) was characterized by XPS, and is shown in Fig. 5.9. The S 2p spectrum
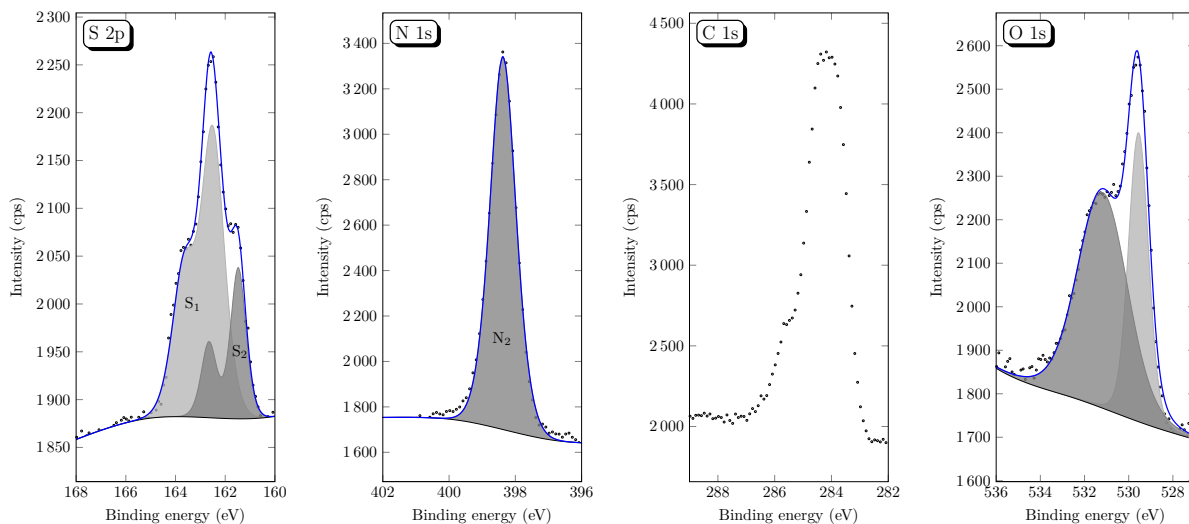
Figure 5.9: XPS spectra of the S 2p, N 1s, C 1s and O 1s core levels after 191 L 2-MBI exposure on pre-oxidized Cu(111) surface at 1×10^{-9} mbar and RT.

shows the presence of two components S_1 and S_2, with the $2p_{3/2}$ at 162.5 eV and 161.5 eV, corresponding to S in the non bonded molecule and S bonded to Cu, respectively. Compared to the 2-MBI multilayer adsorbed on metallic Cu(111), the total intensity of S 2p spectrum decreases to half, mainly associated to the decrease of the S_2 component, accompanied by a decrease in the FWHMs of S_1 and S_2 components, indicating a difference in the structure of the adsorbed layer. This decrease in the intensity of S bonded to Cu may be explained by a reduced decomposition of the molecule. The N 1s spectrum shows a component N_2 at 398.4 eV as for adsorption on metallic Cu(111), indicating an interaction of N with Cu. As previously, the decomposition of C 1s spectrum is not performed, but a slight shift of 0.2 eV to lower binding energy is observed. The intensity of the O 1s spectrum is 1.6 times that obtained on metallic Cu(111) with 2-MBI multilayer, but remains low compared to that with 2-MBI monolayer. Similarly, the equivalent thickness of the 2-MBI multilayer was estimated to be 0.6 ± 0.1 nm, which is thinner than that formed on metallic Cu(111). This decrease in layer thickness contributes to a decrease in the attenuation of the layer underneath, which confirms a lower concentration of S bonded to copper on pre-oxidized surface.

5.4.3 Thermal stability of 2-MBI multilayer

The stability of the 2-MBI multilayer adsorbed on metallic Cu(111) was investigated by annealing at different temperatures, and the surface was characterized by AES and STM. After annealing at 200°C (Fig. 5.10a), reorganization of the sample surface is observed. The step edges are realigned, and the molecular layer becomes flat and homogeneous. The outermost molecular layer is more compact.

<p style="text-align:center">(a)　　　　　　　　　　　　　　　　　(b)</p>
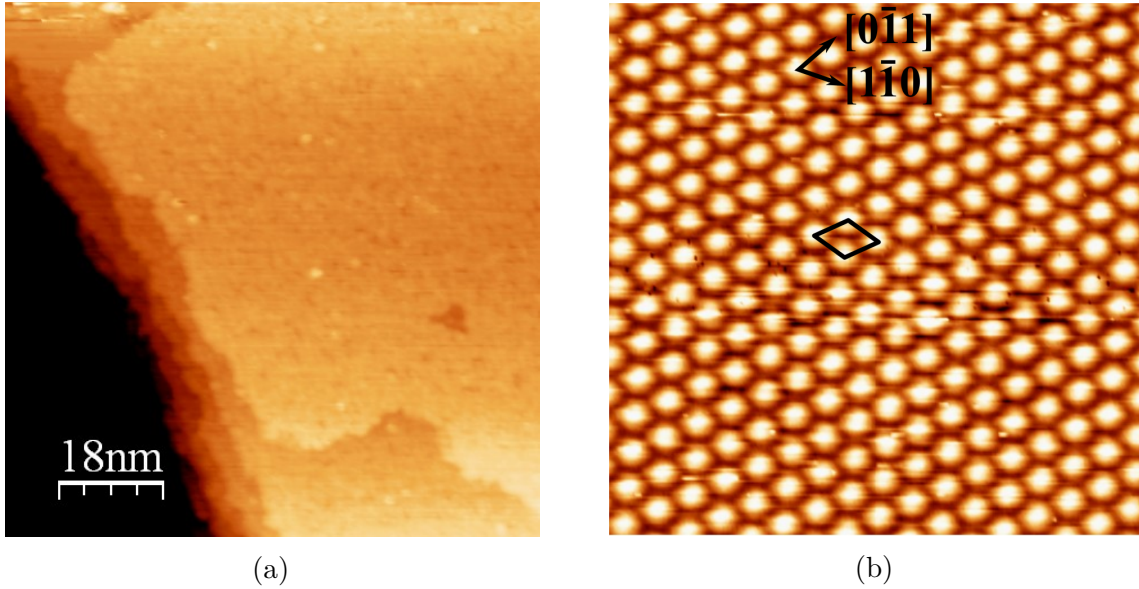
Figure 5.10: STM images of 2-MBI multilayer on metallic Cu(111) surface (a) after annealing at 200°C (90 nm × 90 nm, $V = 0.5$ V, $I = 0.5$ nA); (b) after annealing at 500°C (10 nm × 10 nm, $V = 0.8$ V, $I = 0.3$ nA), main directions of the Cu surface and the $(\sqrt{7} \times \sqrt{7})$R19.1° superstructure unit cell are indicated.

Further annealing results in the formation of an overall $(\sqrt{7} \times \sqrt{7})$R19.1° structure at temperature above 500°C (Fig. 5.10b), corresponding to the adsorption of atomic S on copper. This indicates a dissociation of 2-MBI after annealing above 500°C, and the adsorption of atomic S on Cu(111). No change is evidenced by AES until 500°C. Compared to 2-MBT multilayer which decomposes at 100°C [89], a higher stability is evidenced for 2-MBI. This is consistent with a higher adsorption energy of 2-MBI obtained by DFT calculation [112].

5.4.4　Oxidation inhibition by 2-MBI adsorbed on Cu(111)

In order to test the inhibition efficiency of 2-MBI, the oxidation kinetics of Cu(111) with pre-adsorbed 2-MBI monolayer (5 L) and multilayer (167 L) were recorded at $P_{O_2} = 5 \times 10^{-6}$ mbar at room temperature by AES, and the results are shown in Fig. 5.11.

In the presence of a pre-adsorbed 2-MBI monolayer, a slight increase in the oxygen intensity is observed, much slower compared to the oxidation kinetics of metallic Cu(111) [87, 113]. Since the value of h_O/h_{Cu} is ~ 0.22 for the 2D oxide layer formed on Cu(111) at saturation, the oxide coverage on Cu(111) with pre-adsorbed 2-MBI monolayer at an oxygen exposure of 10^4 L is about 20%. This small oxidation may be explained by the presence of local defects in the 2-MBI monolayer. However, with pre-adsorbed 2-MBI multilayer, no oxygen uptake is observed. The comparison between the oxidation kinetics with and without pre-adsorbed 2-MBI indicates that a multilayer of 2-MBI can effectively protect the copper surface from oxygen adsorption in these conditions of temperature and
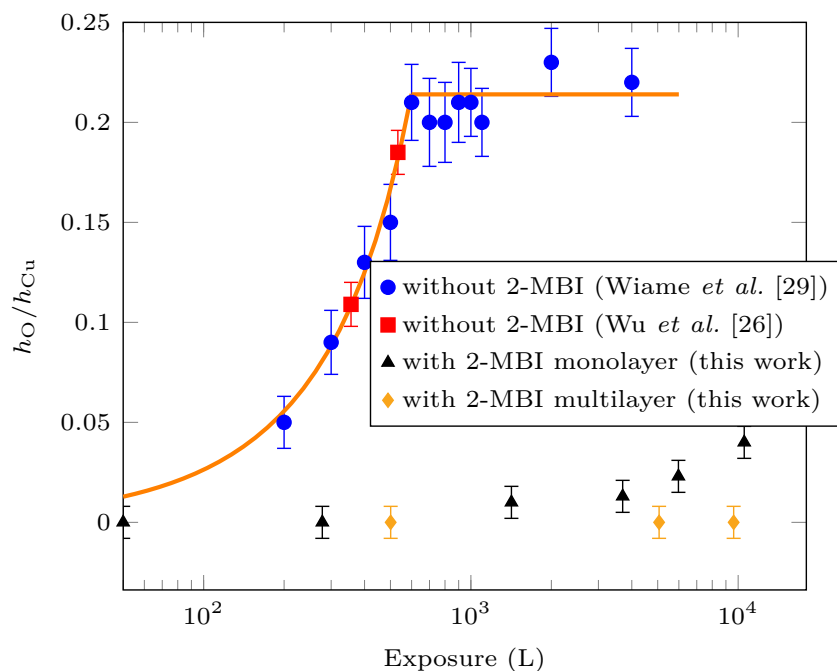
Figure 5.11: Oxidation kinetics of Cu(111): effect of adsorbed 2-MBI monolayer (5 L) and multilayer (167 L) at RT prior to oxidation.

pressure, and thus prevent the the initial stages of oxidation of copper. The molecule may prevent the dissociation of oxygen by blocking the oxygen adsorption sites. In the case of 2-MBT, the oxygen adsorption was blocked by a 2-MBT monolayer, with defective sites representing only about 8% of the surface area [113]. Thus 2-MBT monolayer offers a better protection against the initial stages of oxidation compared to 2-MBI.

5.5 Conclusions

This study reports the investigation of corrosion inhibition of 2-MBI on Cu at the molecular scale. Growth of molecular films on pristine and pre-oxidized Cu(111) surfaces at 1×10^{-9} mbar and room temperature was evidenced by AES, with an excess of S, suggesting a partial decomposition of 2-MBI.

On clean, metallic Cu(111) surface, STM images reveal the formation of a self-assembled monolayer at 5 L, with the coexistence of different structures including a $(\sqrt{7} \times \sqrt{7})$R19.1° structure due to the adsorption of atomic S, and a (8×8) structure which may be assigned to the adsorption of 2-MBI clusters. An incomplete second layer is formed at 11 L with a thickness of 1.2 Å, further exposure results in multilayer adsorption with incomplete topmost molecular layer of thickness of 1.7 Å, indicating flat-lying molecules on the sample surface. XPS analysis indicates that S and N both interact with copper, as confirmed by the presence of a S $2p_{3/2}$ peak at 161.7 ± 0.2 eV and a N 1s peak at 398.5 ± 0.1 eV.

2-MBI exposure on pre-oxidized Cu(111) leads to the formation of a flat, homogeneous and complete molecular layer through bonding of S and N to copper. No ordered structure is observed by STM. A substitution of oxygen in the 2D oxide layer is evidenced by AES.

A surface reorganization of the molecular layer adsorbed on metallic Cu(111) is observed at 200°C, followed by the appearance of $(\sqrt{7} \times \sqrt{7})$R19.1° structure on the whole surface, indicating the decomposition of 2-MBI at 500°C. Moreover, Cu(111) oxidizes much slower with a pre-adsorbed 2-MBI monolayer, while the presence of a multilayer of 2-MBI prevents the initial stages of oxidation of Cu(111) at low O_2 pressure and room temperature.

Finally, the comparison with 2-MBT indicates that the molecular layer formed by 2-MBI on pristine Cu(111) is more stable, but is less effective on corrosion protection due to the presence of local defects. Furthermore, 2-MBI interacts much more slowly with pre-oxidized Cu(111) surface. Thus 2-MBT may offer a better corrosion inhibition for copper at room temperature.

CHAPTER 6

2-MBT DEPOSITION ON Cu(111) SURFACE AT MILD TEMPERATURE

6.1   Abstract

The adsorption of 2-mercaptobenzothiazole (2-MBT) vapor on Cu(111) surface under ultra low pressure was investigated. For an exposure of 45 L at 150°C, a Moiré pattern was observed, resulting from the superposition of a underlying $(\sqrt{3} \times \sqrt{3})$R30° structure and an outer layer compressed by 18% and rotated by 1.2°. The Moiré pattern is rich in S bonded to Cu resulting from molecular decomposition and partial desorption, and was transformed to a $(\sqrt{7} \times \sqrt{7})$R19.1° structure when increasing the sample temperature during deposition above 250°C. This pre-adsorbed Moiré structure leads to a sharp decrease of the oxidation kinetics, better protecting copper against corrosion than the non-ordered 2-MBT monolayer formed at room temperature. Upon further exposure to 2-MBT at room temperature, an equivalent monolayer of molecule was adsorbed on the Moiré structure at saturation, whereas a multilayer is formed for direct deposition on Cu(111) at room temperature.

6.2   Introduction

2-mercaptobenzothiazole (2-MBT) is used commercially in oils, greases, and cooling fluids as a corrosion inhibitor for copper and its alloys. The molecule may be heated during application, so it is of great importance to elucidate the adsorption of 2-MBT not only at

room temperature but also at higher temperature. However, the interaction of 2-MBT with copper surface is not well understood, since in practice empirical tests are performed to evaluate the effectiveness of different compounds for industrial application. Several studies have been carried out in solution in order to investigate the inhibiting effect of 2-MBT on copper corrosion [51, 116, 117]. It is believed that 2-MBT forms a complex layer on copper through bonding with sulfur and/or nitrogen atoms, which can protect copper from corrosion. However, the inhibition mechanism of the molecular layer is still debated.

Structural aspects of molecular adsorption at model interfaces is thus of great interest. Our previous study on 2-MBT adsorption by sublimation at ultra low pressure on Cu(111) at room temperature presented the formation of non-ordered monolayer, followed by flat-lying multilayers at saturation [89]. It has been shown that 2-MBT forms a self-assembled monolayer from liquid phase, with flat-lying molecules on the Au(111) surface [96, 118, 119]. A Moiré pattern was observed for the adsorption of sulfate anions on the Cu(111) surface, accompanied by a reconstruction of the Cu(111) substrate [120]. Moreover, the adsorption of S on Cu(111) under ultra-high vacuum (UHV) has been widely studied, with the formation of various structures including $(\sqrt{3} \times \sqrt{3})$R30° and $(\sqrt{7} \times \sqrt{7})$R19.1° depending on S coverage [110, 111, 121]. A reconstruction to form a pseudo-(100) structure was also evidenced for the adsorption of nitrogen on Cu(111) [122, 123].

In this work, 2-MBT exposure on Cu(111) surface by sublimation at ultra low pressure and 150°C, and the resulting formation of an interfacial layer characterized by a Moiré pattern (thereafter denoted "Moiré structure") were investigated. The inhibition efficiency of the Moiré structure was studied by exposure to gaseous oxygen and ambient air at room temperature, as well as its effect on the buildup of 2-MBT mutilayer at room temperature. The sample surfaces were characterized by Scanning Tunneling Microscopy (STM), X-ray Photoelectron Spectroscopy (XPS), Auger Electron Spectroscopy (AES) and Low Energy Electron Diffraction (LEED). The influence of temperature on the molecular deposition was also studied. The results provide new insight on the chemical and structural interaction between inhibitor molecule and copper surface, and contribute to the design of new inhibitors which better protect the metals.

6.3 Experimental

Experiments were carried out in a UHV system with base pressure in the 10^{-10} mbar and equipped with a reactor for 2-MBT evaporation. Different surface analytical techniques were used: STM (Omicron, STM1 with SCALA system), AES (Omicron, CMA-100) and LEED (Omicron, SpectaLEED). The sample was a high purity (99.999%) Cu(111) single-crystal. It was mechanically polished to 0.25 μm (diamond paste), electropolished in phosphoric acid and then prepared in the UHV system by cycles of ion sputtering

($P_{\text{Ar}} = 1 \times 10^{-5}$ mbar, 600 V, 20 mA, 30 min) and annealing (600°C, 30 min) until a clean copper surface was obtained, i.e. no contamination was evidenced by AES, a sharp (1×1) pattern was observed by LEED, as well as large and flat terraces by STM.

The clean metallic Cu(111) surface was exposed to 2-MBT vapor at ultra low pressure (2×10^{-9} mbar) in the UHV reactor. Exposures are expressed in langmuirs (1 L = 1×10^{-6} Torr.s). The 2-MBT powder (99% purity, Sigma-Aldrich) was placed in a vacuum-sealed glass mounted on the reactor. The pressure in the reactor is limited by the vapor pressure of 2-MBT at room temperature. The Cu(111) sample was heated to 150°C during molecule deposition. The temperature was selected to avoid total desorption of molecules from the surface, and to allow the reorganization of the molecular layer.

The STM characterization was carried out at room temperature and in constant current mode. W tip was prepared by electrochemical attack in NaOH solution followed by voltage pulses under UHV. Image processing was performed using WSxM software (5.0 Develop 9.1) [80]. No filtering was applied. All images were corrected by plane subtraction.

Quantitative chemical analysis was performed by transferring quickly the sample to another UHV system equipped with XPS (Thermo Electron Corporation, ESCALAB 250) of base pressure of 10^{-10} mbar. A monochromatic Al K_α source (1486.6 eV) was used. The survey spectrum was recorded with a pass energy of 100 eV corresponding to an overall resolution of 1.8 eV, the high resolution spectra were recorded with a pass energy of 20 eV corresponding to an overall resolution of 360 meV. The XPS measurements were performed at a take-off angle of 90°, and the data analysis was preformed using the CasaXPS software (version 2.3.19) [82].

In order to verify the inhibition properties of the adsorbed Moiré layer formed at 150°C, further exposure to 2-MBT at room temperature and 2×10^{-9} mbar was performed, as well as exposure of the surface with the Moiré structure to oxygen at low pressure (1×10^{-5} mbar) for up to 1 h 30 min and to ambient air at atmospheric pressure. Finally, in order to investigate the influence of temperature on the adsorption of 2-MBT, exposure was also performed at higher temperature.

6.4   Results and discussion

6.4.1   Exposure at 150°C: Moiré structure formation

STM images of the Cu(111) surface before and after exposure to 2-MBT at 150°C are shown in Fig. 6.1. On clean Cu(111), the step edges were aligned according to the disorientation of the single-crystal, with multi-atomic steps (1–3 atomic planes), as shown in Fig. 6.1a. The step edges appear to be fuzzy because of the high mobility of copper atoms at room temperature. After exposure to 2-MBT at 150°C (45 L), as shown in Fig. 6.1b, the step edges became straight, suggesting a reduced surface mobility of Cu

atoms after exposure to 2-MBT. Moreover, they were reoriented in three directions forming an angle of 120° with each other. Large terraces are favored by the formation of higher multi-atomic steps (1–6 atomic planes). The terraces remained atomically flat, suggesting the formation of an organized layer after exposure to 2-MBT.

(a)   (b)
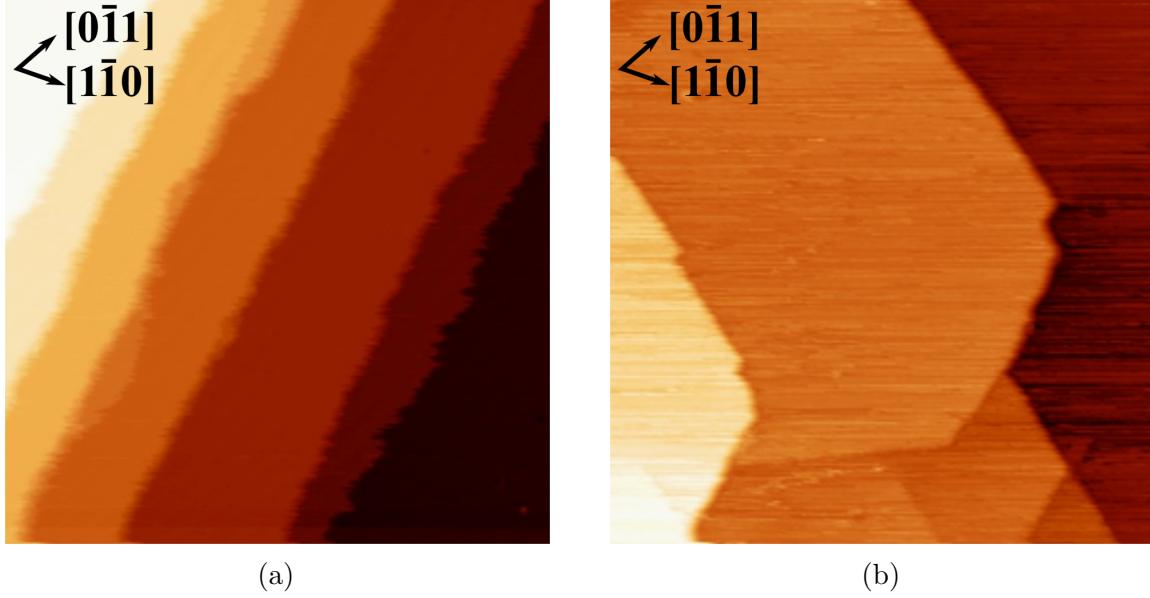
Figure 6.1: STM images of (a) clean Cu(111) surface (100 nm × 100 nm, $V = 0.7$ V, $I = 0.2$ nA) and (b) Cu(111) surface exposed to 45 L of 2-MBT at 150°C (100 nm × 100 nm, $V = 0.1$ V, $I = 2.5$ nA).

By zooming in on the terraces obtained after 2-MBT exposure, a Moiré structure is observed, with the presence of two hexagonal structures, as indicated in Fig. 6.2a and modeled in Fig. 6.2b. The short-range hexagonal unit cell is marked in blue, with a lattice parameter of 3.5 ± 0.5 Å, and a rotation of $31 \pm 4°$ with respect to the directions of the substrate. This is also confirmed by the Fast Fourier transform (FFT) (Fig. 6.2c) and LEED (Fig. 6.2d), which shows the same direction and gives a lattice parameter of 3.7 Å. Moreover, two overlapped mirror domains are observed by LEED. The long-range hexagonal lattice (Moiré structure) is indicated in black, with a lattice parameter 5.6 times larger (19.6 ± 0.6 Å) and a rotation of 6.4° compared to the short-range structure (25 ± 5° with respect to the substrate). According to Moiré pattern mathematical formalism [124], we found that the observed Moiré structure may be explained by the superposition of two molecular layers: the 3.5 Å lattice observed in the STM image and an underlying hexagonal lattice not observed in the STM image with a lattice parameter mismatch of 18% and a rotation of 1.2° between the two, as shown in Fig. 6.2b. The lattice parameter for the underlying layer is 4.1 ± 0.6 Å, corresponding to $\sqrt{3}$ times the lattice constant of Cu(111), with a rotation of $30 \pm 4°$ with respect to the substrate. It thus forms a $(\sqrt{3} \times \sqrt{3})$R30° structure.
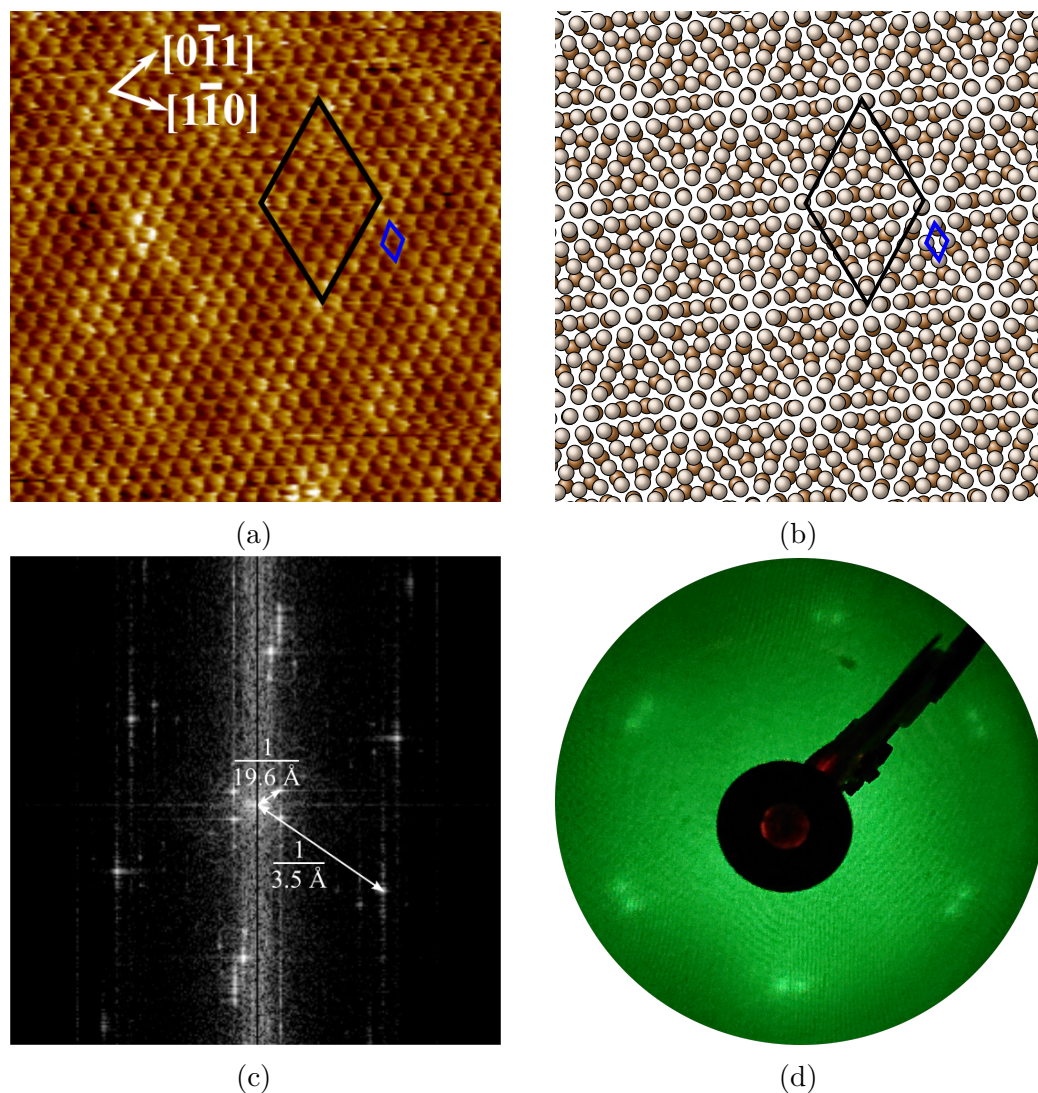
Figure 6.2: Moiré structure for 45 L of 2-MBT deposited on Cu(111) surface at 150°C (a) STM image (10 nm × 10 nm, $V = 0.05$ V, $I = 4.0$ nA); (b) Model of Moiré structure consisting of two superimposed molecular layers with the unit cells observed in the STM image marked (substrate not shown); (c) FFT of the image in (a) with Moiré structure and top molecular layer structure marked; (d) LEED pattern (Ep = 55 eV).

AES peak-to-peak height ratios of S (151 eV) and N (380 eV) to C (271 eV) signals were calculated for the Moiré structure, and their relative ratios were corrected using the relative sensitivities of the Auger transitions. The results give a S/C atomic ratio of 3.57, which is about 12.5 times the theoretical (molecule stoichiometry) value (2/7), and a N/C atomic ratio of 0.05, which is about 0.4 times the theoretical value (1/7). These differences suggest that the Moiré structure is rich in S, resulting from a partial decomposition of 2-MBT by the cleavage of the C=S and/or C–S bonds for exposure at 150°C, probably due to the high affinity of sulfur to copper [90–94]. The moiré structure also appears poor in N, suggesting the desorption of molecular fragments after decomposition.

The surface with this Moiré structure was then transferred to the XPS system for quantitative analysis, and the results are shown in Fig. 6.3. For the peak fitting of S

2p spectra, spin-orbit doublets S $2p_{1/2}$ and S $2p_{3/2}$, with a branching ratio of 0.5 and a spin-orbit splitting of 1.18 eV were considered [45, 54]. The Moiré structure is mainly composed of a component S_3, with S $2p_{3/2}$ at 161.7 eV. This component is slightly shifted to higher binding energy (0.2 eV) compared to that of the $(\sqrt{7} \times \sqrt{7})$R19.1° S/Cu(111) surface obtained by exposing clean Cu(111) surface to H_2S, which may be explained by an interaction with oxygen during transfer in air. The S_3 component is assigned to S bonded to metallic copper [113]. A N 1s component at 399.0 eV is observed, corresponding to N in non bonded molecule [113]. XPS spectra obtained on the 2-MBT monolayer formed on Cu(111) at room temperature are also shown for comparison. The intensity of S 2p spectrum was found to be 0.6 times that obtained on the Moiré structure, and the intensity of N 1s spectrum was found to be 1.3 times that obtained on the Moiré structure, suggesting that the Moiré structure is richer in S than the 2-MBT monolayer formed at room temperature.
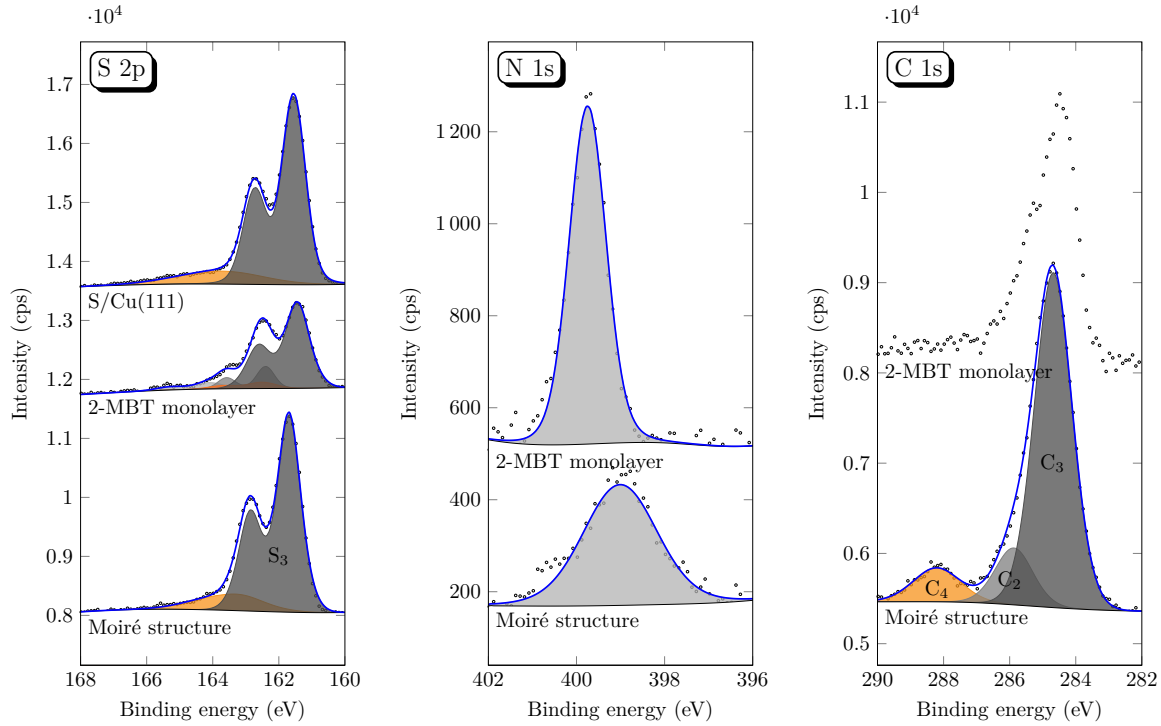
Figure 6.3: XPS spectra of the S 2p, N 1s and C 1s core levels for Cu(111) exposed to 45 L 2-MBT at 150°C (Moiré structure) and 15 L 2-MBT at RT (2-MBT monolayer [113]) for comparison. S 2p spectrum for a $(\sqrt{7} \times \sqrt{7})$R19.1° S/Cu(111) surface is also shown for comparison [113].

The atomic ratios of S and N versus C were calculated for the Moiré structure. We found a S to C atomic ratio 1.4 times the theoretical value for the stoichiometry of the molecule (2/7), and a N to C atomic ratio 0.4 times the theoretical value (1/7), confirming the decomposition of the molecule. We assume three types of carbon, C_2, C_3 and C_4, for the peak fitting of the C 1s spectrum. The full width at half maximum (FWHM) (1.3 eV)
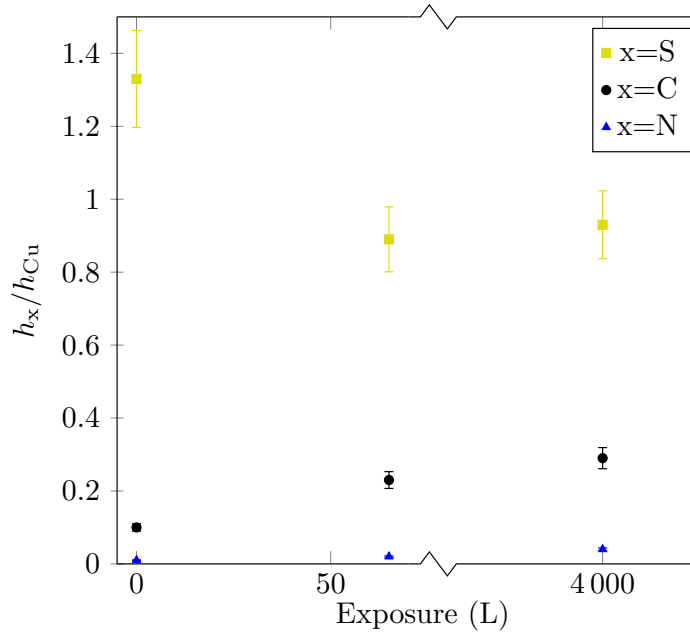
Figure 6.4: Growth of 2-MBT layer on pre-adsorbed Moiré structure at 2×10^{-9} mbar and RT. Change in the AES peak-to-peak height ratios h_S/h_{Cu}, h_C/h_{Cu} and h_N/h_{Cu} as a function of 2-MBT exposure.

of the C_2 and C_3 components was set to be the same, and the fit is in agreement with the measured spectrum. The C_4 component at binding energy of 288.2 eV indicates the presence of carboxylic groups (air contamination) [69], which explains the difference with S and N to C atomic ratios obtained by AES. The C_2 and C_3 components at binding energies of 285.8 ± 0.2 eV and 284.7 ± 0.1 eV correspond to C–N bond and the remaining C atoms in the benzene ring, respectively [113]. The intensity of C_3 is 5–6 times that of C_2. This confirms the decomposition of 2-MBT by the cleavage of the C=S and C–S bonds.

In order to study the influence of temperature on the adsorption of 2-MBT, exposures were also carried out on Cu(111) at different temperatures, and the surface structure was characterized by LEED. The Moiré structure formed at 150°C was transformed to $(\sqrt{7} \times \sqrt{7})$R19.1° structure when increasing the deposition temperature to 250°C.

6.4.2 Growth of 2-MBT layer on pre-adsorbed Moiré structure at room temperature

The surface with the Moiré structure was then exposed to 2-MBT under ultra low pressure (2×10^{-9} mbar) at room temperature, and the AES peak-to-peak height ratios of S (151 eV), C (271 eV) and N (380 eV) to Cu (920 eV) signals were calculated and plotted as a function of exposure (see Fig. 6.4). The values at 0 L correspond to that for the Moiré structure.

After exposure to 65 L 2-MBT, a slight decrease of the S signal is firstly observed. This may be explained by the attenuation of the Moiré structure (rich in S) by the adsorbing 2-MBT molecules. On the contrary, N and C signals were observed to increase, confirming the adsorption of molecules on the surface. Further exposure of 2-MBT until 4000 L shows no obvious increase of the S, C and N signals. By comparing the AES peak-to-peak height ratios to that obtained for 2-MBT deposited on the clean Cu(111) surface [89], we estimate that only one equivalent monolayer of 2-MBT is adsorbed, whereas 2-MBT multilayers are grown on the clean Cu(111) surface.

The sample was also analyzed by XPS in order to obtain information on the chemical composition (Fig. 6.5). The S 2p spectrum shows that the growth of 2-MBT on the Moiré structure at room temperature gives rise to two other components S_1 and S_2, with the $2p_{3/2}$ peaks at 164.2 eV and 162.8 eV, corresponding to the endocyclic and exocyclic S atoms in the 2-MBT molecule non bonded to copper, respectively [54, 113]. This confirms the adsorption of molecules on the Moiré structure. The comparison of the intensity of XPS spectra with those obtained on Cu(111) with the pre-adsorbed 2-MBT monolayer [113] confirms the formation of one equivalent 2-MBT monolayer on the Moiré structure at room temperature. The binding energies of S_2 and S_3 components are found to be slightly superior to that found in our previous study on 2-MBT [113], which may be explained by the influence of exposure to air during transfer to XPS in this case. Increase in the intensities of C and N is also observed, with a slight shift to higher binding energy (0.3 eV) and a decrease in FWHM (1.5 eV) of about 25 % for N 1s spectrum. A component C_1 at binding energy of 286.4 eV is also observed, which is assigned to C=S bond [113]. Similarly, the C_4 component at 288.2 eV is assigned to carboxylic groups (air contamination) [69].

The topography of the surface obtained after exposure at room temperature of the Moiré structure to 2-MBT was characterized by STM, and is shown in Fig. 6.6 and Fig. 6.7. After an exposure of 65 L (Fig. 6.6), the surface is homogeneous with the presence of multi-atomic steps with height of about 7 Å (3–4 atomic planes). The step edges remain straight. By zooming in on the terraces (Fig. 6.6b), we can see that the adsorbed molecular layer is almost complete and relatively flat with a maximal height difference of around 1.5 Å. The size of protrusions is 1–2 nm, which could be assigned to the adsorption of 2-MBT molecules. FFT shows no ordered structure.

At higher exposure until 4000 L, Fig. 6.7a shows that the step edges are reorganized, and the surface is always flat and homogeneous, as confirmed by Fig. 6.7b. The molecular layer is very similar to that observed at 65 L with a maximal height difference of around 1.7 Å, and protrusions of 1–2 nm, and no ordered local structure revealed by FFT.
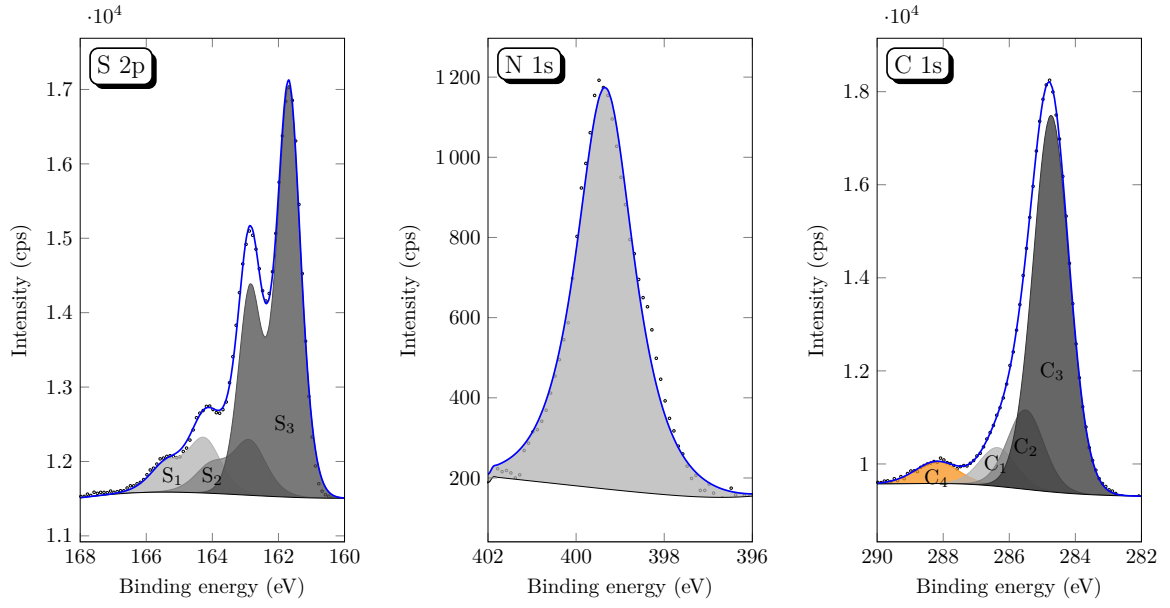
Figure 6.5: XPS spectra of the S 2p, N 1s and C 1s core levels for pre-adsorbed Moiré structure exposed to 65 L 2-MBT at RT.

(a)

(b)
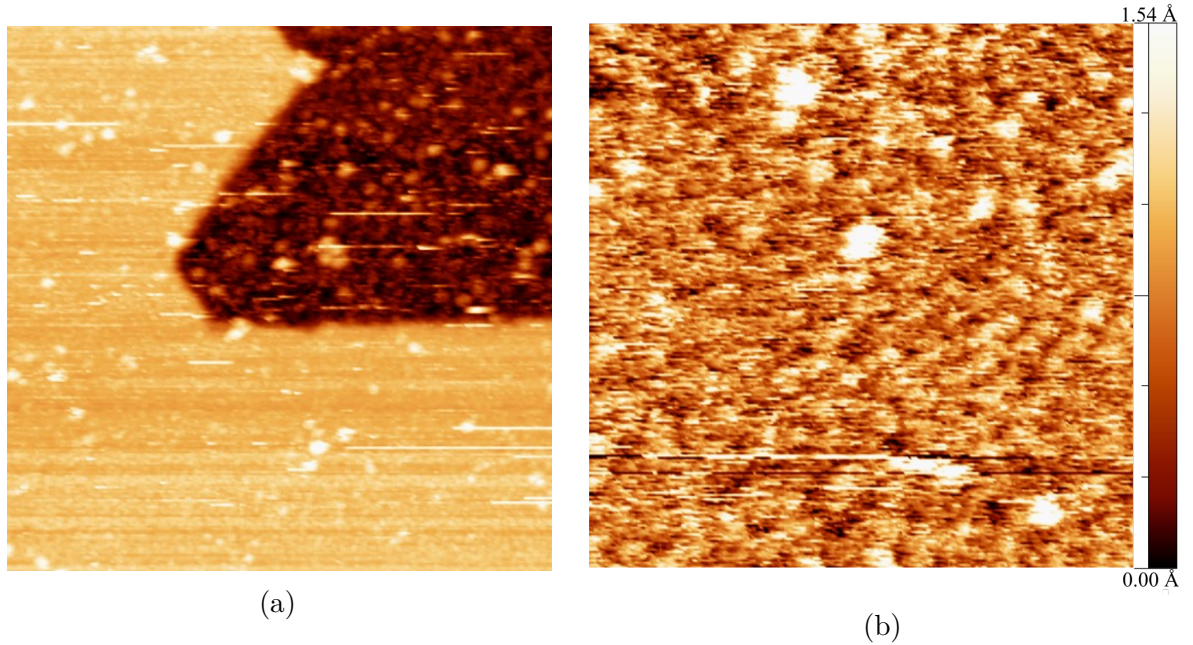
Figure 6.6: STM images of Moiré pattern exposed at RT to 65 L 2-MBT (a) 100 nm × 100 nm, $V = 1.0$ V, $I = 0.1$ nA; (b) 25 nm × 25 nm, $V = 0.5$ V, $I = 0.5$ nA).
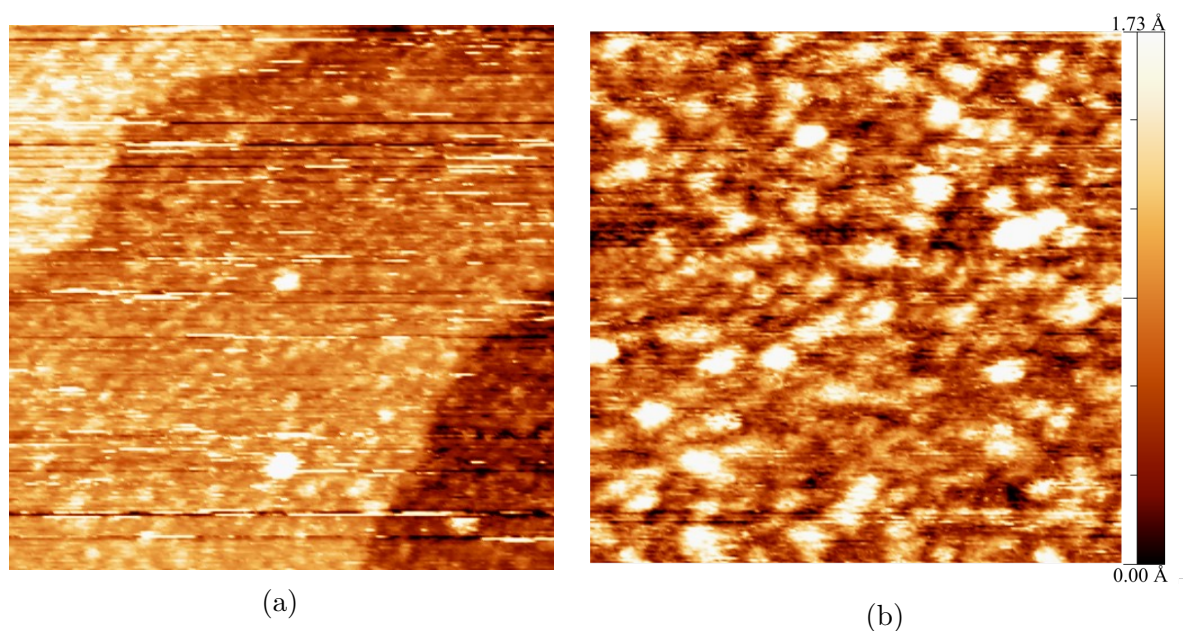
Figure 6.7: STM images of Moiré pattern exposed at RT to 4000 L 2-MBT (a) 50 nm $\times$ 50 nm, $V = 1.0$ V, $I = 0.2$ nA; (b) 30 nm $\times$ 30 nm, $V = 1.0$ V, $I = 0.3$ nA).

6.4.3 Inhibition effect of pre-adsorbed Moiré structure on the oxidation of Cu(111)

In order to clarify the inhibition properties of the interfacial Moiré structure, the Cu(111) surface with the pre-adsorbed Moiré structure was exposed to oxygen under low pressure (until 10^{-5} mbar) at room temperature. The oxidation kinetics was followed by AES, as shown in Fig. 6.8. When the copper surface is pre-covered by the Moiré structure, there is almost no uptake of oxygen, in contrast to the oxidation kinetics on clean Cu(111) surface [87]. This confirms the effective protection of copper by the Moiré structure at low O_2 pressure and room temperature. Because of the well organized pre-adsorbed structure, no residual uptake of oxygen is observed as in the case of Cu(111) with a non-ordered pre-adsorbed 2-MBT monolayer formed at room temperature [113], suggesting a better protection of copper against corrosion by the Moiré structure.

When exposed to ambient air, the sample surface was slightly oxidized, as indicated by the XPS spectra shown in Fig. 6.9. The results were compared to those obtained on the metallic Cu(111) surface after exposure to air. Firstly, we can see that the intensities of Cu 2p, O 1s and Cu LMM core levels decrease largely in the presence of the pre-adsorbed Moiré structure. The decrease of Cu 2p intensity can be explained by a strong attenuation of the signal by the pre-adsorbed Moiré structure. Moreover, weak satellite structures are observed between the $2p_{1/2}$ and $2p_{3/2}$ peaks, indicating the formation of Cu(II) in the two cases [125, 126]. Analysis of the O 1s spectrum obtained on metallic Cu(111) gives two components O_1 and O_2 at binding energies of 531.5 eV and 530.3 eV, respectively. O_1 component may be attributed to the interface OH groups resulting from dissociative
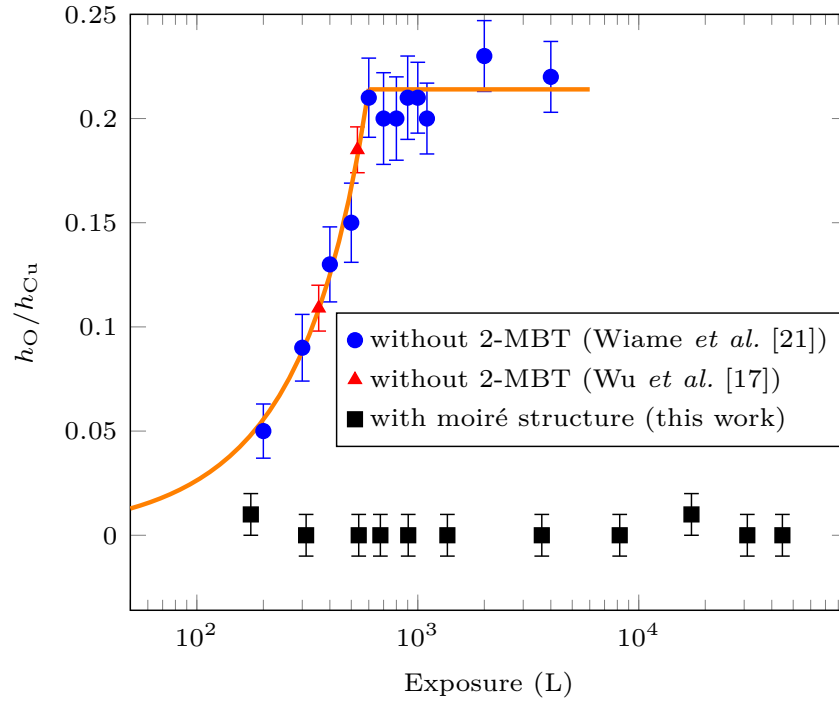
Figure 6.8: Oxidation kinetics of Moiré structure: effect of pre-adsorbed 2-MBT (45 L at 150°C prior to oxidation).

adsorption of water and/or oxygenated contaminations, while O_2 component is usually assigned to the bulk oxide [114, 115]. The decrease in O 1s spectrum (both O_1 and O_2 components) with the Moiré structure indicates that the metallic Cu(111) sample is more oxidized and contaminated. This confirms that the Moiré pattern offers good protection of copper against oxidation even in ambient air.

In order to elucidate the nature of oxide formed on the sample surface, decomposition of the Cu LMM spectra was also carried out using three reference spectra obtained by analyzing the metallic Cu sample and copper oxides [127]. The results show the formation of 34% of cuprous oxide (Cu_2O) and 19% of cupric oxide (CuO) on metallic Cu(111). In the presence of the Moiré structure, the intensities of Cu(I) and Cu(II) components decrease, but the relative proportion of Cu(I) component increases to 76%. This can be explained by a preferential Cu(I) oxidation occurring upon formation of the Moiré structure, with the Cu(I) component assigned to oxidized copper bonded to S in the Moiré structure. The results confirm that the Moiré structure can protect the copper substrate from oxidation when exposed to air.

6.5 Conclusions

The adsorption of 2-MBT on Cu(111) at ultra low pressure was investigated at mild temperature by STM, XPS, AES and LEED. The STM images show that a Moiré structure was formed for exposure at 150°C, with a short-range unit cell and a underlying
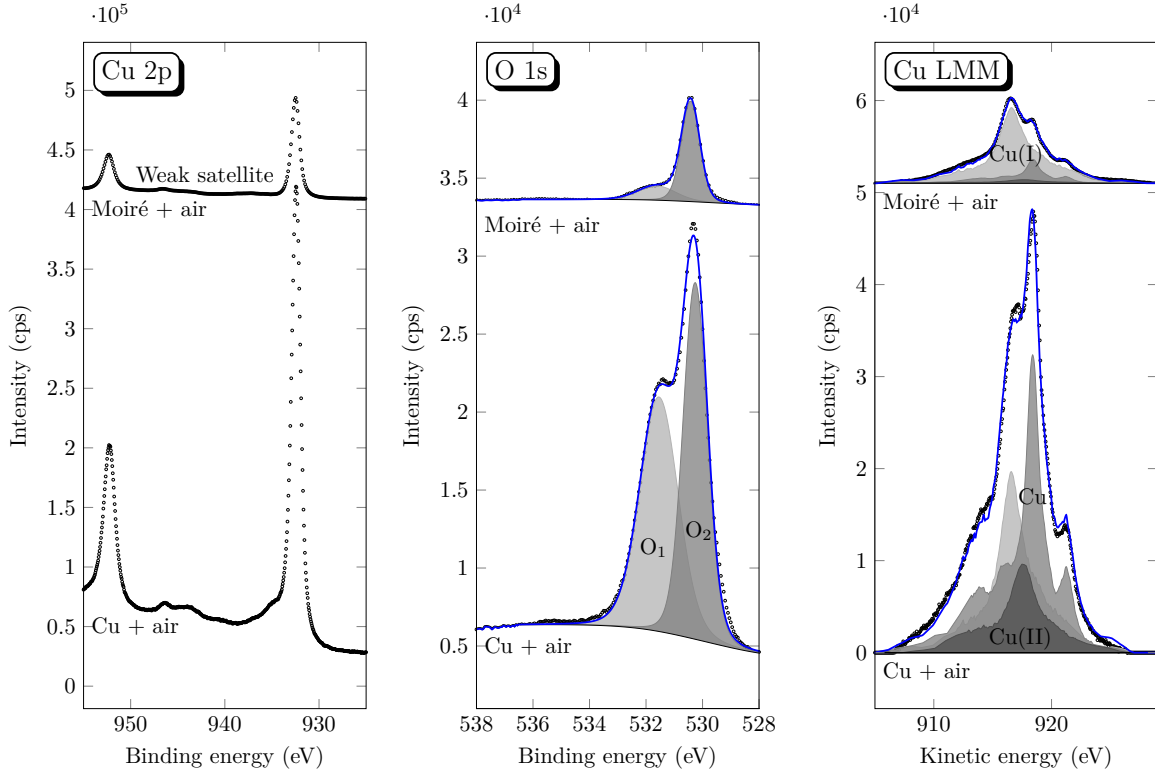
Figure 6.9: XPS spectra of the Cu 2p, Cu LMM and O 1s core levels for metallic Cu(111) and Moiré structure exposed to air.

superimposed $(\sqrt{3} \times \sqrt{3})$R30° structure. XPS spectra show that the Moiré structure is rich in S bonded to Cu resulting from 2-MBT decomposition and partial desorption. When increasing the deposition temperature, the Moiré structure formed at 150°C was transformed to $(\sqrt{7} \times \sqrt{7})$R19.1° structure at 250°C, assigned to atomic S bonded to Cu.

The corrosion inhibition efficiency of the interfacial Moiré structure was determined by dosing oxygen to the pre-adsorbed Moiré structure. No uptake of oxygen was observed until an oxygen partial pressure of 10^{-5} mbar, and the sample was only slightly oxidized when exposed to ambient air. This indicates the good protection against oxidation of the Cu(111) surface by pre-adsorbed Moiré structure, which is more efficient than 2-MBT monolayer formed at room temperature.

Upon further exposure to 2-MBT of the Moiré structure at 2×10^{-9} mbar and room temperature, an equivalent monolayer of molecules was formed, which is flat and homogeneous. However, no further growth was evidenced until an exposure of 4000 L, suggesting that the pre-adsorbed Moiré structure does not enable the formation of multilayers of 2-MBT, observed on the clean Cu(111) surface.

Conclusions and perspectives

In this work, the growth and corrosion inhibition mechanisms of two structurally related organic corrosion inhibitors, 2-MBT and 2-MBI, deposited by sublimation under ultra low pressure on pristine and pre-oxidized Cu(111) surfaces were investigated using advanced surface characterization techniques: STM, XPS, AES and LEED.

2-MBT deposition at room temperature

For 2-MBT deposition on pristine Cu(111) surface at room temperature, *in situ* XPS and AES measurements show the growth of a molecular layer, with an excess of sulfur compared to the stoichiometry of the molecule, indicating a partial decomposition of 2-MBT. High resolution XPS analysis shows the presence of only one S 2p component in the monolayer, with the $2p_{3/2}$ at 161.5 ± 0.1 eV. This component is at the same position as that of the Cu(111) surface exposed to H$_2$S, confirming the decomposition of 2-MBT and the adsorption of atomic sulfur on copper. Moreover, the two sulfur atoms in the non-dissociated 2-MBT molecules are involved simultaneously in the interaction with copper, giving rise to one component at the same binding energy. This component is not observed after 2-MBT deposition in the same conditions on Cu(111) prepared in air, indicating that the pre-formed 3D oxide prevents the direct interaction with metallic Cu and the decomposition of the molecule. The formation of 2-MBT multilayer is observed from an exposure of 15 L, confirmed by the presence of two additional S 2p components with the $2p_{3/2}$ at binding energy of 164.1 eV and 162.5 eV, corresponding to the endocyclic and exocyclic sulfur atoms in the 2-MBT molecule non-bonded to copper, respectively. The thicknesses of the 2-MBT monolayer and multilayer are calculated to be 0.2 nm and 0.6 nm, respectively, indicating that the molecules are lying flat on Cu(111).

The STM images obtained on the metallic Cu(111) surface at initial stage of deposition show the formation of local $(\sqrt{7} \times \sqrt{7})$R19.1° ordered triangular structures, typical of atomic sulfur adsorption on Cu(111), confirming the partial decomposition of 2-MBT and the adsorption of atomic sulfur on copper. A complete non-ordered monolayer is observed at an exposure of about 10 L, with molecules lying flat on the surface, followed

by non-ordered multilayer with flat-lying molecules, confirming the results obtained by XPS.

The influence of oxygen on the adsorption of the 2-MBT molecule was investigated. XPS and AES measurements show the substitution of oxygen in the 2D oxide layer by 2-MBT, without decomposition of the molecule. A monolayer of 2-MBT is observed at about 0.5 L, indicating that the pre-adsorbed 2D oxide accelerates the initial uptake of 2-MBT on copper. The thickness of the monolayer is calculated to be 0.4 nm, suggesting the adsorption of 2-MBT in a tilted configuration. STM characterization shows that the pre-oxidation of copper favors the formation of a complete and homogeneous molecular layer.

The thermal stability of the adsorbed molecular layer on metallic and pre-oxidized Cu(111) surfaces was elucidated. Decomposition of 2-MBT is observed after annealing to temperature above 100°C, accompanied by a partial desorption of nitrogen and carbon, while sulfur remains adsorbed on copper, forming a $(\sqrt{7} \times \sqrt{7})$R19.1° structure.

The corrosion inhibition efficiency of 2-MBT was tested by exposing Cu(111) with pre-adsorbed molecules to oxygen, and a monolayer of 2-MBT effectively prevents the oxidation of Cu(111) at low O_2 pressure and room temperature.

2-MBI deposition at room temperature

Growth of the molecular layer on pristine and pre-oxidized Cu(111) surfaces at ultra low pressure and room temperature is evidenced by AES, giving an excess of sulfur. XPS analysis shows the presence of the interfacial sulfur component as observed for the adsorption of 2-MBT, indicating the bonding of sulfur with copper. A N 1s peak at 398.5 ± 0.1 eV is also observed, suggesting that nitrogen atoms are also involved in the interaction with copper. The formation of multilayer is confirmed by the presence of a S 2p component at binding energy of 162.4 eV for $2p_{3/2}$, corresponding to sulfur in the 2-MBI molecule non-bonded to copper. The thicknesses of the multilayers formed on metallic and pre-oxidized Cu(111) surfaces at saturation are calculated to be 1.0 nm and 0.6 nm, respectively.

The STM images reveal the formation of a self-assembled monolayer of 2-MBI on metallic Cu(111) surface for an exposure of 5 L, including a $(\sqrt{7} \times \sqrt{7})$R19.1° structure resulting from the adsorption of atomic sulfur, and a (8×8) structure which may be assigned to the adsorption of 2-MBI clusters. This confirms the partial decomposition of 2-MBI on metallic Cu(111). Further exposure to 2-MBI leads to the formation of multilayer with flat-lying molecules. The pre-adsorbed 2D oxide layer favors the formation of a flat, homogeneous and complete molecular layer, while being substituted by 2-MBI.

When heated to 200°C, a surface reorganization of the molecular layer adsorbed on metallic Cu(111) is observed, followed by the decomposition of 2-MBI forming the

$(\sqrt{7} \times \sqrt{7})$R19.1° structure at 500°C. Moreover, a multilayer of 2-MBI blocks the oxidation of Cu(111) at low O$_2$ pressure and room temperature, while a slight uptake of oxygen is observed with pre-adsorbed 2-MBI monolayer.

The comparison with 2-MBT indicates that the monolayer formed by 2-MBI on pristine Cu(111) is self-assembled, and the multilayer is thicker and more stable. However, the 2-MBI monolayer is less effective on corrosion protection due to the presence of local defects. Furthermore, 2-MBI interacts much more slowly with pre-oxidized Cu(111) surface. Thus 2-MBT may offer a better corrosion inhibition for copper at room temperature. From the above analysis, we may conclude that the replacement of one nitrogen atom by sulfur in 2-MBI improves its corrosion inhibition efficiency, probably due to the high affinity of sulfur to copper.

2-MBT deposition at mild temperature

The influence of temperature on the adsorption of 2-MBT was studied for its potential use in high temperature environment. The STM images show the formation of a Moiré pattern on Cu(111) exposed to 2-MBT at 150°C, with a short-range unit cell and a underlying $(\sqrt{3} \times \sqrt{3})$R30° structure. AES measurement shows that the Moiré structure is richer in S than the non-ordered monolayer of 2-MBT formed on Cu(111) at room temperature. XPS analysis shows only one S 2p component corresponding to interfacial sulfur, indicating that the Moiré structure is rich in S bonded to Cu resulting from 2-MBT decomposition and partial desorption. Moreover, the Moiré structure is stable up to 250°C before transformation to the $(\sqrt{7} \times \sqrt{7})$R19.1° structure.

When exposed to oxygen at low pressure, the Moiré structure offers a good protection of the Cu(111) surface against oxidation, which is more effcient than 2-MBT monolayer formed at room temperature. Moreover, the Moiré structure protects copper against oxidation in ambient air. However, the pre-adsorbed Moiré structure does not enable the formation of multilayers of 2-MBT at room temperature, which is observed on the clean Cu(111) surface.

Perspectives

Further work can be envisaged to complete the present study, especially for the corrosion inhibition investigation of 2-MBI.

Firstly, the experimental conditions can be improved, with the installation of an evaporator for the *in situ* deposition of organic molecules in the UHV systems. This would allow us to follow precisely the growth of 2-MBI on pristine and pre-oxidized Cu(111) surfaces while characterizing its chemical composition in the XPS system without transfer in air.

Secondly, since the adsorption of 2-MBT at 150°C and the formation of the Moiré structure protects well the copper surface underneath, it would also be interesting to study the adsorption of 2-MBI at higher temperature and the corrosion inhibition efficiency of the adsorbed molecular layer.

Finally, theoretical simulations such as DFT calculations can be conducted to confirm our experimental results, and to offer a rational base for the design of new inhibitors which protects better the copper surface.

Acknowledgments

Bibliography

[1] http://impact.nace.org/economic-impact.aspx.

[2] M. A. Kelland, Production Chemicals for the Oil and Gas Industry, CRC Press, 2016.

[3] M. M. Antonijević, M. B. Petrović Mihajlović, Copper corrosion inhibitors. A review, International Journal of Electrochemical Science 3 (1) (2008) 1–28.

[4] M. Finšgar, I. Milošev, Inhibition of copper corrosion by 1,2,3-benzotriazole: A review, Corrosion Science 52 (2010) 2737–2749.

[5] A. Kokalj, Ab initio modeling of the bonding of benzotriazole corrosion inhibitor to reduced and oxidized copper surfaces, Faraday Discussions 180 (2015) 415–438.

[6] C. Gattinoni, A. Michaelides, Understanding corrosion inhibition with van der Waals DFT methods: the case of benzotriazole, Faraday Discussions 180 (2015) 439–458.

[7] A. Kokalj, S. Peljhan, DFT study of adsorption of benzotriazole on Cu_2O surfaces, The Journal of Physical Chemistry C 119 (21) (2015) 11625–11635.

[8] F. Grillo, D. W. Tee, S. M. Francis, H. Früchtl, N. V. Richardson, Initial stages of benzotriazole adsorption on the Cu(111) surface, Nanoscale 5 (12) (2013) 5269–5273.

[9] F. Grillo, D. W. Tee, S. M. Francis, H. Früchtl, N. V. Richardson, Passivation of copper: Benzotriazole films on Cu(111), The Journal of Physical Chemistry C 118 (16) (2014) 8667–8675.

[10] M. R. Vogt, W. Polewska, O. M. Magnussen, R. J. Behm, In situ STM study of (100) Cu electrodes in sulfuric acid solution in the presence of benzotriazole adsorption, Cu corrosion, and Cu deposition, Journal of the Electrochemical Society 144 (5) (1997) 113–116.

[11] M. R. Vogt, R. J. Nichols, O. M. Magnussen, R. J. Behm, Benzotrizole adsorption and inhibition of Cu(100) corrosion in HCl: A combined in situ STM and in situ FTIR spectroscopy study, Journal of Physical Chemistry B 102 (1998) 5859–5865.

[12] M. Sugimasa, L.-J. Wan, J. Inukai, K. Itaya, Adlayers of benzotriazole on Cu(111), (100), and (111) in $HClO_4$ solution, Journal of the Electrochemical Society 149 (10) (2002) 367–373.

[13] W. Polewska, M. R. Vogt, O. M. Magnussen, R. J. Behm, In situ STM study of Cu(111) surface structure and corrosion in pure and benzotriazole-containing sulfuric acid solution, Journal of Physical Chemistry B 103 (1999) 10440–10451.

[14] O. M. Magnussen, M. R. Vogt, J. Scherer, R. J. Behm, Double-layer structure, corrosion and corrosion inhibition of copper in aqueous solution, Applied Physics A 66 (1998) 447–451.

[15] M. A. Amin, K. Khaled, Copper corrosion inhibition in O_2-saturated H_2SO_4 solutions, Corrosion Science 52 (2010) 1194–1204.

[16] E. B. Hart, H. Steenbock, J. Waddell, C. A. Elvenhjem, Iron nutrition. VII. copper is a supplement to iron for hemoglobin building in the rat, The Journal of Biological Chemistry 77 (1928) 797–833.

[17] A. Maurel, Dessalement de l'eau de mer et des eaux saumâtres, 2006.

[18] S. B. Adeloju, H. C. Hughes, The corrosion of copper pipes in high chloride-low carbonate mains water, Corrosion Science 26 (10) (1986) 851–870.

[19] A. Fateh, M. Aliofkhazraei, A. R. Rezvanian, Review of corrosive environments for copper and its corrosion inhibitors, Arabian Journal of Chemistry 13 (1) (2020) 481–544.

[20] N. Takeno, Atlas of Eh-pH diagrams, Geological survey of Japan open file report 419 (2005) 102.

[21] D. Knight, Humphry Davy, Cambridge University Press, 1992.

[22] H. Gräfen, E.-M. Horn, H. Schlecker, H. Schindler, Corrosion, Ullmann's Encyclopedia of Industrial Chemistry, Wiley-VCH: Weinheim, 2002.

[23] C. Fiaud, C. Lemaitre, N. Pebere, Inhibiteurs de corrosion, in: G. Beranger, H. Mazille (Eds.), Corrosion et anticorrosion (pratique industrielle), Mécanique et ingénierie des Matériaux, Hermès Science Publications, Lavoisier, 2002, pp. 245–266.

[24] E. E. Oguzie, Y. Li, S. G. Wang, F. Wang, Understanding corrosion inhibition mechanisms—experimental and theoretical approach, RSC Advances 1 (5) (2011) 866–873.

[25] B. E. Brycki, I. H. Kowalczyk, A. Szulc, O. Karczewska, M. Pakiet, M. Aliofkhazraei, Organic corrosion inhibitors, in: InTech Open, no. 1, Corrosion Inhibitors, Principles and Recent Applications, 2017.

[26] A. I. Muñoz, J. G. Antón, J. Guiñón, V. P. Herranz, Comparison of inorganic inhibitors of copper, nickel and copper–nickels in aqueous lithium bromide solution, Electrochimica Acta 50 (4) (2004) 957–966.

[27] M. Stern, The mechanism of passivating-type inhibitors, Journal of the Electrochemical Society 105 (11) (1958) 638–647.

[28] P. R. Roberge, Handbook of corrosion engineering, McGraw-Hill, 2000.

[29] Procter, Gamble, Ltd. British Patent 652339 (1947).

[30] J. I. Bregman, Corrosion Inhibitors, Collier MacMillan Co., London, 1963.

[31] C. C. Nathan, Corrosion Inhibitors, National Association of Corrosion Engineers (NACE), Houston, Texas, 1973.

[32] N. Putilova, S. A. Balezin, V. P. Barannik, Metallic Corrosion Inhibitors, Pergamon Press, London, 1966.

[33] M. W. Ranney, Inhibitors-Manufacture and Technology, Noyes Data Corp, New Jersey, 1976.

[34] C. D. Taylor, P. Marcus, Molecular modeling of corrosion processes: scientific development and engineering applications, Wiley Online Library, 2015.

[35] J. Vosta, J. Eliasek, Study on corrosion inhibition from aspect of quantum chemistry, corrosion science 11 (4) (1971) 223–229.

[36] G. Gece, The use of quantum chemical methods in corrosion inhibitor studies, Corrosion science 50 (11) (2008) 2981–2992.

[37] S. Sun, Y. Geng, L. Tian, S. Chen, Y. Yan, S. Hu, Density functional theory study of imidazole, benzimidazole and 2-mercaptobenzimidazole adsorption onto clean Cu(111) surface, Corrosion Science 63 (2012) 140–147.

[38] A. Kokalj, S. Peljhan, Density functional theory study of ATA, BTAH, and BTAOH as copper corrosion inhibitors: Adsorption onto Cu(111) from gas phase, Langmuir 26 (18) (2010) 14582–14593.

[39] M. B. Petrović Mihajlović, M. M. Antonijević, Copper corrosion inhibitors. period 2008-2014. A review, International Journal of Electrochemical Science 10 (2015) 1027–1053.

[40] M. M. Antonijević, S. M. Milić, M. B. Petrović, Films formed on copper surface in chloride media in the presence of azoles, Corrosion Science 51 (2009) 1228–1237.

[41] R. Walker, Benzotriazole as a corrosion inhibitor for immersed copper, Corrosion 29 (7) (1973) 290–298.

[42] Y. Jiang, J. B. Adams, D. Sun, Benzotriazole adsorption on $Cu_2O(111)$ surfaces: A first-principles study, Journal of Physical Chemistry B 108 (34) (2004) 12851–12857.

[43] B.-S. Fang, C. G. Olson, D. W. Lynch, A photoemission study of benzotriazole on clean copper and cuprous oxide, Surface Science 176 (1986) 476–490.

[44] J. Jia, A. Giglia, M. F. Carrasco, O. Grizzi, L. Pasquali, V. A. Esaulov, 1,4-benzenedimethanethiol interaction with Au(110), Ag(111), Cu(100) and Cu(111) surfaces: Self-assembly and dissociation processes, Journal of Physical Chemistry C 118 (46) (2014) 26866–26876.

[45] J. Jia, A. Kara, L. Pasquali, A. Bendounan, F. Sirotti, V. A. Esaulov, On sulfur core level binding energies in thiol self-assembly and alternative adsorption sites: An experimental and theoretical study, Journal of Chemical Physics 143 (2015) 104702.

[46] M. Beccari, A. Kanjilal, M. G. Betti, C. Mariani, L. Floreano, A. Cossaro, V. Castro, Characterization of benzenethiolate self-assembled monolayer on Cu(100) by XPS and NEXAFS, Journal of Electron Spectroscopy and Related Phenomena 172 (2009) 64–68.

[47] F. M. A. Kharafi, N. A. Al-Awadi, I. M. Ghayad, R. M. Abdullah, M. R. Ibrahim, Novel technique for the application of azole corrosion inhibitors on copper surface, Materials Transactions 51 (9) (2010) 1671–1676.

[48] G. Gece, Drugs: A review of promising novel corrosion inhibitors, Corrosion Science 53 (12) (2011) 3873–3898.

[49] C. W. Yan, H. C. Lin, C. N. Cao, Investigation of inhibition of 2-mercaptobenzoxazole for copper corrosion, Electrochimica Acta 45 (2000) 2815–2821.

[50] J. C. Marconato, L. O. Bulhões, M. L. Temperini, A spectroelectrochemical study of the inhibition of the electrode process on copper by 2-mercaptobenzothiazole in ethanolic solutions, Electrochimica Acta 43 (7) (1998) 771–780.

[51] M. Ohsawa, W. Suëtaka, Spectro-electrochemical studies of the corrosion inhibition of copper by mercaptobenzothiazole, Corrosion Science 19 (7) (1979) 709–722.

[52] D. Chadwick, T. Hashemi, Electron spectroscopy of corrosion inhibitors: Surface film formed by 2-mercaptobenzothiazole and 2-mercaptobenzimidazole on copper, Surface Science 89 (1-3) (1979) 649–659.

[53] R. Woods, G. A. Hope, K. Watling, A SERS spectroelectrochemical investigation of the interaction of 2-mercaptobenzothiazole with copper, silver and gold surfaces, Journal of Applied Electrochemistry 30 (2000) 1209–1222.

[54] M. Finšgar, D. K. Merl, An electrochemical, long-term immersion, and XPS study of 2-mercaptobenzothiazole as a copper corrosion inhibitor in chloride solution, Corrosion Science 83 (2014) 64–175.

[55] R. Subramanian, V. Lakshminarayanan, Effect of adsorption of some azoles on copper passivation in alkaline medium, Corrosion Science 44 (2002) 535–554.

[56] F. Altaf, R. Qureshi, S. Ahmed, Surface protection of copper by azoles in borate buffers-voltammetric and impedance analysis, Journal of electroanalytical chemistry 659 (2) (2011) 134–142.

[57] H. Nishizawa, O. Sugiura, Y. Matsumura, M. Kinoshita, Evaluation of mercaptobenzothiazole anticorrosive layer on cu surface by spectroscopic ellipsometry, Japanese journal of applied physics 46 (5R) (2007) 2892.

[58] G. Contini, V. D. Castro, S. Stranges, R. Richter, M. Alagia, Gas-phase photoemission study of 2-mercaptobenzothiazole, The Journal of Physical Chemistry A 106 (2002) 2833–2837.

[59] J. P. Chesick, J. Donohue, The molecular and crystal structure of 2-mercaptobenzothiazole, Acta Crystallographica Section B 27 (7) (1971) 1441–1444.

[60] E. M. M. Sutter, F. Ammeloot, M. J. Pouet, C. Fiaud, R. Couffignal, Heterocyclic compounds used as corrosion inhibitors: correlation between ^{13}C and ^{1}H NMR spectroscopy and inhibition efficiency, Corrosion Science 41 (1999) 105–115.

[61] L. P. Kazansky, I. A. Selyaninov, Y. I. Kuznetsov, Adsorption of 2-mercaptobenzothiazole on copper surface from phosphate solutions, Applied Surface Science 258 (2010) 6807–6813.

[62] N. Sandhyarani, G. Skanth, S. Berchmans, V. Yegnaraman, T. Pradeep, A combined surface-enhanced Raman–X-Ray photoelectron spectroscopic study of 2-mercaptobenzothiazole monolayers on polycrystalline Au and Ag films, Journal of Colloid and Interface Science 209 (1999) 154–161.

[63] A. L. R. Silva, M. D. M. C. Ribeiro da Silva, Energetic, structural and tautomeric analysis of 2-mercaptobenzimidazole, Journal of Thermal Analysis and Calorimetry 129 (3) (2017) 1679–1688.

[64] G. R. Form, E. S. Raper, T. C. Downie, The crystal and molecular structure of 2-mercaptobenzimidazole, Acta Crystallographica Section B: Structural Crystallography and Crystal Chemistry 32 (2) (1976) 345–348.

[65] G. Xue, X.-Y. Huang, J. Dong, J. Zhang, The formation of an effective anti-corrosion film on copper surfaces from 2-mercaptobenzimidazole solution, Journal of Electroanalytical Chemistry 310 (1991) 139–148.

[66] G. Xue, X. Huang, J. Ding, Surface reaction of 2-mercaptobenzimidazole on metals and its application in adhesion promotion, Journal of the Chemical Society, Faraday Transactions 87 (8) (1991) 1229–1232.

[67] G. Xue, Q. Dai, SERS and IR studies of the reaction of an oxidized surface and an etched surface of copper with 2-mercaptobenzimidazole, Spectroscopy Letters 27 (3) (1994) 341–351.

[68] B. Trachli, M. Keddama, H. Takenouti, A. Srhiri, Protective effect of electropolymerized 2-mercaptobenzimidazole upon copper corrosion, Progress in Organic Coatings 44 (2002) 17–23.

[69] M. Finšgar, 2-mercaptobenzimidazole as a copper corrosion inhibitor: Part I. long-term immersion, 3D-profilometry, and electrochemistry, Corrosion Science 72 (2013) 82–89.

[70] M. Finšgar, 2-mercaptobenzimidazole as a copper corrosion inhibitor: Part II. surface analysis using X-ray photoelectron spectroscopy, Corrosion Science 72 (2013) 90–98.

[71] F. X. Perrin, J. Pagetti, Characterization and mechanism of direct film formation on a Cu electrode through electro-oxidation of 2-mercaptobenzimidazole, Corrosion Science 40 (10) (1998) 1647–1662.

[72] J. Izquierdo, J. J. Santana, S. González, R. M. Souto, Scanning microelectrochemical characterization of the anti-corrosion performance of inhibitor films formed by 2-mercaptobenzimidazole on copper, Progress in Organic Coatings 74 (3) (2012) 526–533.

[73] Y. Tooru, An X-ray photoelectron spectroscopic study of several metal complexes of 2-mercaptobenzimidazole and 2-mercaptobenzoxazole, The Chemical Society of Japan 53 (5) (1980) 1449–1450.

[74] M. G. Hosseini, T. Shahrabi, R. J. Nichols, Characterization of mercaptobenzimidazole adsorption on an Au(111) electrode, Iranian Journal of Science & Technology, Transaction A 29 (A1) (2005) 49–63.

[75] N. Kovačević, I. Milošev, A. Kokalj, The roles of mercapto, benzene, and methyl groups in the corrosion inhibition of imidazoles on copper: II. inhibitor–copper bonding, Corrosion Science 98 (2015) 457–470.

[76] National toxicology program chemical repository database (1992).

[77] G. Binning, H. Rohrer, Scanning tunneling microscopy, Surface Science 126 (1983) 236–244.

[78] M. Schmid, Institut für angewandte physik, technische universität Wien STM gallery, http://www.iap.tuwien.ac.at/www/surface/STM_Gallery/stm_schematic.html.

[79] C. J. Chen, Introduction to scanning tunneling microscopy, Vol. 4, Oxford University Press on Demand, 1993.

[80] I. Horcas, R. Fernández, J. M. Gómez-Rodríguez, J. Colchero, J. Gómez-Herrero, A. M. Baro, WSXM: A software for scanning probe microscopy and a tool for nanotechnology, Review of Scientific Instruments 78 (2007) 013705.

[81] http://faculty.chem.queensu.ca/people/faculty/horton/research.html.

[82] Casaxps manual 2.3.15, Casa Software Ltd (2009).

[83] S. Tanuma, C. J. Powell, D. R. Penn, Calculations of electron inelastic mean free paths . IX . Data for 41 elemental solids over the 50 eV to 30 keV range, Surface and Interface Analysis 43 (2011) 689–713.

[84] M. P. Seah, W. Dench, Quantitative electron spectroscopy of surfaces: A standard data base for electron inelastic mean free paths in solids, Surface and interface analysis 1 (1) (1979) 2–11.

[85] P. Auger, Sur l'effet photoélectrique composé, Journal de Physique et Le Radium 6 (6) (1925) 205–208.

[86] P. M. V. Raja, A. R. Barron, Physical methods in chemistry and nano science, LibreTexts libraries.

[87] F. Wiame, V. Maurice, P. Marcus, Initial stages of oxidation of Cu(111), Surface Science 601 (2007) 1193–1204.

[88] A. K. Rai, R. Singh, K. Singh, V. Singh, FTIR, Raman spectra and ab initio calculations of 2-mercaptobenzothiazole, Spectrochimica Acta Part A 63 (2006) 483–490.

[89] X. Wu, F. Wiame, V. Maurice, P. Marcus, Adsorption and thermal stability of 2-mercaptobenzothiazole corrosion inhibitor on metallic and pre-oxidized cu (111) model surfaces, Applied Surface Science 508 (2020) 145132.

[90] C. Vericat, M. E. Vela, G. Corthey, E. Pensa, E. Cortes, M. H. Fonticelli, F. Ibanez, G. Benitez, P. Carro, R. C. Salvarezza, Self-assembled monolayers of thiolates on metals: a review article on sulfur-metal chemistry and surface structures, RSC Advances 4 (53) (2014) 27730–27754.

[91] G. Ertl, Reactions at surfaces: from atoms to complexity (nobel lecture), Angewandte Chemie International Edition 47 (19) (2008) 3524–3535.

[92] F. Wiame, V. Maurice, P. Marcus, Reactivity to sulphur of clean and pre-oxidised Cu(111) surfaces, Surface science 600 (18) (2006) 3540–3543.

[93] H. Keller, P. Simak, W. Schrepp, J. Dembowski, Surface chemistry of thiols on copper: an efficient way of producing multilayers, Thin Solid Films 244 (1-2) (1994) 799–805.

[94] R. M. Issa, M. K. Awad, F. M. Atlam, Quantum chemical studies on the inhibition of corrosion of copper surface by substituted uracils, Applied Surface Science 255 (5) (2008) 2433–2441.

[95] Y. S. Tan, M. P. Srinivasan, S. O. Pehkonen, S. Y. M. Chooi, Self-assembled organic thin films on electroplated copper for prevention of corrosion, Journal of Vacuum Science & Technology A 22 (4) (2004) 1917–1925.

[96] C. M. Whelan, M. R. Smyth, C. J. Barnes, N. M. D. Brown, C. A. Anderson, An XPS study of heterocyclic thiol self-assembly on Au (111), Applied Surface Science 134 (1998) 144–158.

[97] C. M. Whelan, M. R. Smyth, C. J. Barnes, HREELS, XPS, and electrochemical study of benzenethiol adsorption on Au(111), Langmuir 15 (1999) 116–126.

[98] N. Petrova, I. Yakovkin, Mechanism of associative oxygen desorption from Pt(111) surface, The European Physical Journal B 58 (3) (2007) 257–262.

[99] D. B. Rao, K. Heinemann, D. Douglass, Oxide removal and desorption of oxygen from partly oxidized thin films of copper at low pressures, Oxidation of Metals 10 (4) (1976) 227–238.

[100] M. Zharnikov, M. Grunze, Spectroscopic characterization of thiol-derived self-assembling monolayers, Journal of Physics: Condensed Matter 13 (49) (2001) 11333.

[101] F. Eberle, M. Metzler, D. M. Kolb, M. Saitner, P. Wagner, H.-G. Boyen, Metallization of ultra-thin, non-thiol SAMs with flat-lying molecular units: Pd on 1, 4-Dicyanobenzene, ChemPhysChem 11 (13) (2010) 2951–2956.

[102] L. P. Kazansky, Y. E. Pronin, I. A. Arkhipushkin, XPS study of adsorption of 2-mercaptobenzothiazole on a brass surface, Corrosion Science 89 (2014) 21–29.

[103] Y.-H. Chen, A. Erbe, The multiple roles of an organic corrosion inhibitor on copper investigated by a combination of electrochemistry-coupled optical in situ spectroscopies, Corrosion Science 145 (2018) 232–238.

[104] T. Yoshida, K. Yamasaki, S. Sawada, An X-ray photoelectron spectroscopic study of 2-mercaptobenzothiazole metal complexes, Bulletin of the Chemical Society of Japan 52 (10) (1979) 2908–2912.

[105] M. Zheludkevich, K. Yasakau, S. Poznyak, M. Ferreira, Triazole and thiazole derivatives as corrosion inhibitors for AA2024 aluminium alloy, Corrosion Science 47 (12) (2005) 3368–3383.

[106] T. Matsumoto, R. Bennett, P. Stone, T. Yamada, K. Domen, M. Bowker, Scanning tunneling microscopy studies of oxygen adsorption on Cu(111), Surface Science 471 (2001) 225–245.

[107] R.W.Judd, P. Hollins, J. Pritchard, The interaction of oxygen with Cu(111): Adsorption, incorporation and reconstruction, Surface Science 171 (1986) 643–653.

[108] E. Wahlström, I. Ekvall, H. Olin, S.-A. Lindgren, L. Walldén, Observation of ordered structures for S/Cu(111) at low temperature and coverage, Physical Review B 60 (15) (1999) 10699–10702.

[109] E. Wahlström, I. Ekvall, T. Kihlgren, H. Olin, S.-A. Lindgren, L. Walldén, Low-temperature structure of S/Cu(111), Physical Review B 64 (2001) 155406.

[110] L. Ruan, I. Stensgaard, F. Besenbacher, E. Laegsgaard, A scanning tunneling microscopy study of the interaction of S with the Cu(111) surface, Ultramicroscopy 42-44 (1992) 498–504.

[111] C. T. Campbell, B. E. Koel, H_2S/Cu(111): A model study of sulfur poisoning of water-gas shift catalysts, Surface Science 183 (1-2) (1987) 100–112.

[112] E. Vernack, D. Costa, P. Tingaut, P. Marcus, Theoretical studies of 2-mercaptobenzothiazole and 2-mercaptobenzimidazole as corrosion inhibitors for copper, Submitted to Corrosion Science (2020).

[113] X. Wu, F. Wiame, V. Maurice, P. Marcus, 2-mercaptobenzothiazole corrosion inhibitor deposited at ultra-low pressure on model copper surfaces, Corrosion Science (2020) 108464.

[114] T. H. Fleisch, Reduction of copper oxides by UV radiation and atomic hydrogen studied by XPS, Applications of Surface Science 10 (1982) 51–62.

[115] F. Wiame, F.-R. Jasnot, J. Światowska, A. Seyeux, F. Bertran, P. L. Fèvre, A. Taleb-Ibrahimi, V. Maurice, P. Marcus, Oxidation of α-brass: A photoelectron spectroscopy study, Surface Science 641 (2015) 51–59.

[116] J. Li, C. W. Du, Z. Y. Liu, X. G. Li, M. Liu, Inhibition film formed by 2-mercaptobenzothiazole on copper surface and its degradation mechanism in sodium chloride solution, International Journal of Electrochemical Science 11 (2016) 10690–10705.

[117] L. Kazansky, I. Selyaninov, Y. Kuznetsov, Adsorption of 2-mercaptobenzothiazole on copper surface from phosphate solutions, Applied Surface Science 258 (2012) 6807– 6813.

[118] C. M. Whelan, M. R. Smyth, C. J. Barnes, The influence of heterocyclic thiols on the electrodeposition of Cu on Au(111), Journal of Electroanalytical Chemistry 441 (1998) 109–129.

[119] D. Zerulla, I. Uhlig, R. Szargan, T. Chassé, Competing interaction of different thiol species on gold surfaces, Surface Science 402-404 (1998) 604–608.

[120] M. Wilms, P. Broekmann, C. Stuhlmann, K. Wandelt, In-situ STM investigation of adsorbate structures on Cu(111) in sulfuric acid electrolyte, Surface Science 416 (1998) 121–140.

[121] J.-L. Domange, J. Oudar, Structure et conditions de formation de la couche d'adsorption du soufre sur le cuivre, Surface Science 11 (1) (1968) 124–142.

[122] A. Soon, L. Wong, M. Lee, M. Todorova, B. Delley, C. Stampf, Nitrogen adsorption and thin surface nitrides on Cu(111) from first-principles, Surface Science 601 (2007) 4775–4785.

[123] J. F. Skelly, T. Bertrams, A. W. Munz, M. J. Murphy, A. Hodgson, Nitrogen induced restructuring of Cu(111) and explosive desorption of N_2, Surface Science 415 (1998) 48–61.

[124] K. Hermann, Periodic overlayers and moire patterns: theoretical studies of geometric properties, Journal of Physics: Condensed Matter 24 (2012) 314210.

[125] J. C. Klein, C. P. Li, D. M. Hercules, J. F. Black, Decomposition of copper compounds in X-ray photoelectron spectrometers, Applied Spectroscopy 38 (5) (1984) 729–734.

[126] S. Poulston, P. M. Parlett, P. Stone, M. Bowker, Surface oxidation and reduction of CuO and Cu_2O studied using XPS and XAES, Surface and Interface Analysis 24 (1996) 811–820.

[127] B. E. T. Bautista, A. J. Wikieł, I. Datsenko, M. Vera, W. Sand, A. Seyeux, S. Zanna, I. Frateur, P. Marcus, Influence of extracellular polymeric substances (EPS) from pseudomonas NCIMB 2021 on the corrosion behaviour of 70Cu-30Ni alloy in seawater, Journal of Electroanalytical Chemistry 737 (2015) 184–197.

Annexe : Résumé étendu de thèse

Chapitre I : État de l'art

Le cuivre est un métal mou et ductile qui présente de hautes performances thermique et électrique, et une bonne résistance à la corrosion. Il est présent dans un grand nombre d'applications telle que l'électronique, comme conducteur de chaleur et d'électricité, ou comme constituant d'alliages métalliques.

Le cuivre réagit lentement avec l'air humide pour former une couche de carbonate hydraté de cuivre (vert-de-gris) qui protège le métal sous-jacent. En solution aqueuse neutre ou alcaline, le cuivre réagit avec l'eau pour former une couche d'oxyde protectrice dite couche passive. Cependant, ce métal n'est pas totalement immunisé contre la corrosion. Dans des conditions acides ou en présence d'ions chlorure, la couche protectrice n'est pas stable et le cuivre se corrode.

La corrosion du cuivre peut entraîner d'énormes pertes économiques en raison des nombreuses utilisations du cuivre et de ses alliages dans les domaines industriel, militaire et civil. Il est donc particulièrement important de trouver un moyen de limiter ce phénomène. L'utilisation d'un inhibiteur de corrosion est une approche efficace pour contrôler la corrosion des métaux et des alliages qui sont en contact avec un environnement agressif.

Un inhibiteur de corrosion est un composé chimique qui est ajouté en petites quantités dans l'environnement corrosif (liquide ou gaz) pour ralentir ou même arrêter le processus de corrosion d'un métal. Les inhibiteurs sont souvent faciles à appliquer et offrent l'avantage d'une application *in situ* sans provoquer de perturbations significatives du système. Les applications industrielles ont conduit à des traitements basés sur l'utilisation d'inhibiteurs de corrosion dans divers domaines tels que l'aéronautique, les chaudières à vapeur, le pétrole et les raffineries et les systèmes de refroidissement.

Pour chaque matériau, il existe une famille d'inhibiteurs efficaces pour limiter les phénomènes de corrosion. Les azoles et leurs dérivés sont très souvent utilisés comme inhibiteurs de corrosion pour le cuivre et présentent une efficacité remarquable. Les azoles sont une classe de composés hétérocycliques à cinq atomes contenant un atome d'azote et quatre atomes de carbone. La présence d'un atome d'azote leur donne la possibilité de

se coordonner avec d'autres substances et en particulier avec les ions métalliques. Cette capacité de complexation conduit à des applications intéressantes dans l'inhibition de la corrosion des métaux et d'alliages.

Le benzotriazole (BTA, $C_6H_5N_3$) et ses dérivés sont les inhibiteurs de corrosion les plus utilisés pour le cuivre. L'utilisation du BTA comme inhibiteur de corrosion du cuivre est étudiée depuis 1947. Il a été constaté qu'en solution, le BTA se chimisorbe sur le cuivre, avec la formation de fortes liaisons chimiques N–Cu et d'un complexe polymère Cu(I)-BTA qui recouvre totalement la surface du cuivre, entraînant une forte inhibition de la corrosion. L'adsorption du BTA en phase gazeuse a également été étudiée sous ultra-haut vide (UHV), et une monocouche chimisorbée se forme au début, avec l'azote lié au cuivre, puis des multicouches physisorbées qui sont moins stables et désorbent à environ 100°C.

En plus du BTA, le 2-mercaptobenzothiazole (2-MBT, $C_7H_5NS_2$) est aussi utilisé dans l'industrie. Des travaux montrent qu'il est encore plus efficace que le BTA sous certaines conditions. La présence d'azote et de soufre dans la molécule pourrait améliorer sa capacité d'inhibition de corrosion en formant des liaisons avec le cuivre. Le mécanisme d'inhibition est influencé par le milieu de corrosion. À quelques exceptions près, les recherches expérimentales ont été effectuées par immersion dans des solutions contenant la molécule. En milieu aqueux, le 2-MBT dissous en solution peut réagir avec le cuivre pour former un mince film polymère de Cu(I)-MBT insoluble dans l'eau qui agit comme une couche protectrice à la surface du cuivre. Il se fixe à la surface du métal par interaction avec le soufre et/ou l'azote.

Une autre molécule inhibitrice, structurellement proche du 2-MBT, est le 2-mercapto-benzimidazole (2-MBI, $C_7H_6N_2S$). Des recherches portant principalement sur l'interface métal/solution indiquent une chimisorption du 2-MBI sur la surface du cuivre pour former un film polymère qui protège le métal contre la corrosion. Il y a deux atomes d'azote et un atome de soufre dans la molécule 2-MBI, qui peuvent être liés simultanément ou individuellement au cuivre. Des études montrent que la molécule se décompose sur la surface métallique par la rupture de la liaison C=S. En outre, des études en théorie de la fonctionnelle de la densité suggèrent que le 2-MBI neutre en phase gazeuse peut être chimisorbé perpendiculairement à la surface par une liaison N–Cu ou S–Cu et physisorbé presque parallèlement à la surface.

Cependant, une controverse existe sur la nature chimique du complexe formé, ainsi que sur les mécanismes fondamentaux de l'interaction entre les molécules inhibitrices et le cuivre. Les structures résultantes de la couche protectrice formée sur le cuivre ne sont pas non plus très claires. Plus particulièrement, le rôle exact de l'oxyde de surface dans la fonction inhibitrice reste à identifier. Afin d'élucider les mécanismes d'inhibition, le dépôt de molécules en phase gazeuse sous UHV pourrait être plus efficace, car il permet de

maîtriser chaque étape du dépôt dans un environnement bien contrôlé et sur une surface bien définie.

Ce travail vise à apporter un nouvel éclairage et à approfondir les connaissances sur la relation entre la structure locale ainsi que la composition chimique des films inhibiteurs et l'efficacité d'inhibition de la corrosion en présence d'oxygène. L'objectif est d'obtenir les informations détaillées et nécessaires pour mieux comprendre les mécanismes d'inhibition de la corrosion, et ainsi d'offrir une base rationnelle pour la conception de nouveaux inhibiteurs.

Dans ce but, une approche de surface a été utilisée, faisant intervenir le dépôt des molécules sous ultra basse pression par sublimation en phase gazeuse sur des surfaces monocristallines bien définies. La cinétique d'adsorption des inhibiteurs sur la surface du Cu(111) métallique et pré-oxydée est suivie par la spectroscopie d'électrons Auger (AES). La composition chimique pendant la croissance des couches moléculaires est analysée *in situ* par la spectroscopie de photoélectrons induits par rayons X (XPS). La structure et la topographie des couches moléculaires formées sur le cuivre à différentes étapes du dépôt sont caractérisées par la microscopie à effet tunnel (STM) et la diffraction d'électrons lents (LEED).

Chapitre II : Matériaux et méthodes expérimentales

Dans ce travail, les expériences ont été réalisées dans trois systèmes UHV différents. L'un est équipé d'un réacteur pour le dépôt des molécules et d'un STM (Omicron, STM1), d'un AES (Omicron, CMA-100) ainsi que d'un LEED (Omicron, SpectaLEED) pour la caractérisation *in situ* de la surface de l'échantillon, et sera appelé le système STM par la suite. Un deuxième système est équipé d'un réacteur de dépôt identique et d'un XPS (Thermo Electron Corporation, ESCALAB 250) ainsi que d'un LEED (Thermo VG Scientific, Rear View LEED) pour l'analyse *in situ* de la croissance des inhibiteurs, et sera désigné comme le système XPS ci-après. La pression de base dans ces deux systèmes est de 10^{-10} mbar. Enfin, une plate-forme UHV équipée d'un STM (Omicron, VT STM XA), d'un XPS (Omicron, ARGUS) et d'un LEED (Omicron, SpectaLEED) a été utilisée pour étudier les propriétés des couches inhibitrices après exposition à l'air, avec une pression de base de 10^{-11} mbar, et sera par la suite dénommée la plate-forme d'analyse et d'imagerie des surfaces (PAIS). Ces trois systèmes sont équipés d'un canon de bombardement ionique et d'un système de recuit pour la préparation d'échantillon sous UHV.

La technique STM est basée sur un concept quantique, l'effet tunnel, et est utilisée pour déterminer la morphologie et la densité d'états de surfaces conductrices ou semi-conductrices, avec une résolution spatiale qui peut être égale ou inférieure à la taille d'un atome. Avec cette résolution, les atomes sur la surface de l'échantillon peuvent être imagés et manipulés individuellement.

Le principe du STM est relativement simple : une pointe conductrice balaie la surface d'un échantillon. Nous avons choisi de travailler en mode à courant constant, c'est-à-dire que nous ajustons en temps réel la hauteur de la pointe pour maintenir un courant constant et enregistrons cette hauteur qui permet de reconstituer la topographie de la surface. La caractérisation STM a été réalisée à température ambiante. Le traitement d'image a été effectué à l'aide du logiciel WSxM (5.0 Develop 9.1). Aucun filtrage n'a été appliqué sauf mentionné et toutes les images ont été corrigées par la soustraction d'un plan.

L'XPS est une technique d'analyse quantitative qui permet de déterminer la composition chimique des éléments présents à la surface d'un matériau. Pour cela, l'échantillon est bombardé par les rayons X, des photoélectrons sont ainsi produits par effet photoélectrique et détectés. Deux géométries ont été utilisées : afin d'étudier les éléments présents plus profondément dans l'échantillon, l'angle entre la surface de l'échantillon et l'analyseur a été fixé à 90° pour avoir un angle d'émission normal. Afin de caractériser les premières couches de la surface de l'échantillon, un angle d'émission de 45° a également été utilisé dans la plate-forme PAIS.

La source de photons utilisée dans les deux systèmes est une source de rayons X Al K_α monochromatique qui produit des photons monoénergétiques ($h\nu = 1486,6$ eV). La transmission de l'analyseur a été calibrée par la mesure d'échantillons de référence. Dans le système XPS, les spectres généraux ont été enregistrés avec une énergie de passage de 100 eV correspondant à une résolution globale de 1,8 eV, les spectres haute résolution ont été enregistrés avec une énergie de passage de 20 eV correspondant à une résolution globale de 360 meV. Dans le système PAIS, des énergies de passage de 50 eV et 20 eV ont été utilisées respectivement pour les spectres généraux et les spectres haute résolution. Le traitement des données a été effectué à l'aide du logiciel CasaXPS (version 2.3.19).

L'AES est une technique analytique largement utilisée pour étudier la composition de surface en se basant sur un phénomène physique appelé effet Auger. Pour la mesure AES, l'échantillon est bombardé par un faisceau d'électrons et les électrons Auger émis sont collectés et analysés. L'énergie cinétique des électrons Auger est caractéristique de l'énergie des niveaux électronique des éléments présents sur la surface et est indépendante de l'énergie du faisceau incident. Les spectres de référence sont utilisés pour identifier les éléments présents à la surface.

Le LEED est une technique de détermination de la structure cristalline d'une surface monocristalline par le bombardement d'un faisceau d'électrons collimaté à basse énergie (généralement comprise entre 20 et 200 eV). L'énergie du faisceau d'électrons est ajustée de telle sorte que sa longueur d'onde associée soit comparable aux distances interatomiques. Un écran fluorescent est utilisé pour afficher le motif de diffraction, qui est une image du réseau réciproque de la surface. L'existence de domaines symétriquement équivalents doit être prise en compte lors de l'analyse du motif LEED.

L'échantillon utilisé dans ce travail est un monocristal de Cu(111) de haute pureté (99,999%). Afin de préparer une surface propre et plane, l'échantillon a d'abord été poli mécaniquement de 6 à 0,25 μm à l'aide d'une pâte diamantée, et abondamment rincé à l'eau ultra pure (UP) (résistivité > 18 MΩ·cm) entre chaque étape pour éliminer les résidus de l'étape précédente. Il a ensuite été rincé successivement avec de l'acétone, de l'éthanol et de l'eau UP. Après cela, l'échantillon a été électropoli dans une solution à 60% en poids de H_3PO_4 à 1,4 V pendant 5 min, puis rincé avec une solution à 10% en poids de H_3PO_4 et de l'eau UP pour améliorer la finition de surface. Enfin, l'échantillon a été recuit sous un flux continu de H_2 à 725°C pendant 20 h pour reconstruire et recristalliser la surface avant l'introduction dans le système UHV.

L'échantillon a ensuite été préparé sous UHV dans le système STM par des cycles de bombardement ionique et de recuit. Le bombardement ionique a été effectué sous une pression de 1×10^{-5} mbar d'Ar^+ à une tension de 600 V et un courant d'émission de 20 mA, pendant 30 min. Ensuite, afin d'éliminer les défauts créés par le bombardement ionique et afin de réorganiser la surface de l'échantillon, un recuit thermique à 600°C a été effectué pendant 30 min. De même, dans le système XPS, le bombardement ionique ($P_{Ar} = 5 \times 10^{-6}$ mbar, 600 V, 10 mA, 10 min) et le recuit (600°C, 10 min) ont été répétés jusqu'à d'obtenir une surface propre et bien structurée.

La qualité de surface a été systématiquement vérifiée par AES, XPS, LEED et STM jusqu'à ce qu'aucune contamination ne soit détectée dans les spectres AES et XPS, et une bonne organisation de la surface soit observée par LEED et STM, caractérisée par un motif LEED (1×1) intense et une topographie STM présentant de larges terrasses sans défauts.

L'oxydation du Cu(111) a été réalisée en introduisant l'oxygène à $P_{O_2} = 5 \times 10^{-6}$ mbar à température ambiante jusqu'à saturation. Dans ces conditions, un oxyde de surface 2D est formé. Le dépôt des molécules inhibitrices a été réalisé par sublimation sous ultra basse pression dans le réacteur, avec une pression de vapeur du 2-MBT de 2×10^{-9} mbar et celle du 2-MBI de 1×10^{-9} mbar à température ambiante. Un système de chauffage est disponible dans le réacteur pour réaliser des dépôts à haute température.

Chapitre III : Dépôt de 2-MBT sur la surface du Cu(111) propre et pré-oxydée à température ambiante

Ce chapitre est dédié à l'étude de la composition chimique et de la topographie de l'échantillon suite à l'adsorption de 2-MBT sur la surface du Cu(111) propre et pré-oxydée à température ambiante. Pour cela, l'échantillon a été exposé au 2-MBT *in situ* dans les systèmes XPS et STM pour ensuite être analysé directement sous UHV sans être contaminé par l'air.

Les analyses XPS et AES montrent la croissance du 2-MBT sur la surface du Cu(111) propre, avec un excès de S par rapport à la stœchiométrie de la molécule. Une analyse détaillée des spectres XPS haute résolution montre la présence d'une composante de S à la même position que sur la surface $(\sqrt{7} \times \sqrt{7})$R19,1° S/Cu(111) obtenue en exposant la surface du Cu(111) propre à H_2S, indiquant une décomposition partielle des molécules 2-MBT par la rupture des liaisons C=S et C–S lors de l'interaction avec le cuivre métallique et l'adsorption de S atomique. De plus, les molécules qui s'adsorbent sur la surface sans se décomposer se lient au Cu par les deux S et donnent lieu à une composante d'énergie identique. Cette composante d'interface n'est pas observée après dépôt de 2-MBT sous vide sur une surface du Cu(111) pré-oxydée à l'air, ce qui montre que l'oxyde 3D pré-adsorbé empêche l'interaction directe avec le Cu métallique et la décomposition de la molécule. Les spectres XPS obtenus à plus haute exposition montrent l'apparition de deux composantes supplémentaires de S en plus de celle d'interface, correspondant au S endocyclique et exocyclique dans la molécule non liée au Cu, indiquant la formation de multicouches sur la surface du Cu(111) à partir d'une exposition de 15 L.

Le dépôt de 2-MBT sur la surface du Cu(111) pré-oxydée sous UHV formant une couche d'oxyde 2D a également été réalisé afin d'étudier l'effet de l'oxygène sur l'adsorption de la molécule. La croissance du 2-MBT est observée par AES et XPS, accompagnée d'une substitution de l'oxygène. Les spectres XPS à haute résolution montrent la présence de la composante de S d'interface, indiquant une liaison entre le S et le Cu. Cependant, la présence d'une couche d'oxyde 2D empêche la décomposition du 2-MBT. Une illustration schématique de l'adsorption du 2-MBT sur la surface du Cu(111) propre et pré-oxydée est résumée dans la figure 6.10. L'angle d'inclinaison entre la molécule et la surface de l'échantillon n'est pas pris en compte.

L'épaisseur des couches de molécules formées sur la surface du Cu(111) propre et pré-oxydée a été calculée. Une épaisseur d'environ 0,2 nm est obtenue à 15 L pour la monocouche de 2-MBT formée sur la surface du Cu(111) propre. Étant donné que la taille d'une molécule de 2-MBT est d'environ 7,2 Å × 10,2 Å, on en déduit que le 2-MBT dans la monocouche s'adsorbe avec son plan presque parallèle à la surface de l'échantillon. Les multicouches se forment avec une épaisseur totale de 0,6 nm à saturation. Sur la surface du Cu(111) pré-oxydée, la monocouche formée est de 0,4 nm après une exposition de 0,2 L, ce qui indique que la molécule s'adsorbe en position inclinée. Des multicouches d'épaisseur de 0,7 nm se forment à 17 L.

La topographie de la surface du cuivre à différentes étapes de dépôt a été caractérisée par STM. Sur la surface du Cu(111) propre, la formation de structures locales triangulaires le long des bords de marches et sur les terrasses est observée à faible exposition (4 L), avec un ordre local à l'intérieur de ces triangles qui peut être attribué à la structure $(\sqrt{7} \times \sqrt{7})$R19,1°. Ceci confirme la décomposition de 2-MBT observée précédemment par AES et XPS. Une monocouche de 2-MBT non ordonnée est observée à 10 L, avec des
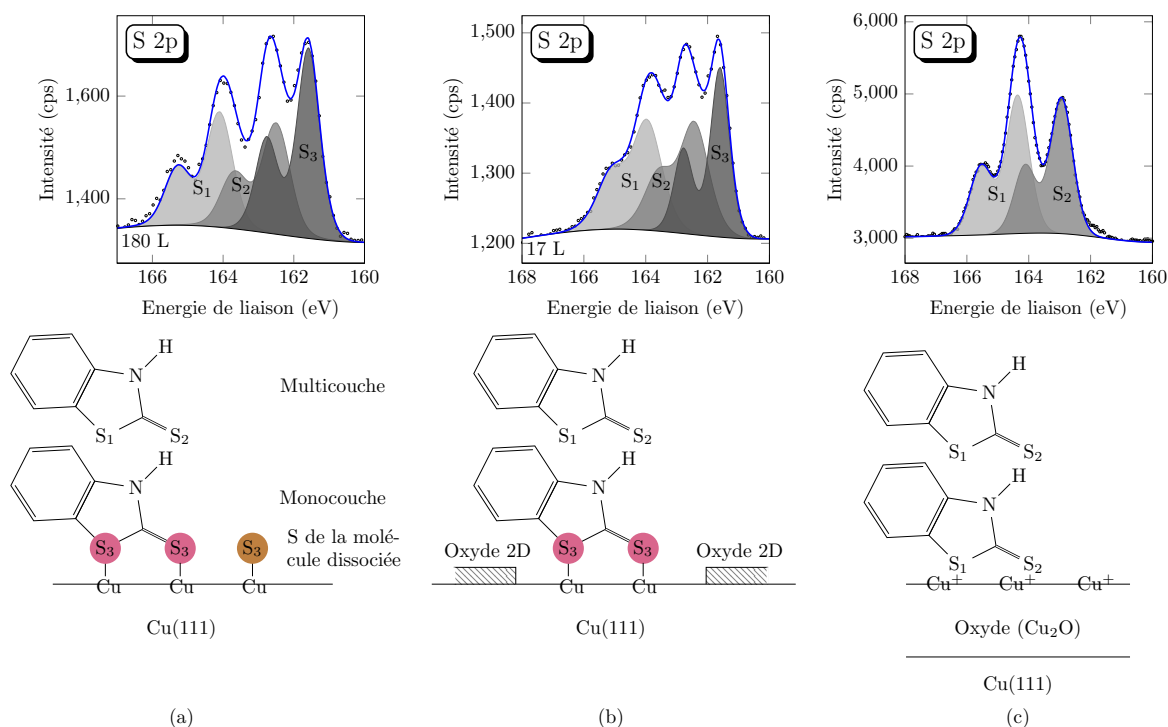
Figure 6.10: Illustration schématique de l'adsorption du 2-MBT sur différentes surfaces de cuivre et de l'état chimique correspondant du S mesuré par XPS : (a) métallique; (b) oxydée (oxyde 2D); (c) oxydé (oxyde 3D).

molécules qui s'adsorbent à plat sur la surface. Ceci est en bon accord avec l'analyse XPS. Des multicouches se forment à plus haute exposition. La dernière couche moléculaire est incomplète avec une épaisseur de 1,2 Å, qui indique que les molécules s'adsorbent aussi à plat dans les multicouches. La présence d'une couche d'oxyde 2D à la surface du Cu(111) avant dépôt change la morphologie de la surface en formant des multicouches de molécules complètes et homogènes.

Afin d'évaluer la stabilité thermique des couches de 2-MBT formées sur la surface du Cu(111) propre et pré-oxydée, un recuit des multicouches moléculaires à différentes températures a été réalisé. L'analyse XPS indique la décomposition et la désorption partielle de la molécule lorsque l'échantillon a été chauffé au-dessus de 100°C. Le STM montre la formation d'une couche ordonnée de structure $(\sqrt{7} \times \sqrt{7})$R19,1°, et confirme donc la décomposition de 2-MBT après recuit, et l'adsorption du S atomique.

Enfin, l'efficacité d'inhibition de la corrosion du 2-MBT a été étudiée en exposant à de l'oxygène la surface d'une monocouche de 2-MBT (8 L) pré-adsorbée sur Cu(111) propre, à température ambiante. La pression d'oxygène a été maintenue à 5×10^{-6} mbar. La mesure de la cinétique d'oxydation par AES montre qu'une monocouche de 2-MBT peut protéger efficacement la surface du cuivre contre l'oxydation dans ces conditions de température et de pression. Une adsorption résiduelle d'oxygène est observée, probablement due à

la formation localisée d'oxyde de cuivre là où la protection par la couche de 2-MBT est défectueuse. Les sites défectueux couvrent environ 8% de la surface.

Chapitre IV : Dépôt de 2-MBI sur la surface du Cu(111) propre et pré-oxydée à température ambiante

Dans ce chapitre, sont décrites les différentes étapes de dépôt et de caractérisation des couches adsorbées de 2-MBI. Le dépôt de 2-MBI sur la surface du Cu(111) propre et pré-oxydée a été réalisé *in situ* dans le système STM à température ambiante, et la surface après dépôt a été analysée par AES, STM et LEED. Ensuite, l'échantillon a été transféré vers le système XPS avec un passage à l'air réduit au minimum pour limiter les contaminations.

Les mesures AES montrent la croissance du 2-MBI sur la surface du Cu(111) propre et pré-oxydée, avec un excès de S par rapport à la stœchiométrie de la molécule, suggérant la décomposition du 2-MBI. Les images STM obtenues sur la surface du Cu(111) propre exposée au 2-MBI montrent la formation d'une monocouche auto-assemblée à une exposition de 5 L. Différentes structures sont mises en évidence sur la surface de l'échantillon, y compris une structure $(\sqrt{7} \times \sqrt{7})$R19,1° due à l'adsorption du S atomique, confirmant la décomposition du 2-MBI sur la surface du Cu(111) métallique. Une structure (8×8) est aussi observée, qui peut être attribuée à l'adsorption de la molécule. Des multicouches se forment à plus haute exposition, et la dernière couche est incomplète avec une épaisseur de 1–2 Å. Étant donné la taille d'une molécule 2-MBI d'environ 7,9 Å × 9,7 Å, on en déduit que le 2-MBI dans les multicouches s'adsorbe avec son plan presque parallèle à la surface de l'échantillon.

L'analyse XPS montre la présence d'une composante de S d'interface dans la mono-couche, indiquant une liaison entre le S et le Cu. La multicouche est marquée par l'apparition d'une composante de S supplémentaire, correspondant au S dans la molécule non-liée au Cu. De plus, le pic d'azote est déplacé vers une énergie de liaison plus faible par rapport à celui dans la poudre seule, suggérant une liaison entre l'azote et le cuivre. L'épaisseur de la multicouche de 2-MBI est estimée à $1,0 \pm 0,2$ nm, qui est presque 2 fois celle formée par le 2-MBT.

Pour le dépôt de 2-MBI sur la surface du Cu(111) pré-oxydée, une substitution de l'oxygène est également observée pendant la croissance de la molécule, comme pour le 2-MBT. Cependant, la cinétique d'adsorption est beaucoup plus lente, ce qui indique que le 2-MBI est moins réactif sur la surface du Cu(111) pré-oxydée.

Les images STM obtenues après le dépôt de 2-MBI sur la surface de Cu(111) pré-oxydée montrent la formation d'une couche complète de molécule. L'analyse XPS indique la formation de liaisons entre le S, le N et le Cu, avec une diminution de la proportion relative
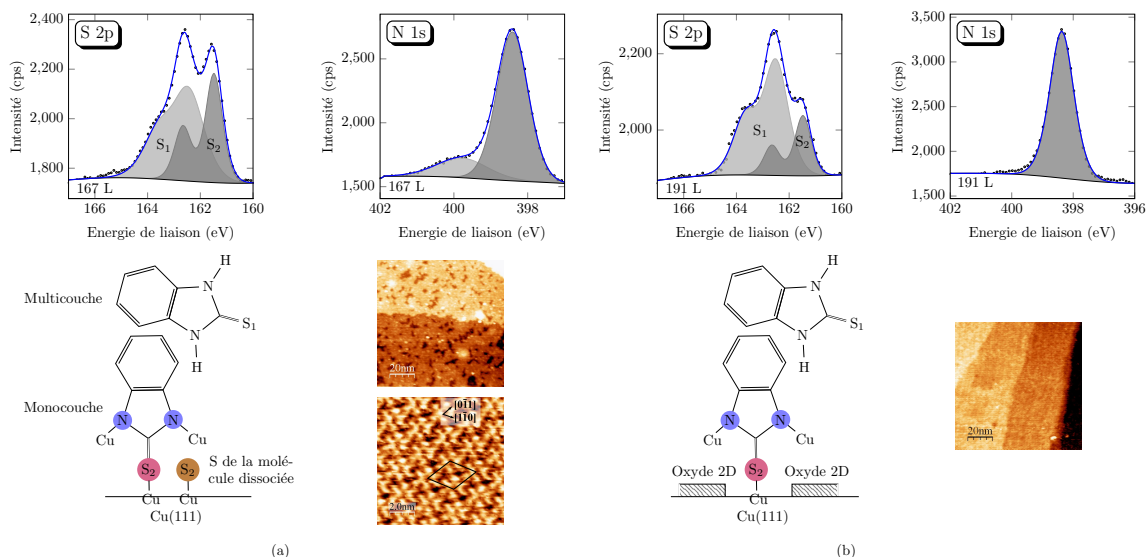
Figure 6.11: Illustration schématique de l'adsorption du 2-MBI sur différentes surfaces de cuivre et de l'état chimique correspondant du S et d'azote mesuré par XPS : (a) métallique; (b) oxydée (oxyde 2D).

du S d'interface. L'épaisseur de la multicouche de 2-MBI est estimée à $0,6 \pm 0,1$ nm, qui est plus mince que celle formée sur la surface du Cu(111) propre. Une illustration schématique de l'adsorption du 2-MBI sur la surface du Cu(111) propre et pré-oxydée est résumée dans la figure 6.11. L'angle d'inclinaison entre la molécule et la surface de l'échantillon n'est pas pris en compte.

La stabilité thermique des couches de 2-MBI formées sur Cu(111) a également été étudiée par un recuit des multicouches moléculaires à différentes températures. Une réorganisation de la surface est observée après recuit à 200°C, suivi de la formation de la structure $(\sqrt{7} \times \sqrt{7})$R19,1° après recuit à 500°C. Comparé aux multicouches de 2-MBT qui se décomposent à 100°C, les multicouches de 2-MBI sont plus stables.

Enfin, une monocouche et une multicouche de 2-MBI pré-adsorbées sur la surface du Cu(111) ont été exposées à l'oxygène à température ambiante pour tester leur efficacité d'inhibition de la corrosion. La pression d'oxygène a été maintenue à 5×10^{-6} mbar. La cinétique d'oxydation mesurée par AES montre que la multicouche de 2-MBI protège efficacement la surface du cuivre contre l'oxydation sous basse pression d'oxygène et à température ambiante. Cependant, il y a une légère augmentation de l'intensité d'oxygène en présence de la monocouche de 2-MBI, qui représente une couverture d'oxyde d'environ 20%. Comparé aux 8% de sites défectueux observé sur la monocouche de 2-MBT, on en déduit que la monocouche de 2-MBT offre une meilleure protection contre l'oxydation que celle de 2-MBI.

Chapitre V : Dépôt de 2-MBT sur la surface du Cu(111) à plus haute température

Ce chapitre est consacré à l'étude de l'effet de la température sur le dépôt de 2-MBT. Pour cela, l'échantillon a été chauffé à plus haute température pendant le dépôt de molécules dans le système STM, et l'état de la surface a été caractérisé *in situ* par AES, STM et LEED. Ensuite, l'échantillon a été transféré vers le système XPS pour l'analyse de la composition chimique.

En faisant varier la température de l'échantillon pendant le dépôt, une structure de Moiré est observée à 150°C, comme présenté dans la figure 6.12. Le Moiré est expliqué par la superposition de deux structures hexagonales, avec une différence de paramètre de réseau de 18% et une rotation de 1,2°. La couche inférieure est identifiée comme étant une structure $(\sqrt{3} \times \sqrt{3})$R30°.

Le spectre AES enregistré sur le Moiré montre un excès de S par rapport à la stœchiométrie de la molécule, suggérant une décomposition du 2-MBT. Ce phénomène est également observé pour le dépôt de 2-MBT sur la surface du Cu(111) propre à température ambiante. Cependant, le Moiré est plus riche en S que la monocouche de 2-MBT formée à température ambiante.

L'analyse XPS montre la présence d'un seul doublet de S correspondant au S d'interface, caractéristique de la liaison entre le S et le Cu. La décomposition du spectre C 1s confirme la dissociation de 2-MBT par la rupture des liaisons C=S et C–S. En plus, le Moiré est stable jusqu'à une température de dépôt de 250°C avant d'être transformé à une structure $(\sqrt{7} \times \sqrt{7})$R19,1°.

La croissance de 2-MBT sur le Moiré à température ambiante a été étudiée, et a montré qu'une couche d'épaisseur équivalente à seulement une monocouche de 2-MBT est formée, contrairement à la formation de multicouches pour le dépôt sur la surface du Cu(111) propre à température ambiante. Les images STM montrent la formation d'une couche homogène et complète.

L'efficacité de l'inhibition de la corrosion en présence du Moiré a aussi été étudiée. Pour cela, la structure de Moiré a été exposée à l'oxygène à température ambiante jusqu'à une pression de 10^{-5} mbar. La cinétique d'oxydation mesurée par AES révèle une protection efficace du Cu, meilleure que celle de la monocouche de 2-MBT formée à température ambiante. De plus, l'analyse XPS montre que le Moiré offre une bonne protection du Cu contre l'oxydation à l'air, confirmée par une forte diminution d'intensité d'oxygène par rapport au Cu propre et une oxydation préférentielle de la structure interfaciale de Moiré, qui protège le substrat métallique sous-jacent.
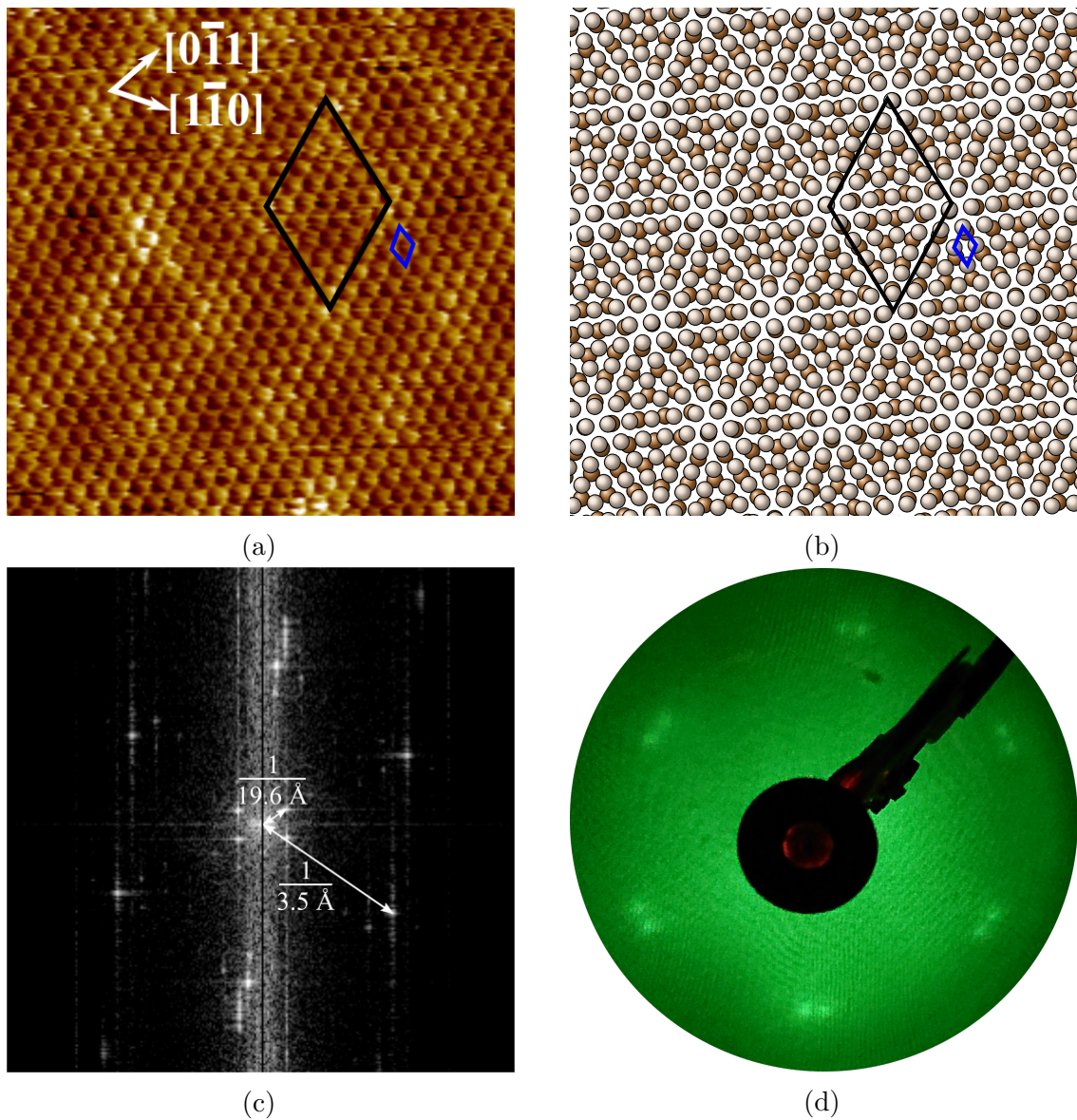
(a)

(b)

(c)

(d)

Figure 6.12: Moiré pour 45 L de 2-MBT déposés sur Cu(111) à 150°C (a) image STM (10 nm × 10 nm, $V = 0,05$ V, $I = 4,0$ nA); (b) modèle de Moiré composé de deux couches moléculaires superposées avec les cellules unitaires observées dans l'image STM marquées (substrat non représenté); (c) transformée de Fourier de l'image (a) avec la structure de Moiré et la structure de la couche moléculaire supérieure marquées; (d) diagramme LEED (Ep = 55 eV).

RÉSUMÉ

L'adsorption et l'inhibition de la corrosion par deux molécules organiques de strcuture comparable, le 2-mercaptobenzothiazole (2-MBT) et le 2-mercaptobenzimidazole (2-MBI), déposées sous ultra basse pression par sublimation en phase gazeuse sur la surface du Cu(111) propre et pré-oxydée ont été étudiées par spectroscopie d'électrons Auger, spectroscopie de photoélectrons induits par rayons X, microscopie à effet tunnel et diffraction d'électrons lents. Sur la surface du Cu(111) propre, la croissance des couches moléculaires à température ambiante est accompagnée d'une décomposition partielle des inhibiteurs, donnant une structure locale $(\sqrt{7} \times \sqrt{7})$R19,1°, caractéristique de l'adsorption du soufre atomique. Le 2-MBT non-dissocié se lie à plat au cuivre par ses deux atomes de soufre. Le 2-MBI s'adsorbe aussi à plat avec ses deux atomes d'azote liés au cuivre en plus du soufre. La pré-formation d'une couche d'oxyde 2D sur Cu(111) favorise la formation d'une couche moléculaire complète et homogène, accompagnée d'une substitution de l'oxygène. De plus, l'oxyde 2D empêche la décomposition de 2-MBT. Une monocouche de 2-MBT non-ordonnée formée à environ 10 L protège le cuivre contre l'oxydation sous basse pression d'oxygène à température ambiante, alors qu'une légère oxydation du cuivre est observée en présence d'une monocouche de 2-MBI auto-assemblée formée à 5 L, à cause de la présence des défauts locaux. La multicouche de 2-MBT se décompose lors du chauffage au-dessus de 100°C, alors que celle de 2-MBI est stable jusqu'à 500°C. En augmentant la température du Cu(111) propre pendant le dépôt de 2-MBT, une structure de Moiré est observée à 150°C, résultant de la superposition de deux structures hexagonales avec une structure $(\sqrt{3} \times \sqrt{3})$R30° sous-jacente. Le Moiré est riche en soufre et protège le cuivre contre l'oxydation à l'air à température ambiante.

MOTS CLÉS

2-MBT, 2-MBI, cuivre, adsorption, structure, corrosion, inhibition, UHV, STM, XPS, AES, LEED

ABSTRACT

The adsorption and corrosion inhibition by two structurally related organic molecules, 2-mercaptobenzothiazole (2-MBT) and 2-mercaptobenzimidazole (2-MBI), deposited under ultra low pressure by sublimation in gaseous phase on pristine and pre-oxidized Cu(111) surfaces were investigated by Auger Electron Spectroscopy, X-ray Photoelectron Spectroscopy, Scanning Tunneling Microscopy and Low Energy Electron Diffraction. On pristine Cu(111) surface, the growth of molecular layers at room temperature is accompanied by a partial decomposition of the inhibitors, resulting in a $(\sqrt{7} \times \sqrt{7})$R19,1° local structure, characteristic of the adsorption of atomic sulfur. The non-dissociated 2-MBT is lying flat on copper through bonding with the two sulfur atoms. 2-MBI is also lying flat with the two nitrogen atoms bonded to copper besides sulfur. The pre-formed 2D oxide layer on Cu(111) favors the formation of a complete and homogeneous molecular layer, accompanied by a substitution of oxygen. Moreover, the 2D oxide prevents the decomposition of 2-MBT. A non-ordered 2-MBT monolayer formed at about 10 L protects copper against oxidation under low oxygen pressure at room temperature, while a slight oxidation is observed with a self-assembled 2-MBI monolayer formed at 5 L, due to the presence of local defects. Decomposition of 2-MBT multilayer is observed after annealing to temperature above 100°C, while the 2-MBI multilayer is stable until 500°C. By increasing the temperature of metallic Cu(111) during 2-MBT deposition, a Moiré structure is observed at 150°C, resulting from the superposition of two hexagonal structures with a underlying $(\sqrt{3} \times \sqrt{3})$R30° structure. The Moiré structure is rich in sulfur and protects copper against oxidation in air at room temperature.

KEYWORDS

2-MBT, 2-MBI, copper, adsorption, structure, corrosion, inhibition, UHV, STM, XPS, AES, LEED